Zeolite-Modified Fischer-Tropsch Synthesis

By

Rashed Shah

Submitted to the University of Cape Town in partial requirements for the degree of

MASTERS OF SCIENCE IN CHEMICAL ENGINEERING

July 2011

Centre for Catalysis Research
Department of Chemical Engineering
University of Cape Town

SYNOPSIS

The improvement of the gasoline selectivity and quality with the addition of HZSM-5 to the Fe-FT process is evident from literature, and such a process is further supported by the demand of high-quality gasoline. The catalytic performance of the combined Fe-FT/HZSM-5 system has, however, been observed to considerably decline with time-on-stream, a phenomenon which has been attributed to the migration of alkali from the Fe-FT catalyst to the HZSM-5 zeolite. There is, however, no conclusive proof that this migration occurs during syngas conversion, nor whether it is the cause of the observed decline in catalytic performance with time-on-stream.

The objective of this study, therefore, is to characterize and confirm the reported performance of the Fe-FT and combined Fe-FT/HZSM-5 catalyst systems in a stirred from top internal recycle reactor (STIRR) under typical high temperature FT conditions. Moreover, this study seeks to establish evidence for the hypothesized migration of potassium from the Fe-FT catalyst to the HZSM-5 zeolite, and to determine any relationship that may exist between potassium migration and changes in the observed performance of the combined Fe-FT/HZSM-5 catalyst system.

Catalytic tests were conducted in a Stirred from Top Internal Recycle Reactor (STIRR) comprising beds of physically mixed potassium-promoted iron powder and HZSM-5 extrudates at 330^{o}C and 20 bar. The potassium content in the fresh and spent Fe-FT and HZSM-5 catalysts was measured via atomic emission (ICP-AES), atomic absorption (AAS) and X-Ray fluorescence (XRF) spectroscopy.

The results of this investigation confirmed the Fe-FT catalyst performance in a STIRR under typical high temperature FT conditions and reconfirmed the significant increase in the gasoline selectivity and quality with the addition of HZSM-5 to the Fe-FT process, as well as the observed decline in performance of the combined Fe-FT/HZSM-5 catalyst system with time-on-stream.

Furthermore, this study confirmed the migration of potassium from the Fe-FT catalyst to the HZSM-5 zeolite in the combined Fe/HZSM-5 experiment, but it was found that no

relationship exists between potassium migration and changes in the observed performance of the combined Fe-FT/HZSM-5 catalyst system with time-on-stream. The deactivation of HZSM-5 was primarily a result of the zeolite coking in this study, which was also ascribed to be the cause of the observed increase in the CH_4 selectivity in the combined system.

ACKNOWLEDGEMENTS

The main credit goes to my supervisor, Prof. Jack C. Q. Fletcher, without whom this dissertation would not be possible. Thank you for giving me the opportunity to carry out this project and for your support, advice and encouragement throughout the period of this project. I would also like to thank you for your valuable input and the patience needed in editing and compilation of this dissertation.

I would like to express my sincere thanks to Roald Brosius for your assistance in practically everything entailing this project; operation of the rig, conduction of experiments, and your insightful ideas and input to put me on the right track. Thank you for keeping sane through the vicissitudes of this project.

A special thanks to Walter Böhringer for your invaluable input in the technical aspects of this dissertation and for always lending an ear, whenever I needed one. Thank you for always making time for me and lightening the mood with your 'amusing' comments.

I would also like to thank; UCT and the Department of Chemical Engineering for the use of their facilities and other resources, the Centre of Catalysis Research for your financial support, and to all my colleagues for providing an 'entertaining' work environment.

Finally, but most importantly, I would like to thank God for…everything, my parents for your invariable support and love, my friends who kept me sane and Taryn for your support and help in editing this dissertation.

TABLE OF CONTENTS

Page

LIST OF TABLES

LIST OF FIGURES

LIST OF SYMBOLS

A_i	Area response of component *i* (GC-FID)
$A_{i,corrected}$	Corrected Area response of component *i* (GC-FID)
$A_{i,sample}$	Area of component *i* (GC-TCD product sample)
$A_{i,calibration}$	Area of component *i* (GC-TCD calibration sample)
$C_{i,sample}$	Concentration of component *i* (GC-TCD product sample)
$C_{i,calibration}$	Concentration of component *i* (GC-TCD calibration sample)
C_p	Specific heat capacity [J/mol.K]
$f_{o,i}$	Correction factor of component *i* (GC-FID)
$\Delta \underline{G}^{rxn}$	Gibbs free energy for reaction [J/mol]
$\Delta \underline{H}^{rxn}$	Enthalpy of reaction [J/mol]
k_i	Correction factor of component *i* (GC-TCD)
K_p	Equilibrium constant
$m_{C[i]}$	Mass of carbon in component *i*
m_i	Mass of component *i*
$M_{[i]}$	Molar mass of component *i*
$n_{C[i]}$	Moles of carbon in component *i*

n	Carbon number (ASF polymerization equation)
n_i	Moles of component *i*
$N_{C[i]}$	Number of carbon atoms in component *i*
$N_{C,i}$	Number of carbon atoms of component *i* (GC-FID)
$N_{C(no\_O),i}$	Number of carbon atoms not bonded to an oxygen atom of component *i* (GC-FID)
$N_{C(O),i}$	Number of carbon atoms bonded to an oxygen atom of component *i* (GC-FID)
P^*_i	Vapour pressure of component *i* [bar]
P_i	Partial pressure of component *i* [bar]
S_i	Selectivity of component *i* [C-%]
V_i	Volume of component *i* [ml/min]
$V_{i,sample}$	Volume of component *i* (GC-TCD sample)
W_n	Sum of mass fractions of hydrocarbons in carbon number *n*
X_i	Conversion of component *i*
y_i	Mole fraction of component *i*
z_i	Response of component *i* (GC-FID)
Å	Armstrong
α	ASF chain growth probability

GLOSSARY

AAS	Atomic Absorption Spectroscopy
ASF	Anderson-Schulz-Flory
FID	Flame Ionization Detector
FT	Fischer-Tropsch
GC	Gas Chromatogram
GC-FID	Gas Chromatogram fitted with a Flame Ionization Detector
GC-TCD	Gas Chromatogram fitted with a Thermal Conductivity Detector
HTFT	High Temperature Fischer-Tropsch
ICP	Inductively Coupled Plasma
LTFT	Low Temperature Fischer-Tropsch
MFC	Mass Flow Controller
MS	Mass spectrometer
STIRR	Stirred from Top Internal Recycle Reactor
TCD	Thermal Conductivity Detector
TOS	Time-on-stream
XRF	X-ray Fluorescence
WGS	Water-Gas Shift
ZSM-5	Zeolite Socony Mobil 5

1 INTRODUCTION

The High Temperature Fischer-Tropsch (HTFT) process is currently being operated to produce gasoline and higher value fine chemicals as the desired products. The hydrocarbons in the gasoline range mainly comprise of linear hydrocarbons (Dry, 1981) and, consequently, this naphtha cut is of a low octane value due to its chemical nature. To convert the naphtha cut to high-octane gasoline, further work-up is required, which is an expense to the Fischer-Tropsch industry. Conceptually, acid catalysts may be co-fed with the FT catalyst to improve the gasoline quality since the presence of the acid co-catalyst will convert the linear hydrocarbons into highly branched and aromatic hydrocarbons.

The Fischer-Tropsch product distribution follows the Anderson-Schulz-Flory model (Anderson, 1956; Schulz et al., 1988a; Schulz et al., 1988b) and the maximum gasoline selectivity ($C_5 - C_{11}$) attainable from this model is 48 wt-% (at an optimized α value of 0.76). These limitations arise from the polymerization kinetics governing chain growth but can be, in principle, circumvented by the addition of an acid co-catalyst, which can extend the gasoline fraction by oligomerization of C_3 and C_4 olefins. In particular, the pore structure of zeolites coupled with their propensity for light olefin oligomerization can both extend the yield and octane quality of the gasoline fraction.

Most combined FT catalyst/zeolite processes have been carried out with HZSM-5 as the acid co-catalyst and it seems to be the preferred choice due to the following reasons (Polinski et al., 1984; Udaya et al., 1990):

- The medium pore opening (5.5 Å) provides a shape-selective effect, minimizing the formation of product molecules above C_{10}, which coincides with the gasoline fraction.
- The highly acidic nature of HZSM-5 helps catalyze oligomerization, cracking, isomerization and aromatization reactions.

- ZSM-5 limits the formation of coke precursors due to its medium pore size.
- ZSM-5 is stable under hydrothermal conditions and is resistant to dealumination under typical FT conditions.

The FT catalysts used for the combined process are mainly iron and cobalt, whereby cobalt could be applied as the FT catalyst for the combined process, but studies (Stencel et al., 1983; Shamsi et al., 1984; Rao et al., 1985) showed that the CH_4 selectivities obtained tend to be high at temperatures above 300^{o}C. Moreover, when operated at temperatures below 300^{o}C the zeolite activity is not significant (Muller et al., 1982; Guan et al., 1996) and, therefore, at temperatures above 300^{o}C, iron would be the preferred FT catalyst choice in a combined process since iron has a lower selectivity towards CH_4 at high temperatures. Furthermore, a more olefinic product spectrum can be attained with the Fe-FT catalyst as compared to the Co-FT catalyst (Dry, 1981), which is desired since olefins are active for oligomerization over the acid co-catalyst. Alkali promotion is significant for the Fe-FT catalyst in terms of its activity and selectivity as it promotes chain growth, and is also known to increase the ratio of olefins to paraffins (Dry, 1981). The probability of chain growth increases with alkali promotion in the order lithium, sodium, potassium and rubidium, but potassium salts are generally used in practice because of the high prices of rubidium (Dry, 2002).

The addition of HZSM-5 into the high temperature Fe-FT process has in general shown promising results in terms of an increase in the gasoline selectivity, with a highly branched and aromatic product spectrum (Chang and Lang, 1978; Caesar et al., 1979; Brennan et al., 1981; Butter et al., 1981; Haag and Haung, 1981; Varma et al., 1986; Dwyer and Garwood, 1982; Schulz et al., 1991a; Botes and Böhringer, 2004; Botes, 2005; Martinez and Lopez, 2005; Pour et al., 2008a). The combined process has been investigated with various types of Fe-FT/HZSM-5 configurations, but the general characteristic is that the two catalysts are either in physical contact or not. The zeolite can be separated from the FT catalyst by using two reactors in series (dual-reactor arrangement) or by placing the catalysts in sequential beds in the

same reactor (dual-bed arrangement). Physical contact between the two catalysts can be achieved through impregnation of the zeolite with the metal solution, pelletizing a ball-milled mixture of HZSM-5 and Fe-FT catalysts, mixing the powders of HZSM-5 and Fe-FT with a binder followed by grinding and/or by simply mixing the two catalysts.

The main areas of concern related to a combined Fe-FT/HZSM-5 process as compared to an Fe-FT process appear to be as follows:

- A decline in the activity of the Fe-FT catalyst and/or a more rapid increase in the CH_4 selectivity when the two catalysts are in intimate contact (Schulz et al., 1991a; Botes and Böhringer, 2004; Pour et al., 2008a).

- Deactivation of HZSM-5 as observed by a declining aromatics content with time-on-stream (Botes and Böhringer, 2004; Botes, 2005; Martinez and Lopez, 2005; Pour et al., 2008a).

The migration of alkali from the Fe-FT catalyst to HZSM-5 in a combined Fe-FT/HZSM-5 process has been claimed to cause the observed loss in activity and/or selectivity of the Fe-FT catalyst and, concomitantly, playing a role in the deactivation of HZSM-5 (Butter et al., 1981; Udaya et al., 1990; Botes and Böhringer, 2004; Pour et al., 2008a; Gwagwa and van Steen, 2009). There is, however, little conclusive evidence of this phenomenon occurring during the combined Fe-FT/HZSM-5 process, although Gwagwa and van Steen (2009) investigated the migration of potassium in pellets originally containing K-Fe_2O_3 (6.7g K_20/100g Fe) and HZSM-5 (silica/alumina molar ratio of 80). The study was carried out while heating the pellets at 350^oC in air for a number of days with the conclusion that at equilibrium, about 20% of the potassium migrated to the HZSM-5 zeolite and in the process neutralizing about 50% of the acid sites. Nonetheless, the extent of alkali migration would depend on various factors including the potassium loading in the Fe-FT catalyst, the acidity of the zeolite and the amount of zeolite used relative to the Fe-FT catalyst. Schulz et al. (1991a) observed a significant increase in the CH_4 selectivity with the addition of HZSM-5 to the Fe-FT

process but after oxidative regeneration of the Fe-FT/HZSM-5 composite catalyst, the CH_4 selectivity of the regenerated catalyst was much lower than that observed at the end of the test with the fresh catalyst, suggesting that a simple case of alkali migration away from the Fe-FT catalyst was not the cause of the observed increase in the CH_4 selectivity.

The main aims of this study, therefore, are to reconfirm the nature of the change in the catalytic performance (activity and selectivity) of the combined Fe-FT/HZSM-5 system with time-on-stream, to quantitatively determine whether potassium migrates from the Fe-FT catalyst to HZSM-5 and to determine any relationship that may exist between potassium migration and changes in the observed catalytic performance. For this purpose, catalytic tests were conducted in a Berty-type reactor comprising beds of physically mixed potassium-promoted iron powder and HZSM-5 extrudates at 330^{o}C and 20 bar. The potassium content in the fresh and spent Fe-FT and HZSM-5 catalysts was measured via atomic emission (ICP-AES), atomic absorption (AAS) and X-Ray fluorescence (XRF) spectroscopy.

2 LITERATURE REVIEW

2.1 Fischer-Tropsch Process

2.1.1 Overview

There are currently two main Fischer-Tropsch (FT) process technologies: the High Temperature Fischer-Tropsch (HTFT) and the Low Temperature Fischer-Tropsch (LTFT) processes. The LTFT process (200 – 230^{o}C) is at present operated for the production of long linear paraffins (waxes) that are hydrocracked to produce middle-distillate fuels. The HTFT process (300 – 350^{o}C) produces gasoline and low molecular mass olefins, where certain olefins are worked-up to higher value chemicals.

In order to obtain the desired hydrocarbon reactions over zeolite catalysts, reaction temperatures above 300^{o}C are generally required (Muller et al., 1982; Guan et al., 1996) and, therefore, the high temperature condition is the preferred choice for the combined Fe-FT/HZSM-5 process.

The gasoline cut (C_5 – C_{10}) from a HTFT process consists mainly of linear hydrocarbons (Dry, 1981) and small amounts of aromatics (Table 2.1), which limits the quality of the gasoline produced in terms of its octane rating. Linear hydrocarbons and paraffins have low octane numbers because of their tendency to crack easily, resulting in self-ignition before completion of the compression stroke in the cylinders of car engines and is referred to as ‘knocking’, an effect that reduces the potential performance of car engines and, inter-alia, results in higher fuel consumption. Current South African legislation requires petrol with an octane number of 95, which is not met by the ‘straight-run’ FT gasoline and consequently, the gasoline requires either further work-up or the addition of high-octane compounds to improve its octane rating (Horsley et al., 1993). This is an expense for the FT industry, which could potentially be

overcome by the addition of an acid co-catalyst to the FT process. The presence of the acid co-catalyst will convert the linear hydrocarbons into highly branched and aromatic hydrocarbons, as a result of skeletal isomerization and aromatisation reactions occurring over the HZSM-5 zeolite. Branched hydrocarbons and aromatics have high octane numbers mainly due to their ability to stabilize radicals and thus avoid self-ignition.

Table 2.1: Typical product compositions for HTFT and LTFT operations over an Fe-FT catalyst (Jager and Espinoza, 1995)

	Tubular fixed-bed reactor		Sasol slurry phase distillate reactor		High temperature Fischer-Tropsch	
	C_5-C_{12}	C_{13}-C_{18}	C_5-C_{12}	C_{13}-C_{18}	C_5-C_{12}	C_{13}-C_{18}
Paraffins (wt-%)	53	65	29	44	13	15
Olefins (wt-%)	40	28	64	50	70	60
Aromatics (wt-%)	0	0	0	0	5	15
Oxygenates (wt-%)	7	7	7	6	12	10

2.1.2 Chemistry and thermodynamics

There are numerous studies and articles on the conversion of synthesis gas to hydrocarbons (Dry, 1981; Anderson, 1984; Dry, 1996; Dry, 2002; Dry, 2004a; Claeys and van Steen, 2004). The FT synthesis reactions are exothermic and can be described by the following set of reactions (Udaya et al., 1990):

Methanation: $$CO + 3H_2 \rightarrow CH_4 + H_2O \quad (2.1)$$

Paraffins: $$nCO + (2n+1)H_2 \rightarrow C_nH_{2n+2} + nH_2O \quad (2.2)$$

Olefins: $$nCO + 2nH_2 \rightarrow C_nH_{2n} + nH_2O \quad (2.3)$$

Alcohols: $$nCO + 2nH_2 \rightarrow C_nH_{2n+1}OH + (n-1)H_2O \quad (2.4)$$

Other competing reactions include the water-gas shift (WGS) reaction and the Boudouard reaction:

WGS: $$CO + H_2O \rightarrow CO_2 + H_2 \quad (2.5)$$

Boudouard: $$2CO \rightarrow CO_2 + C_s \quad (2.6)$$

The formation of CH_4 is favoured over the entire temperature range of synthesis (200 – 400^{o}C) (Bussemeier et al., 1976). However, since thermodynamic equilibrium is reached slowly in FT synthesis, it is possible to take advantage of kinetic factors by using suitable catalysts and so produce heavier hydrocarbons in substantial quantity (Udaya et al., 1990).

2.1.3 Fischer-Tropsch product distribution

The Anderson-Schulz-Flory (ASF) model describes the hydrocarbon product distribution in FT synthesis (Anderson, 1956; Schulz et al., 1988a; Schulz et al., 1988b). The ASF model is based on simultaneous chain growth and product desorption where the adsorbed hydrocarbon species either could participate in further chain growth or desorb to form the observed products. The probability of chain growth is referred to as the α value in the ASF polymerization equation,

$$\log(W_n/n) = n\log\alpha + \log\left|(1-\alpha)^2/\alpha\right| \quad (2.7)$$

Where W_n = sum of mass fractions of hydrocarbons in carbon number n

n = carbon number

α = ASF chain growth probability (values in range 0 – 1)

If the product carbon number distribution follows the polymerization equation (Equation 2.7), one would expect a linear relation between log (W_n/n) and n, resulting in a non-selective product distribution as a wide range of hydrocarbons are obtained. The theoretical maxima for various hydrocarbons have been calculated (Dry, 1981) and are illustrated in Figure 2.1.

The maximum gasoline ($C_5 - C_{11}$) yield attainable from the ASF model is 48% (optimum α value of 0.76) and the maximum diesel ($C_{12} - C_{18}$) yield is 30% (optimum α value of 0.88). These limitations arise from the polymerization kinetics governing chain growth and can, in concept, be circumvented by the addition of an acid co-catalyst.

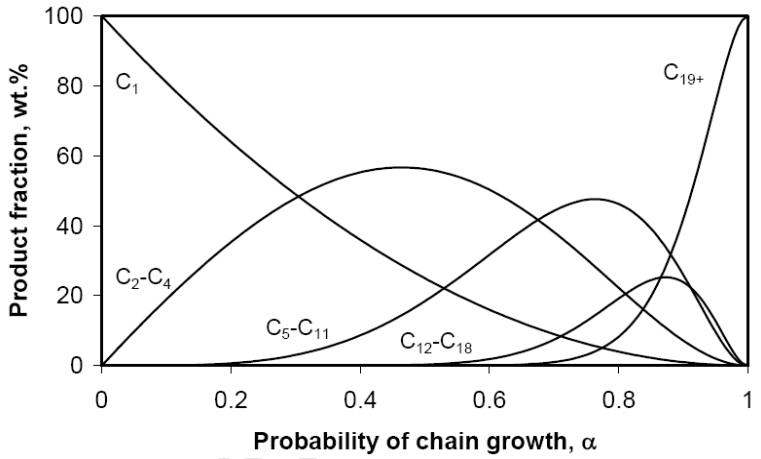

Figure 2.1: Plot of theoretical yields of hydrocarbon products as a function of chain growth probability (Dry, 1981)

2.1.4 HTFT product selectivity

The main products of the FT synthesis are linear α-olefins and linear paraffins, while typical side-products include oxygenates (n-alcohols, aldehydes, ketones, carboxylic acids) and branched compounds (mainly mono-methyl branched) (Claeys and van Steen, 2004).

The high temperature FT process is known to produce more branched and aromatic compounds than the low temperature FT process, and in the commercial HTFT process at Sasol more than 40% of all paraffins are branched, mainly comprising of mono-methyl branched compounds and only small amounts of di- and tri-methyl and ethyl-compounds (Claeys and van Steen, 2004).

The product selectivities obtained from Sasol commercial operations for a synthol reactor at 325^{o}C and 22 bar over an Fe-FT catalyst are shown in Table 2.2.

Table 2.2: Product Selectivities for Sasol Synthol reactor at 325^{o}C (Dry, 1981)

Product	Composition (C-%)
CH_4	10
C_2H_4	4
C_2H_6	4
C_3H_6	12
C_3H_8	2
C_4H_8	9
C_4H_{10}	2
C_5 to C_{11} (gasoline)	40
C_{12} to C_{18} (diesel)	7
$>C_{18}$	4
Water soluble non-acid chemicals	5
Water soluble acids	1

2.1.5 Fischer-Tropsch catalysts

The only known catalysts that have sufficient FT activity for commercial utilization are cobalt, iron, nickel and ruthenium (Dry, 2002). Ruthenium is the most active but due its low availability and consequent high prices, it is generally not used for commercial application. Nickel is very active but since it is also very active for hydrogenation, the selectivity to undesired CH_4 is high and the selectivity to olefins is low. Furthermore, when nickel is used at low temperatures and high pressures for the production of wax, volatile nickel carbonyls are

formed, resulting in a gradual loss of nickel catalyst from the reactor. Rhodium can also be used as an FT catalyst, but it is less active and has a propensity to form large fractions of oxygenates as compared to the other FT catalysts (Dry, 2004b).

Cobalt and iron are the only known commercially viable FT catalysts and the most significant difference between the two catalysts is the effect of water on the FT reaction rate. The proposed kinetic equations (Dry, 2002) are as follows:

For Fe-FT,
$$r = \frac{mP_{H_2}P_{CO}}{P_{CO} + aP_{H_2O}} \tag{2.8}$$

For Co-FT,
$$r = \frac{kP_{H_2}P_{CO}}{(1 + P_{CO})^2} \tag{2.9}$$

With an Fe-FT catalyst (Equation 2.8), water acts as a strongly inhibiting factor, thereby reducing the possibility of attaining a high syngas conversion per pass (Figure 2.2). Since water has no inhibiting effect on the Co-FT catalyst (Equation 2.9), higher degrees of conversion can be achieved. It should, however, be emphasized that due to the much higher prices of cobalt relative to iron, cobalt needs to be highly dispersed and thus very small cobalt crystals will be required on the oxide support. These very small cobalt crystals could potentially deactivate at the high H_2O/H_2 ratios typical of high conversions. Moreover, from Figure 2.2, increasing the number of active sites of the Fe-FT catalyst would better the performance of the Fe-FT catalyst at lower conversions as compared to a less active Co-FT catalyst and, therefore, considering iron is much cheaper than cobalt, there is a big incentive to significantly improve the activity of the Fe-FT catalyst. In addition, Figure 2.2 also shows that for the Fe-FT catalyst, the conversion profile does not change with an increase in total pressure if the residence time and other variables are constant (Dry, 2002).

For the production of gasoline and chemicals at higher temperatures, an Fe-FT catalyst is preferred as a lower CH_4 selectivity and a more olefinic product spectrum can be obtained with

an Fe-FT catalyst as compared to a Co-FT catalyst. In contrast, for the production of diesel at low temperatures, a Co-FT catalyst is preferred to an Fe-FT catalyst as it is more active and the CH_4 selectivity at these low temperatures is not of grave concern (Dry, 1981).

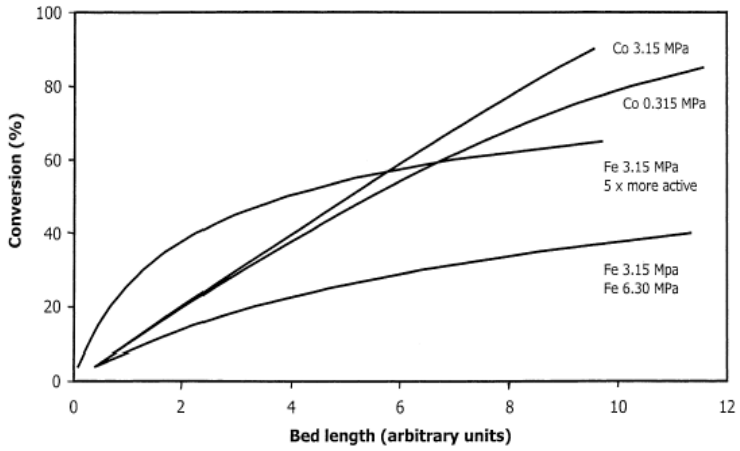

Figure 2.2: Plot of conversion profiles for a LTFT operation with Fe-FT and Co-FT catalysts (Dry, 2002)

2.1.6 Alkali promoters

Fe-FT catalysts require chemical promoters in the form of strong bases (typically alkali metals), as the 'basicity' of the surface is of vital importance for both the activity and selectivity of the Fe-FT catalyst (Dry, 1981). The ability of alkali metals to donate electrons increases the strength of CO chemisorption and so enhances its decomposition to carbon and oxygen atoms (Jager and Espinoza, 1995). The higher the surface concentration of carbon atoms, the higher the coverage by the CH_2 building blocks and thus the higher the probability of chain growth (Dry, 1996). An increase in the strength of CO chemisorption on the Fe-FT catalyst would also result in an increase in the water-gas shift activity (Arakawa and Bell, 1983).

Alkali promotion is known to increase the ratio of olefins to paraffins for reason of the weaker H_2 adsorption on an alkali-promoted Fe-FT catalyst than that of CO and, consequently, alkali increases surface coverage by growing chains and monomers, limiting access for H_2 (Dry, 1981). Alkali promotion of Fe-FT catalysts also inhibits secondary reactions such as oxygenate and olefin re-incorporation and, hence, an increase in oxygenate and olefin content is expected with an increase in alkali content (Claeys and van Steen, 2004). Furthermore, alkali promotion of Fe-FT catalysts is also expected to suppress double bond shift isomerisation, which readily occurs on acidic sites resulting from structural promoters or supports such as silica and alumina, as the presence of alkali lowers the acidity of the catalyst. Consequently, higher contents of α-olefins can be obtained with alkali-promoted Fe-FT catalysts (Claeys and van Steen, 2004).

Despite the advantages of alkali promotion, overdosing the Fe-FT catalyst with alkali is known to reduce catalyst activity, although reasons vary. Some authors claim alkali promotion increases the intrinsic rate of carbon deposition leading to the formation of inactive carbon covering the active sites (Dry, 1981; Arakwa and Bell, 1983). Others claim that the decline in activity is probably due to the blockage of the active iron sites with alkali (van Steen and Claeys, 2008). The decline in catalyst activity with high levels of alkali could also possibly be due to increased diffusion limitations in the porous catalyst – increasing alkali leading to longer-chained products that are more viscous and 'block' feed access to catalyst sites (Dry, 2004b).

The probability of chain growth increases with alkali promotion in the order lithium, sodium, potassium and rubidium, but owing to the high price of rubidium, potassium salts are generally used in practise (Dry, 2002). Co-FT catalysts are less influenced by the presence of chemical or structural promoters (Dry, 2002).

2.1.7 Deactivation of the Fe-FT catalyst

The reason for the loss in the activity of the Fe-FT catalyst and shift in the selectivity towards lower molecular weight products with time-on-stream during the HTFT synthesis is not apparent, although the formation of coke-precursors in the form of aromatics, the Boudouard reaction and the loss of fine catalyst particles have been proposed as possible reasons (Dry, 1990).

The HTFT process in known to produce aromatics and thus there is a possibility that poly-aromatic coke deposits are present, which would cover the active surface sites of the Fe-FT catalyst and, in the process, contribute to the observed loss of the Fe-FT activity (Dry, 1990).

During the HTFT process, the Boudouard reaction readily occurs, resulting in the deposition of elemental carbon on the Fe-FT catalyst at a fairly constant rate throughout the run. However, carbon deposition is not considered to be directly responsible for the decline in activity since the observed decline is quite small (Dry, 2004b). Nonetheless, carbon deposition could have an indirect influence on the loss of activity, since the formation of elemental carbon on the Fe-FT catalyst lowers the density of the catalyst with the possible formation of catalyst fines. In high-gas velocity fluidized beds, the vigorous movement of catalyst particles causes scouring of the carbon rich carbide outer layers of the catalyst particles and could also possibly lead to attrition of the catalyst. Since these small particles have low densities (due to the high free carbon content), they pass through the cyclones and are lost from the reactor, which could be the cause of the observed decline in activity (Dry, 2004b).

2.2 Zeolites

Zeolites have found extensive use in industrial acid-catalyzed processes, as the concentration and strength of the acid sites are controllable. They have also been utilised as supports due to their

molecular sieve and shape-selective character, where their microporous character allows only certain hydrocarbons to enter and leave the zeolite's pore structure, based on molecular size. Zeolites can generally be categorized into 1-, 2- and 3- dimensional pore structures: pathways that are parallel and without cross-section, interconnected channels in 2-dimensional and 3-dimensional patterns. The channel systems are further divided into 8-, 10- and 12- membered ring structures known as small (usually < 5Å), medium and large pore catalysts (Haag et al., 1987; Maxwell et al., 2001).

2.2.1 Acidity and stability

Zeolites are tetrahedrally bound silicon and aluminium ions, which are present within the crystal lattice with interconnecting oxygen ions. Since silicon is tetravalent while aluminium is trivalent, charge compensation at aluminium sites is required in the extended crystalline aluminosilicate network, and this is achieved by the presence of a cation such as NH_4^+ in the vicinity of aluminium. Upon calcination, the ammonium form is transformed to the hydrogen form, or H-zeolite, with the release of ammonia (Rao and Gormley, 1980). The resulting hydroxyl groups (where the hydrogen ion is a delocalised extra framework ion), linking a silicon atom with an aluminium atom in the framework of aluminosilicate zeolites, are responsible for the Bronstead acidity and the catalytic activity, while the oxo-ligands of aluminium that is in interaction with the hydroxyl groups are the corresponding Lewis bases (Figure 2.3). The interaction of the oxygen atom of the hydroxyl group with the aluminium atom leads to the weakening of the hydrogen-oxygen bond, increasing the acidity of that hydrogen atom as well as the basicity of the oxo-ligands of aluminium (Martens and Jacobs, 1997). Therefore, the number of acid sites increases with a decreasing silica/alumina ratio (due to the larger content of aluminium atoms). The strength of each acid site, however, is known to decrease with an increase in the aluminium content (Rastelli et al., 1982; Barthomeuf, 1987).

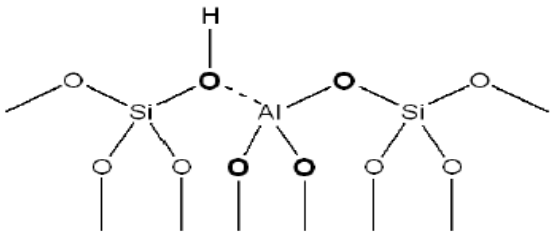

Figure 2.3: Bronstead acid and Lewis base sites for aluminosilicate zeolites (Martens and Jacobs, 1997)

A study carried out by Rastelli et al. (1982) shows the relationship between zeolites (at particular silica/alumina ratios) and their corresponding overall observed zeolite activities (determined by both acid site number and individual strength). From the authors results, at low silica/alumina ratios (ca. below 3.6), the overall observed zeolite activity appeared to decrease with an increase in aluminium, suggesting the dominant factor to be acid site strength. At higher silica/alumina ratios (substantially greater than 8), the overall observed zeolite activity increased with an increase in aluminium content and, hence, the dominant factor was the number of acid sites. Barthomeuf (1987) investigated the effects of varying the aluminium content on specific zeolites and observed similar trends to that of Rastelli et al. (1982). In general, the author observed a maximum point of catalytic activity and effective acidity as a function of silica/alumina ratio for most zeolites tested. Below these maxima (silica/alumina ratios of between 5 and 10), the catalytic activity and effective acidity decreased with an increase in aluminium content, presumably due to the interaction between the aluminium atoms. Above these maxima, at lower aluminium content, the catalytic activity and effective acidity decreased with a decrease in the aluminium content. Therefore, above the maxima, the acid strength of the sites was considered to be independent of the silica/alumina ratio.

A further influence of silica/alumina ratio is the increasing thermal stability, which is observed with increasing silica/alumina ratio. This is because the silicon-oxygen bond has a larger bond strength than the aluminium-oxygen bond, making silica-rich zeolites more stable.

2.2.2 Acid-catalyzed reactions

Primary reactions occurring over a zeolite catalyst in a combined FT catalyst/zeolite process can be briefly summarized as follows (Varma et al., 1986):

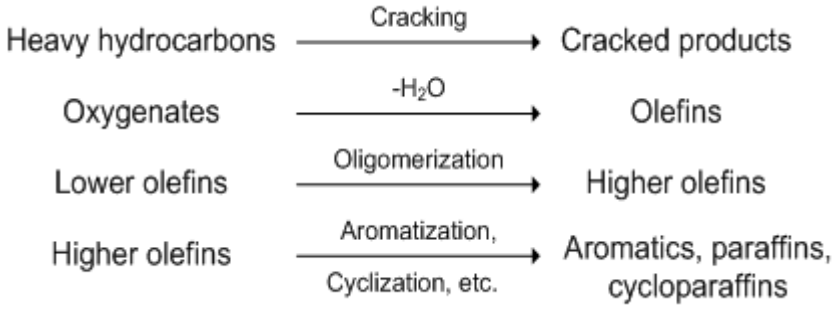

The oligomerization of light olefins over a zeolite is catalyzed by its acid function and will result in longer chain olefins. Olefins are very reactive over an acidic zeolite catalyst due to the double bond, which is easily protonated by the strong Bronstead acid sites to form a carbenium ion (Varma et al., 1987). The suggested oligomerization reaction mechanism, starting from ethylene as an example, is as follows (Udaya et al., 1990):

$$CH_2 = CH_2 + HZ \Leftrightarrow CH_3 - \overset{+}{C}H_2 + \overset{-}{Z} \tag{2.10}$$

$$CH_3 - \overset{+}{C}H_2 + CH_2 = CH_2 \Leftrightarrow CH_3 - CH_2 - CH_2 - \overset{+}{C}H_2 \rightarrow CH_3 - CH_2 - \overset{+}{C}H - CH_3 \tag{2.11}$$

$$CH_3 - CH_2 - \overset{+}{C}H - CH_3 + CH_2 = CH_2 \Leftrightarrow C_6\overset{+}{H}_{13}(etc.) \tag{2.12}$$

$$C_6\overset{+}{H}_{13} + \overset{-}{Z} \Leftrightarrow C_6H_{12} + HZ \tag{2.13}$$

Analogous mechanisms can be written for the oligomerization of other light olefins such as propene and butene. The latter are more abundant than ethene in the FT product stream and react more readily over ZSM-5 than ethene (Varma et al., 1987, Udaya et al., 1990).

The cracking of heavy olefins, by means of ß-scission, also takes place on the acid sites and results in the formation of two olefins. Long chain paraffins are also readily cracked over the zeolite to yield a mixture of lighter olefins and paraffins (Botes, 2002). However, hydrocarbons below C_6 are less readily cracked due to the formation of primary and/or secondary carbenium ions, whereas longer chain hydrocarbons are able to form tertiary carbenium ions.

Oligomerization and cracking reactions involve the carbenium ion mechanism and, hence, a preference for the formation of tertiary carbenium ions due to their high stability. Furthermore, the isomerization of hydrocarbons is a fast reaction in the presence of an acid catalyst and tends to occur via the most stable carbenium ion, resulting in an increase in branched hydrocarbon products. Double bond isomerization of olefins also occurs rapidly over acid catalysts, as the positive charge from a carbenium ion quickly migrates from one carbon atom to another by means of H-shift. Hence, if the carbenium ion is deprotonated, an olefin with the double bond in an internal position is most likely to be formed. Paraffins are significantly less reactive over zeolites than olefins, because the carbenium ions form by means of hydride transfer either to a Lewis acid site on the zeolite or to another carbenium ion (Gates et al., 1979; Botes, 2002).

The oligomerization of lighter olefins can be followed by aromatization that occurs through cyclization and hydrogen transfer reactions. The olefin oligomers are converted to dienes and the dienes are converted to cyclic alkenes, which are subsequently converted to cyclic di-alkenes. Successive abstraction of protons and hydride ions then results in the formation of an aromatic ring (Vedrine et al., 1980). The protons and hydride ions released, during the formation of aromatic rings, are transferred to other olefins to form paraffins. The key step of the aromatization mechanism is suggested to be the hydride transfer between a carbenium ion and a

hydrocarbon (Nenitzescu, 1968). Aromatization occurs under more severe conditions of reaction than those required for olefin oligomerization (Udaya et al., 1990).

2.2.3 Size and shape selective effects

Csicsery (1986) distinguished three types of shape selectivity due to varying size and shape of pores, cages and pore volumes of the intracrystalline zeolite phase (Jacobs and Martens, 1991). However, some catalytic sites also occur on the external surface and pore mouths of zeolite crystals, which can participate in acid-catalyzed reactions and, hence, also affect the nature of the products formed to a certain extent.

Reactant shape-selectivity takes place when some of the reactant molecules are too large or bulky to enter the zeolite pores. An example of reactant shape-selectivity is illustrated in Figure 2.4, where the diffusion and further cracking of 1-methylhexane is restricted as compared to n-heptane.

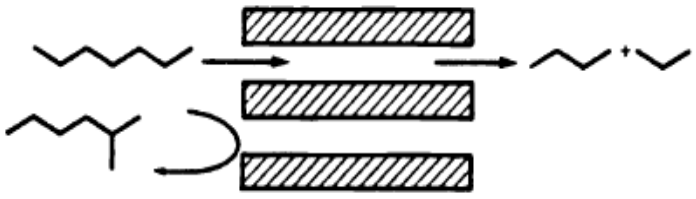

Figure 2.4: Example of reactant shape-selectivity (Csiscery, 1986)

Product shape-selectivity occurs when products formed within the wider sections of the pores (such as the channel intersections of ZSM-5) are too bulky to diffuse out of the narrower channels and eventually deactivate the catalyst by blocking the pores if they are not converted (for example by equilibration or cracking) to less bulky molecules (Csicsery, 1986). Equilibration occurs due to an increase in the local concentration of the more bulky products

within the channels as the less bulky products diffuse out of the pores, resulting in an equilibrium shift towards the less bulky products. This occurrence would force the more bulky products to isomerize into molecules that are more compact and which can diffuse out of the channels as illustrated in Figure 2.5. However, the more bulky products may still form with impunity on the external surfaces of ZSM-5 and other medium pore zeolite crystals.

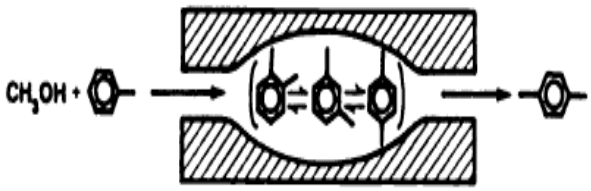

Figure 2.5: Example of product shape-selectivity (Csicsery, 1986)

Transition-state shape-selectivity occurs when certain reactions are prevented because the corresponding transition states are restricted due to spatial constraints within the pores (Csicsery, 1986). An example of transition-state shape-selectivity is illustrated in Figure 2.6, where symmetrical tri-alkylbenzene cannot form directly in H-mordenite because there is not enough space for their bulky transition states, whereas the other tri-alkylbenzenes can form as their transition states are smaller.

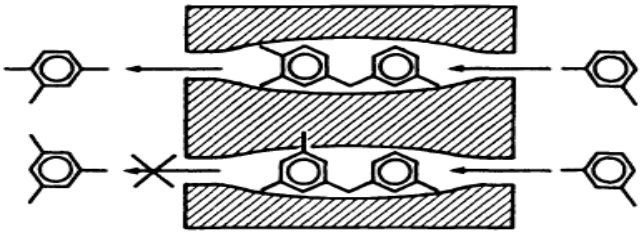

Figure 2.6: Example of transition-state shape-selectivity (Csicsery, 1986)

2.2.4 ZSM-5

ZSM-5 is generally the preferred zeolite for the production of high-octane gasoline for the following summarized reasons (Polinski et al., 1984; Udaya et al., 1990):

- The medium pore opening (5.5 Å) provides a shape-selective effect, minimizing the formation of product molecules higher than C_{10}, which coincides with the upper limit of the gasoline boiling range.

- The highly acidic nature of HZSM-5 helps catalyze oligomerization, cracking, isomerization and aromatization reactions.

- ZSM-5 limits the formation of coke precursors due to its medium pore size. Since bimolecular reactions (such as condensation and hydrogen transfer) between bulky molecules occur with zeolites, steric constraints limit the formation of large coke molecules within the zeolite pores (Guisnet and Magnoux, 1997). Therefore, the selectivity towards coke is expected to decrease with decreasing zeolite pore sizes as was observed by Rollmann and Walsh (1979). Nonetheless, Guisnet and Magnoux (1989) observed a higher coke selectivity for a smaller pore zeolite (ERI) than ZSM-5, despite both the three-dimensional channel structured zeolites being prepared such that they had a similar degree of protonic exchange. This increase in coke selectivity was attributed to the trap cavities (i.e. large cavities with small pore apertures) of ERI that resulted in a rapid blockage of the cavities by coke precursors (Guisnet and Magnoux, 1997; Guisnet et al., 2009).

- ZSM-5 is hydrothermally stable and resistant to dealumination under typical FT conditions.

2.2.4.1 Structure

ZSM-5 exhibits a three-dimensional pore structure consisting of a set of straight 10-member ring pores measuring 5.1 x 5.5 Å, intersecting perpendicularly with a set of sinusoidal 10-member ring pores of 5.3 x 5.6 Å, as illustrated in Figure 2.7. Therefore, the cavities created by the channel intersections are approximately 9 Å at their widest point (van Bekkum et al., 2001).

2.2.4.1 ZSM-5 size and shape-selective effects

The shape-selectivity and high acidity of the HZSM-5 zeolite results in a sharp cut-off of the product spectrum at around C_{11} and also results in a highly aromatic and branched hydrocarbon product distribution as was observed by numerous authors (Chang and Lang, 1978; Caesar et al., 1979; Rao and Gormley, 1980; Brennan et al., 1981; Butter et al., 1981; Dwyer and Garwood, 1982; Varma et al., 1987; Schulz et al., 1991a; Botes and Böhringer, 2004; Botes, 2005; Martinez and Lopez, 2005; Pour et al., 2008a).

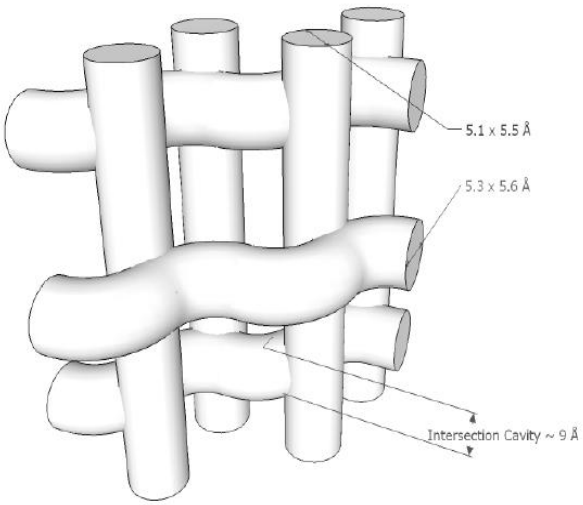

Figure 2.7: Three-dimensional representation of ZSM-5 pore structure with pore dimensions (IZA, 2002)

The ZSM-5 pore diameter of 5.5 Å coupled with the propensity for light alkene oligomerization and cracking of longer chain aliphatics limits the hydrocarbon molecules to the range of C_5-C_{11}, nearly coinciding with the gasoline boiling range. Rao and Gormley (1980) stated that the cracking of heavier molecules could also take place at the acid sites on the external surface of the ZSM-5 crystallites, since the diffusion of reactant molecules larger than C_{11} (especially species other than straight chain paraffins) into the zeolite pores is severely hindered. Fraenkel (1984) subsequently proposed that ZSM-5 has two types of catalytic sites, the first type is located inside the crystals and the second type, which resides on the external surface of the zeolite, is not shape-selective, thus leading to the formation of aromatics above C_{11}.

2.3 Combined Fe-FT/HZSM-5 Fischer-Tropsch Processing

2.3.1 Catalyst bed configurations

A variety of Fe-FT/HZSM-5 catalyst combinations have been employed for the combined FT synthesis and can be generalized as follows:

- Physical contact: physical mixture of the two catalysts (with or without binders), impregnation of the zeolite in an aqueous metal solution, direct decomposition of an organometallic compound on the zeolite and/or pressing the two catalysts into pellets.
- Non-physical contact: the two catalysts placed either in sequential beds in the same reactor (dual-bed arrangement or ‘sandwich’ like arrangement) or in different reactors (dual-reactor arrangement).

2.3.1.1 Physical contact

Chang and Lang (1978) made the first mention of an Fe-FT catalyst mixed with HZSM-5, where different forms of catalyst intimacy were tested: impregnation of the zeolite into an aqueous metal solution after which it was dried and calcined; pelletizing a ball-milled Fe-FT and HZSM-5 mixture; and a physical mixture of the two catalysts. For all the aforementioned catalysts, a significant amount of aromatics was formed as compared to the Fe-FT experiment (experimental run with only the Fe-FT catalyst), but due to the very high synthesis temperature (370^oC), CH_4 selectivities of over 30% were obtained. Caeser et al. (1979) investigated the effect of a potassium-promoted Fe-FT/HZSM-5 composite catalyst at lower synthesis temperatures of about 330^oC. Their results showed a sharp cut-off at C_{11}, a highly aromatic and branched product spectrum and a C_{5+} yield (in the total hydrocarbon product) in excess of 50 wt-% as compared to 6 wt-% obtained by Chang and Lang (1978) in their experiment with the Fe-FT/HZSM-5 composite catalyst at 370^oC. However, Butter et al. (1981) claimed that the use of promoters in Fe-FT catalysts was not desired since most promoters are alkaline in nature and have the tendency to migrate to the acidic crystalline aluminosilicate zeolite. The authors then went on to suggest that alkali promoters might not be necessary for sustained operations in a combined process and, if anything, they are detrimental to the activity of the zeolite. To verify their claim, the authors tested an unpromoted Fe-FT/HZSM-5 composite catalyst at temperatures and pressures ranging from about 288 – 304^oC and 10 – 27 bar, respectively. The results did seem comparable to a promoted Fe-FT catalyst as the authors obtained a $CH_4 + C_2H_6$ composition of less then 20 wt-% of the total hydrocarbon fraction. However, during catalyst preparation, significant amounts of sodium silicate and sodium zirconium were added to prepare a gel in which Fe-FT and HZSM-5 were mixed, with the resulting gel-like mixture homogenized, NH_4^+ exchanged, washed and dried – a process which conceivably could have led to a significant alkali promotion of the Fe-FT catalyst by sodium (Botes and Böhringer, 2004).

Shamsi et al. (1986) investigated the influence of preparative procedures on the activity and selectivity of an Fe-FT/ZSM-5 composite catalyst. The catalyst preparations consisted of:

- The direct decomposition of $(C_5H_5Fe(CO)_2)_2$ on ZSM-5.
- Impregnation of ZSM-5 with an aqueous solution of iron nitrate.
- Physical mixture of precipitated iron oxide with HZSM-5.

The organometallic ($(C_5H_5Fe(CO)_2)_2$) impregnated catalyst resulted in increased metal dispersion in comparison to catalysts prepared by nitrate impregnation or when the two catalysts were physically mixed. Consequently, the organometallic-impregnated catalyst had the slightly higher CO and H_2 conversion but exhibited the lowest selectivity to aromatics, with the physically mixed catalyst exhibiting the highest aromatic selectivity. In the case of the catalyst prepared by aqueous impregnation, there were indications of Fe^{n+} exchange for acidic protons, which affects both catalytic functions of the combined Fe-FT/HZSM-5 process since the non-reducible metal species that are formed after ion exchange are not active for syngas conversion and the acidity of the zeolite is reduced. The number of Bronstead acid sites per gram of catalyst (N_B) and the number of surface iron sites per gram of catalyst (Fe_s) was calculated. The highest value of N_B/Fe_s was obtained for the physically mixed catalyst.

Schulz et al. (1991a) investigated the use of a potassium-promoted Fe-FT/HZSM-5 composite catalyst at 325^{o}C, but at a low H_2/CO ratio of 0.66. The composite catalyst was prepared by mixing the powders of HZSM-5 and the Fe-FT catalyst into an aluminium hydroxide gel, which was then dried, ground and sieved. The authors observed a stable CO conversion (Fe-FT activity) with time-on-stream and a rapid initial increase in the CH_4 selectivity followed by a very slight and gradual increase with time-on-stream. Furthermore, the addition of HZSM-5 to the Fe-FT catalyst, as anticipated, resulted in a higher gasoline selectivity and a more branched and aromatic product spectrum in comparison to the Fe-FT experiment.

Botes and Böhringer (2004) studied the effect of physically mixing the alkali-promoted Fe-FT catalyst with HZSM-5 powder at 330^{o}C and 20 bar. The authors observed a significant decrease in the CO conversion and a substantial increase in the CH_4 selectivity with time-on-stream.

This was claimed to be as a result of extensive alkali migration from the Fe-FT catalyst to the zeolite. The shift towards lighter paraffins was so severe that the commercial viability of physically mixing the two catalysts was questioned.

2.3.1.2 Non-physical contact

Dual-bed arrangement

Brennan et al. (1981) mixed a potassium-promoted Fe-FT catalyst (0.4 cc) with a partially poisoned K-ZSM-5 (1.6 cc) zeolite in the first bed and HZSM-5 (2 cc) in the second bed. The two beds were separated with quartz and a screen. The authors observed a stable Fe-FT activity and C_1 selectivity with time-on-stream, but the zeolite appeared to have deactivated considerably as the aromatics content (in the C_{6+} hydrocarbons) reduced from 53 wt-% initially to 19 wt-% after 7 days on-stream. The experiment was repeated with a similar setup and conditions with the exception that the K-ZSM-5 used in the first bed was replaced by gamma alumina, resulting in a decrease of the aromatics yield by approximately 10 wt-%. The authors concluded that it was more advantageous to have some zeolite in the first bed as well, since it scavenges olefins before they can grow into wax.

Botes and Böhringer (2004) investigated the effect of separating the two catalysts on the gasoline selectivity in a Berty reactor under typical high temperature FT conditions, where contact was avoided by means of a wire mesh. The authors obtained a significantly higher gasoline selectivity and highly aromatic and branched product spectrum over the low acidity HZSM-5 (silica/alumina molar ratio of 280) for the combined Fe-FT/HZSM-5 experiment as compared to the Fe-FT experiment. The authors observed similar CH_4 selectivities for both the Fe-FT and combined Fe-FT/HZSM-5 experiments and, therefore, the authors concluded that there was no or very little alkali migration occurring when the two catalysts were separated.

Dual-reactor arrangement

The main advantages of the dual-reactor arrangement are as follows (Varma et al., 1987):

- Considerable flexibility with respect to both reaction conditions as well as product distributions.
- Operation of each component at its optimum reaction conditions.
- Easier regeneration and replacement of the spent catalyst.

The main drawback with a dual-reactor arrangement is the significant increase in capital and operating costs.

2.3.2 Product selectivity

As discussed earlier, the addition of HZSM-5 to the FT process has generally been observed to increase the gasoline selectivity and produce a highly aromatic and branched hydrocarbon product (Chang and Lang, 1978; Caesar et al., 1979; Rao and Gormley, 1980; Brennan et al., 1981; Butter et al., 1981; Dwyer and Garwood, 1982; Varma et al., 1986; Varma et al., 1987; Schulz et al., 1991a; Botes and Böhringer, 2004; Botes, 2005; Martinez and Lopez, 2005; Pour et al., 2008a; Pour et al., 2009).

Schulz et al. (1991a) and Botes and Böhringer (2004) observed two major differences in the form of enhanced concentrations of certain fractions in the product distribution of the combined Fe-FT/HZSM-5 experiment as compared to the Fe-FT experiment. The first product enhancement was at around C_4 and comprised mainly of iso-butane. Botes and Böhringer (2004) reasoned that the longer aliphatics are not stable in the presence of an active acid catalyst under the prevailing conditions and, therefore, can readily be cracked down to lighter olefins and paraffins – the iso-butane and iso-butene being the preferred products, but with iso-butene subsequently converted to iso-butane through proton and hydride ion transfer during the

formation of aromatics. The second product enhancement was observed at C_8 and this was attributed to the favoured formation of C_8 aromatics and naphthenes over HZSM-5. They also observed a sharp cut-off in the product spectrum around C_{11} and argued that this was due to long chain aliphatics not being stable at the high temperatures used in the HTFT process and thus are readily cracked over the zeolite, while aromatics higher than C_{11} are too large to be formed readily inside the pores of HZSM-5.

A summary of the results obtained by Botes and Böhringer (2004) for the different catalysts and catalyst combinations tested are presented in Table 2.3, although the authors indicated the possibility of errors in the CH_4 selectivities and CO conversions obtained.

Table 2.3: Summarized results obtained in a Berty reactor at 330°C and 20 bar after 3 days on-stream (Botes and Böhringer, 2004)

	Baseline FT	**Physically admixed**	**Dual layers**	
	Fe-FT	*Fe-FT/HZSM-5 (30*)*	*Fe-FT/HZSM-5 (280*)*	*Fe-FT/HZSM-5 (30*)*
CO conversion (%)	77	68	70	53
($CO+CO_2$) conversion (%)	39	31	37	29
CH_4 selectivity$^+$	18	38	15	17
Gasoline (C_5-C_{11}) selectivity$^+$	36	31	52	50
C_{12+} selectivity$^+$	2	0	0	0
Aromatics selectivity$^+$	1	6	14	17

* Silica/alumina molar ratio; $^+$ C-%

2.3.3 Deactivation

2.3.3.1 Deactivation of the Fe-FT catalyst component

In the combined Fe-FT/HZSM-5 process (with physical contact between the two catalysts), a more rapid loss in the activity and/or selectivity of the Fe-FT catalyst with the addition of the HZSM-5 zeolite was observed by various authors (Schulz et al., 1991a;

Botes and Böhringer, 2004; Botes, 2005; Pour et al., 2008a; Pour et al., 2009). Some authors stated or claimed that the more rapid loss of activity and selectivity of the Fe-FT catalyst is due to the potassium migrating away from the Fe-FT catalyst and to the HZSM-5 zeolite (Butter et al., 1981; Udaya et al., 1990; Botes and Böhringer, 2004; Botes, 2005; Pour et al., 2008a; Gwagwa and van Steen, 2009). The possible effects alkali migration would have on the Fe-FT activity and selectivity for the combined Fe-FT/HZSM-5 process are:

- A decrease in the CO conversion and a shift towards a lighter FT product spectrum, with a simultaneous increase in the CH_4 selectivity.
- A decrease in the selectivity and quality of gasoline produced. The loss of alkali from the Fe-FT catalyst would result in an increase in the paraffin/olefin ratio. Whereas, the longer chain paraffins easily crack over the zeolite to form lighter paraffins and olefins under the HTFT conditions, the lighter paraffins do not readily participate in oligomerization and subsequent aromatization reactions over the zeolite and, consequently, the final gasoline selectivity and quality would reduce.

Schulz et al. (1991a) in their study, however, observed a rapid initial increase in the CH_4 selectivity, but after oxidative regeneration of the Fe-FT/HZSM-5 composite catalyst, the CH_4 selectivity of the regenerated catalyst was much lower than that observed at the end of test with the fresh catalyst, hence, suggesting that alkali migration was not the cause of the more rapid loss of the Fe-FT activity and selectivity with the addition of HZSM-5 to the Fe-FT process

2.3.3.2 Deactivation of the acid catalyst function

The zeolite activity is generally represented by its ability to carry out acid-catalyzed reactions and since aromatization is the most demanding of the acid-catalyzed reactions, the amount of aromatics formed would be the best representative of the zeolite's activity with time-on-stream. Studies carried out by Schulz et al. (1991a), Botes and Böhringer (2004), Martinez and Lopez (2005) and Pour et al. (2008a) show that the zeolite deactivates most rapidly

in the initial period of synthesis time for the combined Fe-FT/HZSM-5 process, after which there is a gradual decrease and, in some cases, even an apparent stabilization. Deactivation and deterioration of the zeolite acidity in a combined Fe-FT/HZSM-5 process can be due to the following reasons (Butter et al., 1981; Udaya et al., 1990; Pour et al., 2008a):

- Coke formation on the zeolite.
- Dealumination of zeolite crystals.
- Poisoning of the zeolite's acid sites by alkali.

The extent to which the above-mentioned phenomena contribute to zeolite deactivation is not clear, but since ZSM-5 is assumed to be resistant to dealumination under typical FT conditions (Polinski et al., 1984; Udaya et al., 1990), it would appear that alkali poisoning and/or coking of the zeolite are the most significant contributors to the zeolite deactivation.

Coke formation on the zeolite

The rapid formation of coke on acid catalysts occurs via certain molecules that can be considered as coke-precursors. Typical coke-precursors include olefins (alkenes and dienes) and polyaromatics. Olefins undergo very fast condensation reactions (oligomerization, polymerization) on acid catalysts resulting in heavy and polar products that can easily be retained on the zeolite. Moreover, these products are reactive enough to undergo monomolecular reactions (such as cyclization) and biomolecular reactions (such as hydrogen transfer), leading then to coke molecules (Guisnet and Magnoux, 1997; Guisnet et al., 2009). In the case of polyaromatics, their strong adsorption on the acid sites due to their bulkiness and polarity (basicity) favours their conversion into heavier molecules that cannot desorb and thus remain within the pores and/or on the outer surface of the zeolite. The retention of coke molecules within the pores of the zeolite mainly occurs due to: steric constraints (trapping of coke molecules in the cavities or channel intersections); strong chemisorption of coke molecules

on active sites and their subsequent confinement within the zeolite pores; and/or solubility (liquid phase reaction) or low volatility (gas phase reaction) of the coke molecules under the operating conditions. Coke retention on the outer surface of the zeolite crystals is usually due to the low volatility (or solubility) of the coke molecules (Guisnet and Magnoux, 1997; Guisnet et al., 2009).

Deactivation of zeolites due to coking would generally occur by poisoning (or coverage) of the active sites and/or by pore blockage (Guisnet et al., 2009). For a three-dimensional zeolite with no trap cavities (i.e. large cavities with small pore apertures) such as HZSM-5, the possible restriction of reactants to the active sites within the zeolite pores by coke-precursors is illustrated in Figure 2.8.

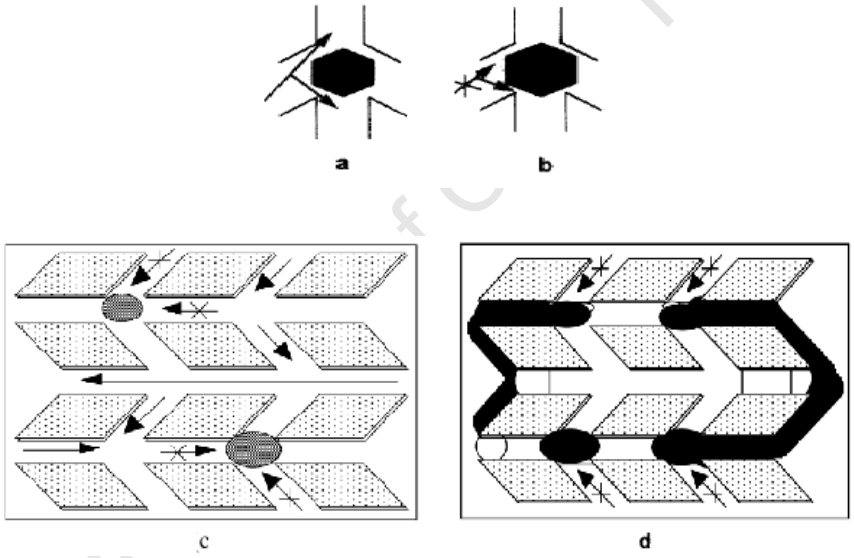

Figure 2.8: Restriction of reactants to the active sites within the pores of a zeolite with interconnecting channels and without trap cavities e.g. HZSM-5; Modes (a, b and c) – site coverage, Mode (d) – pore blockage (Guisnet and Magnoux, 1997; Guisnet et al., 2009)

In modes a, b and c (Figures 2.8a, b and c), the diffusion of reactants to the active site in the cavity is limited or blocked. These restrictions can occur either for steric reasons (a larger

molecule than the pore diameter can form on the cavity intersections) or for chemical reasons (coke molecules are reversibly or quasi-irreversibly adsorbed on the acid sites). Deactivation through these modes is generally limited since only the acid sites on the cavity intersection (often only one site) are partially or totally deactivated (Guisnet and Magnoux, 1997). Mode d (Figure 2.8b) is referred to as pore blockage, as the coke-precursors block or limit access of reactants to the cavities and parts of channels in which coke molecules are not located. Deactivation through this mode is more profound although it mainly appears at high coke contents (Guisnet and Magnoux, 1997), as the reactant would still have access to the active sites through various channels at low coke contents.

Guisnet and Magnoux (1989) examined the occurrence of the different modes of deactivation relative to the C_k/C_{Af} (the ratio between the concentration of coke molecules and active sites of the fresh zeolite) for n-heptane cracking over HZSM-5 at 450^{o}C. It has to be noted that the authors assumed all the active sites had a similar activity and strength, which might not necessarily be the case. At low coke contents ($C_k/C_{Af} < 0.25$), there appeared to be no pore blockage and the slight decrease in activity was attributed to some coke molecules adsorbing onto the protonic sites, as the coke molecules produced in this mode were weakly basic. At medium coke contents, ($0.25 < C_k/C_{Af} < 0.8$), the deactivation appeared to occur by site poisoning and by coke molecules blocking access of adsorbates through a few channel intersections, but with the adsorbates still having access through other channel intersections (Figure 2.8c). At high concentration of coke molecules ($C_k/C_{Af} > 0.8$), the deactivation mainly appeared to be as a result of pore blockage by very bulky molecules overflowing onto the crystal outer surface and/or blockage of channel intersections as illustrated in Figure 2.8d (Guisnet and Magnoux, 2009). Therefore, for HZSM-5, deactivation caused at low coke contents by site poisoning progressively evolves to pore blockage with an increase in coke content (Guisnet and Magnoux, 2009).

Poisoning of the zeolite's acid sites by alkali

The poisoning of the zeolite's acid sites by alkali occurs through the possible migration of alkali promoters from the Fe-FT catalyst to the zeolite co-catalyst in a combined Fe-FT/HZSM-5 process. Butter et al. (1981) mentioned that the use of promoters in Fe-FT catalysts was not preferred since most promoters are alkaline in nature and they have the tendency to migrate to the acidic crystalline aluminosilicate zeolite. Further authors have since claimed that the alkali promoters do migrate from the Fe-FT catalyst to the acid co-catalyst, neutralizing the zeolite's acid sites in the process (Udaya et al., 1990; Botes and Böhringer, 2004; Botes, 2005; Pour et al., 2008a).

Schulz et al. (1991a) observed a rapid initial decrease in the aromatics selectivity, but after regeneration of the Fe-FT/HZSM-5 composite catalyst, the activity could almost be fully restored after burning off any graphitic carbon, coke or organic compounds at temperatures of up to 600^{o}C. This observation suggests that the neutralization of the HZSM-5 acid sites by alkali did not have any significant affect on the overall deactivation of the zeolite. However, this was probably because of the high HZSM-5/Fe-FT ratios (ca. 13/1) used by the authors and thus the amount of potassium that could potentially migrate to HZSM-5 would not have a significant effect on the overall deactivation of the zeolite.

A study by Gwagwa and van Steen (2009) investigated the migration of potassium in pellets originally containing K-Fe_2O_3 (6.7g K_20/100g Fe) and HZSM-5 (silica/alumina molar ratio of 80). The study was carried out while heating the pellets at 350^{o}C in air for a number of days. It was observed that after an extensive period of time (equilibrium), about 20% of the potassium migrated to the HZSM-5 zeolite, neutralizing about 50% of the acid sites in the process. However, the Fe-FT catalyst used by the authors had a high alkali loading, which would mean more alkali available for poisoning of the zeolite sites.

The effect alkali migration would have on the zeolite deactivation depends on various factors including the potassium loading of the Fe-FT catalyst, the acidity of the zeolite, the amount of

zeolite used relative to the Fe-FT catalyst and the extent of contact between the two catalysts. Table 2.4 shows the affect some of the aforementioned factors would have on the poisoning of the zeolite sites (see Section 5.5.2 for equations used). As mentioned previously, a lower alkali loading of the Fe-FT catalyst would mean less alkali available for poisoning the acid sites and a higher acidity zeolite would be influenced less by alkali poisoning as there are more acid sites available. An increase in the HZSM-5/Fe-FT ratio would decrease the influence alkali migration would have on the zeolite, since the ratio of alkali atoms to the number of acid sites available would decrease. The extent of contact between the two catalysts is also expected to affect the rate of alkali migrating away from the Fe-FT catalyst and onto the HZSM-5 zeolite. This is presumably because as the intimacy between the two catalysts is increased, the affinity of alkali towards the acid sites of HZSM-5 also increases. Therefore, the extent to which alkali migration affects the zeolite activity is not apparent and depends on various factors as mentioned above. However, coking of the HZSM-5 does appear to be a significant contributor to the deactivation of the zeolite as was observed from the studies carried out where the possibility of alkali migration was prevented or minimized (Schulz et al., 1991a; Botes and Böhringer, 2004; Botes, 2005). Schulz et al. (1991a) observed that the HZSM-5 deactivates rapidly despite there being minimal alkali poisoning of the zeolite acid sites since it could almost fully be regenerated after synthesis. Botes and Böhringer (2004) also observed rapid zeolite deactivation despite eliminating or minimizing the possibility of alkali migration by separating the two catalysts.

Table 2.4: Comparison of the number of alkali atoms in the Fe-FT catalyst relative to the number of HZSM-5 acid sites available (Botes and Böhringer, 2004; Gwagwa and van Steen, 2009)

	Botes and Böhringer (2004)[a]		Gwagwa and van Steen (2009)[b]	Current Study[b]
SiO_2 / Al_2O_3 ratio	280	30	80	90
g Alkali / 100 g Fe-FT catalyst	0.12	0.12	3.90	0.30
Acid sites (mmol Al) / g HZSM-5	0.11	1.01	0.39	0.35
Percentage of alkali atoms over acid sites	42	5	253	20

[a]Sodium; [b]Potassium

2.3.4 Process parameters

2.3.4.1 The effect of temperature

For the Fe-FT process, an increase in temperature shifts the product spectrum towards a lighter and less olefinic product spectrum, with an increase in the more thermodynamically favoured products such as CH_4, branched alkanes and aromatics (Dry, 1981).

For the combined Fe-FT/HZSM-5 process, an increase in temperature (more severe conditions) is expected to favour the desired and secondary reactions, including coke formation. These reactions will occur essentially on the outer surface of the zeolite crystals where the trapped coke molecules on the outer surface will block diffusion of the reactant molecules into the zeolite pores (Guisnet et al., 2009). However, decreasing the temperature will enhance the retention of the less volatile components and, therefore, there appears to exist an optimum temperature for hydrocarbon conversion over a HZSM-5 zeolite. This also true in respect of the amount of aromatics formed, as Varma et al. (1987) found that the optimum temperature range is between 275 – 300^{o}C for the formation of aromatics in a dual-reactor arrangement depending on the HZSM-5/Fe-FT ratios used.

Botes (2005) investigated the effect of increasing the operating temperature from 330^{o}C to 350^{o}C on the performance of the combined Fe-FT/HZSM-5 catalyst system. The author observed a significant increase in the CH_4 selectivity and a considerable decrease in the gasoline selectivity with an increase in temperature. At higher temperatures, the HTFT product spectrum shifts towards lighter and more paraffinic hydrocarbons (Dry, 1981), concomitantly resulting in an increase in the CH_4 selectivity and a decrease in the gasoline selectivity.

2.3.4.2 The effect of H_2/CO ratio

For the Fe-FT process, a higher H_2/CO syngas ratio results in a lighter and less olefinic product spectrum, as well as a decrease in the carbon deposition (Dry, 1981). Therefore, it is expected that the gasoline selectivity and octane rating would reduce for a combined Fe-FT/HZSM-5 process with an increase in the H_2/CO ratio, as there will be less olefins for the zeolite to oligomerize and thus a subsequent decrease in the aromatics yield. Moreover, the 'straight-run' gasoline yield from the primary FT reaction will also be less. It is also possible that a higher H_2/CO ratio further inhibits coke formation on zeolites (Horsley, 1993), such that the overall stability of the combined catalyst system is expected to improve with increasing H_2/CO ratios.

2.3.4.3 The effect of the HZSM-5 acidity

As discussed earlier (Section 2.2.1), in the case of ZSM-5, the observed zeolite activity is dependent on both the number of acid sites and the strength of each site up to a silica/alumina ratio of approximately 9.5, after which acidity is dependant on the number of acid sites only (Barthomeuf, 1987). Consequently, for commonly used ZSM-5 (with silica/alumina >> 10), the observed zeolite activity is assumed to be independent of the individual acid strength and solely dependent on the number of acid sites. Increasing the aluminium content would, therefore, result in the reactant molecules undergoing a larger number of successive chemical steps along the diffusion pathway within the zeolite crystallites, so enhancing condensation and biomolecular reactions including coking (Guisnet et al., 2009).

Dwyer and Garwood (1982) showed that the main effect of increasing the silica/alumina ratio in a mixed Fe-FT/ZSM-5 bed was a decrease in the aromatics content. The more acidic ZSM-5 (silica/alumina ratio of 70) yielded 50 wt-% aromatics in the hydrocarbon product as compared to the 14 wt-% aromatics obtained from the less acidic ZSM-5 (silica/alumina ratio of 1600). This relationship was also confirmed by Martinez and Lopez (2005) for four commercial ZSM-5 samples (silica/alumina ratios of 30, 50, 80, and 280) and by Botes and Böhringer (2004)

for two ZSM-5 zeolites (silica/alumina molar ratios of 30 and 280). The initial aromatics yield over ZSM-5 increased with decreasing silica/alumina ratios, but in all cases, this was followed by a rapid decrease in the aromatics content with time-on-stream. However, in the study of Botes and Böhringer (2004), the more acidic HZSM-5 deactivated much faster than the less acidic HZSM-5, to an extent that the performance dropped below that of the low acidic HZSM-5 with time-on-stream. These findings suggest, therefore, that an optimum silica/alumina ratio may be found in respect of gasoline yield and catalyst stability.

2.3.4.4 The effect of HZSM-5 addition

An increase in the HZSM-5/Fe-FT ratio, with all other conditions remaining the same, is presumably expected to have the following effects:

- Decrease any negative influence of potassium migration on the zeolite performance as there are more acid sites available.
- Increase the rate of potassium migration from the Fe-FT catalyst due to the larger potassium sink (more acid centres).
- Increase in contact time with the zeolite catalyst relative to the Fe-FT catalyst, resulting in an increase in the formation of aromatics and other acid-catalyzed reaction products, including aromatic side-chain cleavage, the latter reducing gasoline mass yield. Therefore, there also appears to be an optimum HZSM-5/Fe-FT ratio in terms of aromatics yield, as evidenced by Varma et al. (1987), who observed a maximum selectivity of aromatics for an HZSM-5/Fe-FT ratio of between 2 and 4 (dual-reactor arrangement, 300 – 350^{o}C).

2.4 Internal recycle reactors

Bench-scale reactors are used to study, test and develop catalysts for industrial-scale catalyzed reactions and thus it is desirable to perform such tests under conditions similar to those in commercial operation. The FT reaction is highly exothermic and thus it is imperative that there is efficient heat transfer from the catalyst particles to the surrounding medium to prevent an increase in the selectivity of undesired CH_4 and to minimize the loss of catalyst activity due to sintering and fouling. The Berty reactor is recommended for high temperature FT laboratory studies since the high internal recycle ensures a high-gas velocity through the catalyst bed, as encountered in commercial operation. The high-gas velocity and recycle ensure sufficiently long per pass conversions and, consequently, a gradientless reaction zone in respect of concentration and temperature. Even so, overall conversion levels can be varied by altering the fresh feed flow rate (Berty, 1984; Dry, 2008; Brosius and Fletcher, 2010).

Recycle reactors fall in the class of Continuously Stirred Rank Reactors (CSTR) and at recycle ratios greater than 20, they behave as a perfectly mixed CSTR (Berty, 1974). However, different internal recycle reactor embodiments exist, e.g. Carberry reactors (Carberry et al., 1980), Jet Loop recycle reactors (Schermuly and Luft, 1977) and Berty reactors (Berty, 1974), the latter being the most common configuration.

The Berty reactor is an internal recycle reactor with an impeller positioned below the catalyst bed to drive gas flow through the catalyst bed and to recirculate it through the internal gas flow path as shown in Figure 2.9. A common operational problem with the Berty reactors is the accumulation of catalyst particles and heavier hydrocarbons in the bearings of the impeller shaft that ultimately lead to mechanical problems and magnedrive failure. To avoid this problem, a ‘modified’ Berty reactor referred to as the Stirred from Top Internal Recycle Reactor (STIRR), was applied in this study. The STIRR is similar in design to the Berty reactor, with the key difference being that the impeller is positioned on the top of the reactor, above the catalyst bed,

as shown in Figure 2.10. This positioning prevents the accumulation of products and catalyst particles in the magnedrive bearing and has been shown to allow extended operation without mechanical failure.

In the STIRR, the impeller is driven in an anti-clockwise direction so that there is a high-pressure zone created just below the impeller and above the catalyst bed, effectively inducing a downward flow through the catalyst bed and around the internal recirculation path. A detailed characterization of the STIRR used in this study has been presented elsewhere (Brosius and Fletcher, 2010).

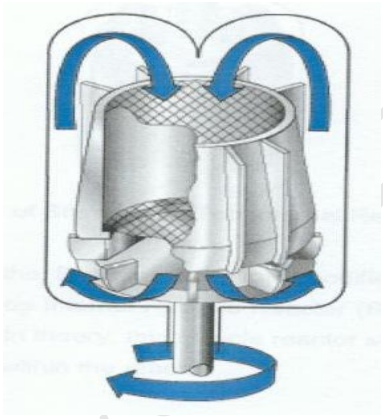

Figure 2.9: Internal view of Berty reactor

Figure 2.10: Internal view of the Stirred from Top Internal Recycle Reactor (STIRR)

3 SUMMARY OF FINDINGS FROM LITERATURE

The demand for high-quality fuels (most noticeably for transport) is of significant importance in the current global energy crisis. The production of gasoline from conventional crude oil appears to have become problematic with the continuous exhaustion of crude oil reserves and the difficulties in meeting the required standards of the gasoline quality. An alternative approach is the conversion of coal and natural gas into syngas, which is further converted into naphtha and middle-distillate fuels via the Fischer-Tropsch (FT) process. The FT process, however, is limited as the product distribution is unselective due to the polymerization kinetics governing chain growth, which can, in principle, be circumvented by the addition of a co-catalyst. The modification of the FT process with HZSM-5 as a co-catalyst has shown a lot of promise and consequently, initiated a more profound interest.

HZSM-5 is the preferred choice in the modified FT process for the production of gasoline due to its medium pore openings, minimizing the formation of product molecules above C_{10}, which coincides with the gasoline fraction. Iron is commonly used as the FT catalyst in the zeolite-modified FT process, as temperatures over 300^{o}C are generally required for an active zeolite and at this temperature range, a lower CH_4 selectivity can be obtained with an Fe-FT catalyst as compared to other FT catalysts. Alkali promotion is imperative for an Fe-FT catalyst, as it affects both the activity and selectivity of the Fe-FT catalyst.

The modified FT process has shown a considerable increase in the initial gasoline selectivity and quality with the addition of HZSM-5, but the main drawback is the decline in the catalytic performance of the combined Fe-FT/HZSM-5 catalysts with time-on-stream when the two catalysts are in intimate contact. A more stable catalytic performance is observed when the two catalysts are separated but the possibility of the zeolite being able to scavenge hydrocarbon species growing on the surface of the FT catalyst and/or to intercept desorbed olefins before they

can readsorb onto the metal surface and be hydrogenated, may influence the preferred arrangement of the catalysts in the combined process.

The change in the catalytic performance of the combined Fe-FT/HZSM-5 system has been claimed to be due to alkali migrating from the Fe-FT catalyst to the HZSM-5 zeolite, which would result in a decline in the activity and selectivity of the Fe-FT catalyst and neutralization of the HZSM-5 acid sites. Potassium has been shown to migrate from the Fe-FT catalyst to the HZSM-5 zeolite in ex-reactor tests, but with no conclusive proof of alkali migration occurring under synthesis conditions, this theory remains to be tested. Furthermore, the existence of a relationship between alkali migration and the observed changes in the catalytic performance of the combined Fe-FT/HZSM-5 system also remains to be tested.

4 OBJECTIVES OF THIS STUDY

The improvement of the gasoline quality and selectivity with the addition of HZSM-5 to the Fe-FT process is evident from literature, and such a process is further supported by the demand of high-quality gasoline. The catalytic performance of the combined Fe-FT/HZSM-5 system has, however, been observed to considerably decline with time-on-stream, a phenomenon which has been attributed to the migration of alkali from the Fe-FT catalyst to the HZSM-5 zeolite. There is, however, no conclusive proof that this migration occurs during syngas conversion, nor whether it is the cause of the observed decline in the catalytic performance of the combined Fe-FT/HZSM-5 system with time-on-stream.

The objective of this study, therefore, is to characterize and confirm the reported performance of the Fe-FT and the combined Fe-FT/HZSM-5 catalyst systems in a STIRR under typical high temperature FT conditions. Moreover, this study seeks to establish evidence for the hypothesized migration of potassium from the Fe-FT catalyst to the HZSM-5 zeolite and to determine any relationship that may exist between potassium migration and changes in the observed performance of the combined Fe-FT/HZSM-5 catalyst system under high temperature FT synthesis conditions.

5 EXPERIMENTAL

5.1 Experimental apparatus

Figure 5.1 presents a process flow diagram of the reactor test unit used for catalytic studies. The reactor system consisted of a Stirred from Top Internal Recycle Reactor (STIRR), followed by a backpressure regulator to maintain the pressure of the reactor, and a needle valve to control subtle changes in flow at high pressures. The product gas passed through an automated six-port valve, where the product gas was sampled for GC-FID analysis with the remainder passing to the GC-TCD via room temperature and cold catch pots. A description of the major components of the system is presented below.

5.1.1 Feed

The total feed, comprising of H_2, CO, CO_2 and Ar, was supplied via the laboratory lines to the STIRR and was controlled by Brooks mass flow controllers. Ar was included as an internal standard. The molar flowrate and composition of the fresh feed is presented in Table 5.1. The feed composition was chosen such that the Ribblett ratio (H_2 / $2CO+3CO_2$) equals one, since the WGS reaction approaches equilibrium under the HTFT conditions and thus CO_2 is best treated as a reactant, and also such that the entry partial pressure factor ($P_{H2}^{0.25}$ / ($P_{CO}+0.7P_{CO2}$) was sufficiently low, as the CH_4 selectivity has been shown to be less at lower entry partial pressure factors (Dry, 2004a).

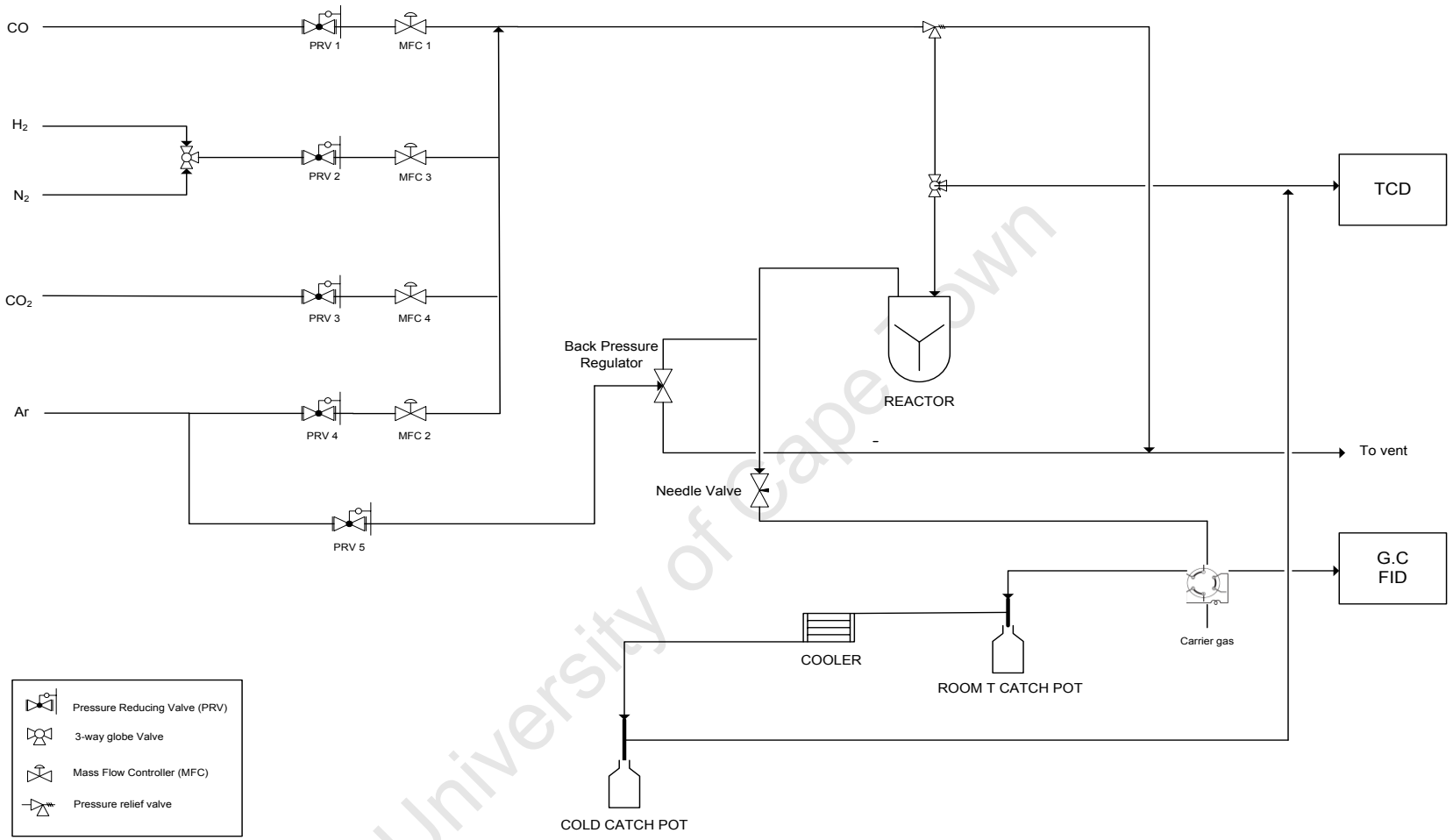

Figure 5.1: Process flow diagram of reactor test unit

Table 5.1: Flowrate and composition of the feed gas

Gas	V_{in} (ml/min)	n_{in} (mols/min)	Mole fraction
H_2	635.3	0.25	0.64
CO	158.8	0.06	0.16
CO_2	105.4	0.04	0.11
Ar	100.0	0.04	0.10
	1000.0	0.39	1.00

5.1.2 Reactor

A schematic of the STIRR is presented in Figure 5.2. The reactor comprised two parts, viz.

- a "lid" which was fixed through mounting to the test unit frame and to which was mounted the magnedrive and impeller assembly, and
- a "body" which formed the internal flow path that included a central draft tube and catalyst bed assembly. The internal draft tube holding the catalyst bed could be removed from the reactor for cleaning and catalyst reloading. The top of the catalyst basket consisted of a wire mesh reinforced 15 μm sintered metal felt (hereafter referred to as felt), which was placed upon a metal sieve plate with 5 mm diameter perforations, while the base of the basket consisted of an identical metal sieve plate and felt but in this case, the metal sieve plate was placed upon the felt.

The bottom thermocouple (just below the catalyst bed) was used to set and control the reactor temperature, while a thermocouple on the side of the catalyst bed was used to monitor the reactor temperature. The impeller was driven in a counter clockwise direction by a variable speed motor (Bonfiglioli, 50 Hz and 0.55 kW) via the magnedrive, so that gas flow was downwards through

the catalyst basket with recycle flow proceeding upwards external to the draft tube. Photographs of the reactor and reactor test unit are presented in Appendix I.

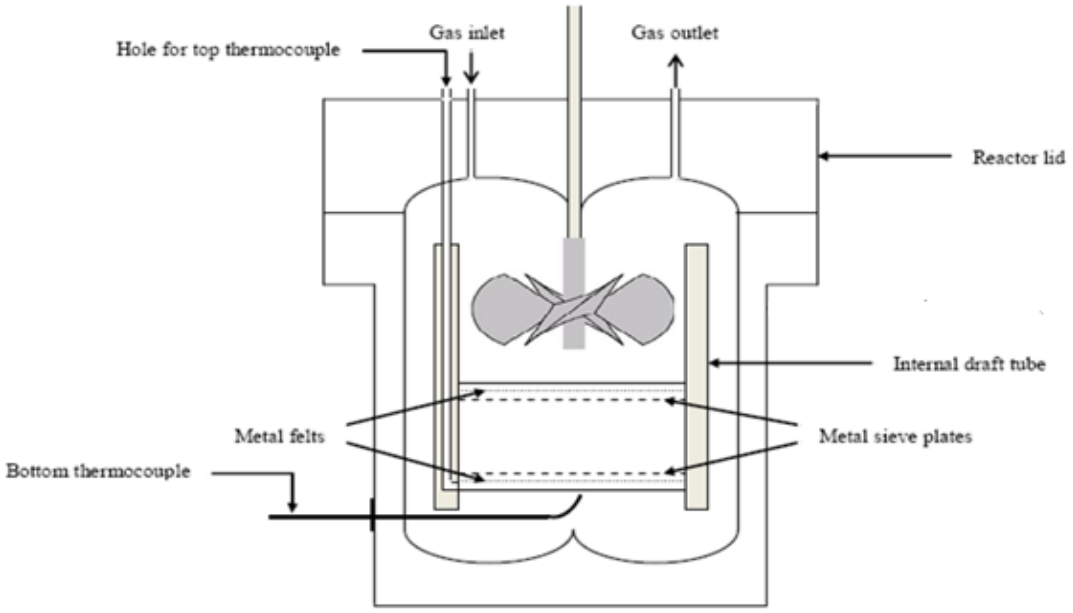

Figure 5.2: Schematic diagram of STIRR

5.1.1 Pressure control

A dome-loaded diaphragm backpressure regulator was installed to regulate the pressure of the reactor. Pressurized Ar was used to set the backpressure to the diaphragm at the desired reactor pressure.

5.1.2 Reactor exit

The exit stream from the reactor flowed through a 6-way multi-port switching valve that was operated and controlled by the Varian Galaxie chromatography workstation, where some of the

product gas was pneumatically injected into the GC-FID and the rest flowed to the GC-TCD via a room temperature catch pot and a cold catch pot (5^{o}C). The hydrocarbons and water from the product gas were condensed in the catch pots before analyzing the permanent gases (CH_4, CO, CO_2, H_2 and Ar) in the GC-TCD.

5.2 Catalyst

A potassium-promoted, precipitated Fe-FT catalyst was used for this study and was prepared in an industrial lab by Vallabh (2008) – an outline of the preparation procedure is provided in Dry (2004b). The Fe-FT catalyst was used in the form of a spray-dried powder with a minimum particle diameter of 25 μm. The acid catalyst used in this study was a commercial HZSM-5 type material supplied by Süd-Chemie Zeolites (Pty) Ltd., comprising alumina-bound extrudates (inch diameter) of a generic MFI powder with a nominal silica/alumina molar ratio of 90. An elemental analysis (XRF) of the fresh Fe-FT and HZSM-5 catalysts is presented in Table 5.2, where the high alumina content in the HZSM-5 catalyst reflects the alumina binder, as the extrudates were ground prior to analysis.

Table 5.2: Elemental analysis (XRF) of the fresh Fe-FT and HZSM-5 catalysts

Major Oxides (wt-%)*	Fresh Fe-FT	Fresh HZSM-5
SiO_2	0.06 ± 0.03	75.25 ± 0.26
Al_2O_3	0.15 ± 0.01	24.62 ± 0.18
Fe_2O_3	97.18 ± 0.02	0.11 ± 0.05
K_2O	0.24 ± 0.01	< 0.01
CuO	2.37 ± 0.01	0.02 ± 0.02
Fe	68.35 ± 0.02	-
K	0.21 ± 0.01	-
K/Fe	0.003	-

* Normalized to Si, Al, Fe, K and Cu oxides content

5.3 Experimental operating conditions

An Fe-FT experiment was carried out to test the validity of the high temperature FT synthesis on the STIRR and to serve as a baseline with which to compare the performance of the combined Fe-FT/HZSM-5 experiment. The reproducibility of the experiments on the STIRR was also tested by repeating both the Fe-FT and the combined Fe-FT/HZSM-5 experiments. A brief summary of the experiments carried out is presented in Table 5.3. All the aforementioned experiments were carried out under the reduction and synthesis conditions presented in Table 5.4.

Table 5.3: Summary of experiments carried out in the STIRR

Experiment	Catalyst loading	Duration
Fe-FT Expt. 1	5g Fe-FT	7 days
Combined Fe-FT/HZSM-5 Expt. 1	5g Fe-FT / 5g HZSM-5	14 days
Fe-FT Expt. 2	5g Fe-FT	14 days
Combined Fe-FT/HZSM-5 Expt. 2	5g Fe-FT / 5g HZSM-5	15 days

Table 5.4: Reduction and reaction conditions

Reduction Conditions	
Temperature	420^{o}C
Pressure	20 bar
Time	16 hours
Reduction Gas	H_2
Flow rate	635.5 ml/min
Gas space velocity	127 ml/min/g unreduced Fe-FT cat.
Reaction Conditions	
Temperature	330^{o}C
Pressure	20 bar
Total feed gas flow rate	1000 ml/min
Syngas flow rate	794 ml/min
Syngas space velocity	159 ml/min/g unreduced Fe-FT cat.

5.4 Experimental operating procedures

5.4.1 Catalyst loading

The Fe-FT experiments were performed with 5 g of Fe-FT catalyst. The catalyst was loaded by removing the internal draft tube containing the felts and metal sieve plates making up the catalyst bed. The metal sieve plate and bottom felt were tightened into position. The catalyst was spread evenly so that it uniformly filled the holes in the metal sieve plate as illustrated in Figure AI.3 in Appendix I. The top felt and metal sieve plate were screwed into position after which the entire catalyst basket and draft tube assembly were placed into position in the reactor. The same procedure was applied for the combined Fe-FT/HZSM-5 experiments with the exception that 5 g of HZSM-5 extrudates were equally dispersed over the Fe-FT catalyst layer before screwing the top felt and metal sieve plate into position.

5.4.2 Reactor operation

5.4.2.1 Start-up procedure

Prior to all the experiments, a pressure test was performed to ensure that there were no leaks in the reactor system. This was done by setting the backpressure regulator to 20 bar and feeding H_2 to test the reactor at pressures of 5, 10, 15 and 20 bar. For each test, the H_2 flow was stopped at the desired pressure and the pressure gauge was observed for about 30 minutes. The test was considered successful if the reactor pressure did not drop by more than 0.5 bar during this time. If the pressure loss exceeded 0.5 bar, the joints were checked for leaks using snoop (liquid leak detector), retightened and the pressure test repeated until a satisfactory pressure test was achieved.

Upon achievement of a satisfactory pressure test, the reactor was depressurized to atmospheric pressure and the reactor thermally insulated. The impeller speed was set to 1800 rpm and a period of 30 minutes was allowed for the reactor to settle in. Thereafter experiments were commenced.

5.4.2.2 Catalyst reduction and synthesis

For reduction, a pure H_2 gas flowrate of 635.5 ml/min was fed to the reactor at 20 bar. The temperature of the reactor was ramped at a heating rate of 2^oC per minute from ambient temperature to 420^oC, and held at this temperature for 16 hours.

For synthesis, the temperature set point was lowered to 330^oC and the reactor temperature was allowed 4 hours to stabilize. The feed gas flows were then set to the synthesis feed composition using the relevant mass flow controllers.

5.4.2.3 Shut down procedure

After completion of the experimental run, the temperature set point was set to 0^oC and the backpressure regulator was set to atmospheric pressure. The impeller was switched off and the gas flow to the reactor was stopped by setting the mass flow controllers to 0 % and closing the corresponding valves from the feed gas line. The reactor was left to cool to ambient temperature, after which the insulation was removed and the catalyst unloaded.

5.5 Feed and product gas analysis

5.5.1 Gas chromatography

5.5.1.1 Sampling procedure

The sampling was achieved by means of an on-line 6-way multi-port switching valve. During normal operation of the experimental apparatus, the product gas passes through a sample loop in the 6-way valve whilst, simultaneously, flushing the GC injector port with the carrier gas. When sampling, the 6-way valve is switched in such a way that the product gas in the sample loop is driven into the GC injector port by the chromatographic carrier gas. After approximately 30 seconds, the valve was switched back to its initial position, in preparation for the next analysis.

5.5.1.2 Hydrocarbon product analysis

Chromatographic conditions

The hydrocarbon product distribution was determined using an on-line Varian 3900 gas chromatograph (GC) fitted with a flame ionisation detector (FID), and a summary of the GC conditions is presented in Table 5.5.

Peak identification

The peaks of the compounds in the GC-FID were identified by taking some of the condensed hydrocarbon sample from the cold catch pot and manually identifying the peak of each compound in a GC fitted with a mass spectrometer (MS).

Table 5.5: Summarized description of the Varian 3900 GC

Model	Varian 3900		
Detector	Flame Ionisation Detector (FID)		
Carrier gas	H_2		
Column head-pressure	2 bar		
Injector	Split injector $T_{Injector}$ = 250°C Split ratio 1:50		
Oven temperature	0°C to 300°C (ramp)		
Ramping programme	Step 1	Step 2	Step 3
Initial temperature (°C)	0	0	50
Ramp rate (°C/min)	0	3.3	8.3
Final temperature (°C)	0	50	300
Hold time (min)	5	0	0
Detector temperature	275°C		

To attain similar retention times, the same column was used in both the GC-FID and GC-MS instruments. A list of compounds with the calculated correction factors and corresponding retention times are presented in Appendix II. Typical FID chromatograms for the Fe-FT and combined Fe-FT/HZSM-5 experiments are also presented in Appendix II.

Data analysis

The mass of compound *i* in the GC-FID was determined as follows:

The chromatographic peak area obtained from the GC-FID (A_i) was corrected with a correction factor (f_0) since the GC-FID response for compounds containing oxygen is less than that for pure hydrocarbons. In order to account for this, specific response factors were determined according to the incremental approach suggested by Kaiser (1969) where the response (z) of all carbon atoms not bonded to an oxygen atom is set to unity and the response of carbon atoms with a single and two oxygen bonds are 0.55 and 0.1, respectively.

Consequently, the corrected area ($A_{i,corrected}$) was determined as follows:

$$A_{i,corrected} = A_i \cdot f_{o,i} \tag{5.1}$$

$$f_{o,i} = \frac{N_{C,i}}{N_{C(no\_O),i} + z_{C-O,i}.N_{C-O,i} + z_{C=O,i}.N_{C=O,i}} \tag{5.2}$$

Where $N_{C,i}$ = number of carbon atoms in a compound *i*

$N_{C(no\_O),i}$ = number of carbon atoms not bonded to an oxygen atom in a compound *i*

$N_{C\text{-}O,i}$ = number of carbon atoms bonded to an oxygen atom in a compound *i*

$N_{C=O,i}$ = number of carbon atoms bonded to two oxygen atoms in a compound *i*

Therefore, the mass of carbon in each compound was calculated as follows:

$$m_{C[i]} = \frac{A_{i,corrected}}{\sum A_{i,corrected}} . \sum m_{C[i]} \tag{5.3}$$

Where the total mass of carbon in the hydrocarbons ($\sum m_{C[i]}$) was calculated from the carbon mass balance as follows:

$$m_{C[CO],in} + m_{C[CO_2],in} = m_{C[CO],out} + m_{C[CO_2],out} + m_{C[CH_4],out} + m_{C[hydrocarbons],out} \tag{5.4}$$

It was further assumed that the mass of carbon in was equal to the mass of carbon out, since no accumulation of hydrocarbons was expected in the product line (see Appendix III), and also since it was assumed there were no hot/cold spots in the STIRR used in this study (previously characterized by Vallabh (2008)). The rate of carbon deposition on the Fe-FT catalyst was assumed negligible compared to the rate of formation of hydrocarbons.

Therefore, the moles and mass of compound *i* were determined as follows:

$$n_{C[i]} = n_i = \frac{m_{C[i]}}{M_{C[i]}.N_{C[i]}} \tag{5.5}$$

$$m_i = n_i.M_i \tag{5.6}$$

5.5.1.3 Permanent gases analysis

Chromatographic conditions

The permanent gases were measured using an on-line Varian 4900 gas chromatograph (GC) fitted with a thermal conductivity detector (TCD), and a summary of the GC conditions is presented in Table 5.6.

Table 5.6: Summarized description of the Varian 4900 GC

Model	Varian CP-4900 Micro gas chromatograph
Detector	Thermal conductivity detectors (TCD)
Detector temperature	200°C
Oven temperature	80°C (constant)
	Channel 1
Carrier gas	Ar
Column head-pressure	300 kPa
Analysis temperature	40°C
Gases detected	H_2
	Channel 2
Carrier gas	H_2
Column head-pressure	200 kPa
Analysis temperature	40°C
Gases detected	CO, CO_2, Ar, CH_4

Data analysis

The GC-TCD signal is a measurement of the relative concentration, therefore the volume of CO in the product gas is:

$$V_{CO,product} = C_{CO,product}.V_{T,product} = \frac{A_{CO,product}}{A_{T,product}}.V_{T,product} \quad (5.7)$$

and the volume of Ar is:

$$V_{Ar,product} = C_{Ar,product}.V_{T,product} = \frac{A_{Ar,product}}{A_{T,product}}.V_{T,product} \quad (5.8)$$

Including the calibration factor to both equations:

$$V_{CO,product} = \frac{A_{CO,product}}{A_{T,product}}.V_{T,product}.\frac{C_{CO,calibration}}{A_{CO,calibration}} \quad (5.9)$$

$$V_{Ar,product} = \frac{A_{Ar,product}}{A_{T,product}}.V_{T,product}.\frac{C_{Ar,calibration}}{A_{Ar,calibration}} \quad (5.10)$$

Since Ar is an inert, the $V_{T,product}$ can be calculated from the $V_{Ar,product}$:

$$V_{T,product} = \frac{A_{T,product}}{A_{Ar,product}}.V_{Ar,product}.\frac{A_{Ar,calibration}}{C_{Ar,calibration}} \quad (5.11)$$

Substituting $V_{T,product}$ into Equation 5.9:

$$V_{CO,product} = \frac{A_{CO,product}}{A_{Ar,product}}.\frac{C_{CO,calibration}}{A_{CO,calibration}}.V_{Ar,product}.\frac{A_{Ar,calibration}}{C_{Ar,calibration}} \quad (5.12)$$

The volumes of CO_2, H_2 and CH_4 were obtained with an analogous approach.

5.5.2 Data work-up

- The following equations were applied in analysing the data:

$$X_{CO} = \frac{V_{CO,out} - V_{CO,in}}{V_{CO,in}}.100 \quad (5.13)$$

$$X_{CO+CO_2} = \frac{\left(V_{CO\,out} - V_{CO\,in}\right) - \left(V_{CO_2\,out} - V_{CO_2\,in}\right)}{V_{CO\,in}}.100 \quad (5.14)$$

$$X_{H_2+CO_2} = \frac{\left(V_{H_2\,out} - V_{H_2\,in}\right) - \left(V_{CO_2\,in} - V_{CO_2\,out}\right)}{V_{H_2\,in}}.100 \quad (5.15)$$

$$H_2 : CO_{usage\_ratio} = \frac{\left(V_{H_2\,in} - V_{H_2\,out}\right) - \left(V_{CO_2\,in} - V_{CO_2\,out}\right)}{\left(V_{CO\,in} - V_{CO\,out}\right) - \left(V_{CO_2\,out} - V_{CO_2\,in}\right)} \quad (5.16)$$

In this study, some of the CO was converted to CO_2 via the WGS reaction. CO_2 is not a desired product nor is it considered part of the FT synthesis and, hence, the volume of CO_2 produced was subtracted from the volume of CO consumed when presenting the conversion of CO and H_2.

All selectivities were calculated on a carbon atom basis as follows:

$$S_i = \frac{m_{C[i],\,formed}}{m_{C[CO],consumed} - m_{C[CO_2],\,formed}}.100 \quad (5.17)$$

where the mass of carbon in compound *i* ($m_{C[i]}$) was determined by the carbon mass balance, as follows:

$$m_{C[i]} = \frac{P.V_i}{R.T}.M_i \quad (5.18)$$

However, the selectivity of CO_2 was determined as follows:

$$S_{CO_2} = \frac{m_{C[CO_2],\,formed}}{m_{C[CO],consumed}}.100 \qquad (5.19)$$

- The chain growth probability (α) is determined from the Anderson-Schulz-Flory (ASF) polymerization equation, where it is assumed that α is independent of the number of carbon atoms in the growing species (Dry, 1981), as follows:

$$\ln\left[\frac{W_n}{n}\right] = n\ln\alpha + \ln\left[\frac{(1-\alpha)^2}{\alpha}\right] \qquad (5.20)$$

A plot of $\ln(W_n/n)$ versus n yields a straight line with slope $\ln(\alpha)$. In determining the slope, only the C_{3+} fraction was taken into account since the C_1 and C_2 selectivities of the FT product deviates from the ideal ASF equation (Dry, 2004).

- The percentage of alkali atoms over acid sites was determined for the fresh Fe-FT catalyst as follows:

$SiO_2 / Al_2O_3 = 90$

$Si/Al = 45$

Unit cell formula for HZSM-5: $H_nAl_nSi_{96-n}O_{192}$

thus $[(96 – n) / n] = 45$

$n = 2.09$

$M_{HZSM-5} = 5954$ g/mol

To determine the mass of zeolite (excluding the binder), it was assumed the total amount of alumina in the zeolite was ca. 25 wt-% (refer to Table 5.2). Therefore,

Mass of alumina in extrudates 5 g x 0.25 = 1.25 g

Mass of alumina in HZSM-5 5 g x 0.75 / 45 = 0.08 g

Mass of binder in extrudates	1.17 g
Mass of HZSM-5	3.8 g

Hence,

Mols of HZSM-5:	(5954 g/mol) x 1000 / 3.8 g (HZSM-5) = 0.84 mmol
Number of acid sites (Al sites)	n x 0.84 = 1.33 mmol

It was assumed that the percentage of potassium in the fresh Fe-FT catalyst was 0.21% (refer to Table 5.2).

Potassium loading	1000 x 5 g (Fe-FT catalyst) x (0.21/100) / M_K = 0.27 mmol

Therefore, the percentage of alkali atoms over acid sites = 100 x (0.27 / 1.33) = 20 %

5.6 Catalyst Characterization

For all HZSM-5 analyses, approximately 2 g of HZSM-5 extrudates were crushed in a pulveriser or mortar and pestle so as to obtain a homogeneous, representative sample for each specific analysis.

5.6.1 Atomic absorption spectroscopy (AAS)

A Varian Spectra AA-30 spectrometer attached to a DS-15 station was used to determine the concentrations of potassium and iron in the fresh and spent Fe-FT and HZSM-5 catalysts. Sample preparation entailed adding 0.1 g catalyst to a mixture of 8 ml hydrochloric acid (30 %) and 2 ml hydrofluoric acid (40 %) in a 250 ml Erlenmeyer flask followed by heating to boil, after which 10 ml of nitric acid (60 %) was added to the flask and boiling continued until the sample volume was reduced to approximately 2 ml, at which point 5 ml of perchloric acid was added.

Upon final sample reduction to approximately 2 ml (at which point a white cloud formed once the reaction took place), the sample solution was quantitatively transferred to a 100 ml volumetric flask and made up to a volume of 100 ml with de-ionized water. The liquid sample was filtered through a Whatman No.1 filter paper and the filtrate analysed by AAS.

5.6.2 Atomic emission spectroscopy (AES)

The potassium and iron concentrations of both the fresh and spent Fe-FT and HZSM-5 catalysts were also determined by means of an inductively coupled plasma atomic emission spectrometer (ICP-AES) at an external (commercial) laboratory.

5.6.3 X-Ray fluorescence (XRF)

The iron, potassium, silicon and aluminium concentrations of both the fresh and spent Fe-FT and HZSM-5 catalysts were further determined on a Philips PW1480 wavelength dispersive XRF spectrometer with a dual target Mo/Sc x-ray tube, according to the procedure given in Willis (1999).

6 RESULTS

6.1 Preliminary findings

6.1.1 Stability of the reactor system and Fe-FT catalyst

The chromatographic peak areas for the permanent gases analyzed on the second channel of the GC-TCD for the Fe-FT Expt. 1 are presented in Figure 6.1. Since Ar is an inert gas, its chromatographic peak area is representative of the stability of the reactor system and, from Figure 6.1, it can be seen that the Ar flow remained stable throughout the Fe-FT experiment after a short initial settling-in period (ca. 1 day). Similarly, CO, CO_2 and CH_4 effluent flows were steady after the initial stabilization period, with the very slight increase in CO effluent indicating a very slight catalyst deactivation with time-on-stream such that the FT catalyst may be considered stable for the duration of the experiments of this study. Likewise, the total chromatographic peak area of components analysed on the GC-FID for the Fe-FT Expt. 1 is presented in Figure 6.2, from which it can be seen that the FT conversion stabilizes after approximately 1 day on-stream and remains so for the duration of the experiment of this study.

6.1.2 Fe-FT catalyst settling-in period

The CO conversion of the Fe-FT Expt. 2 and the combined Fe-FT/HZSM-5 Expt. 2 are presented in Figure 6.3, from which it can be seen that the CO conversion for both experiments stabilized after approximately 1 day on-stream – a trend that was observed for the FT conversions in all the experiments presented henceforth. This phenomenon was attributed to the Fe-FT catalyst settling-in period and, consequently, the performance of the Fe-FT catalyst is considered significant only after at least 1 day on-stream for all further discussions.

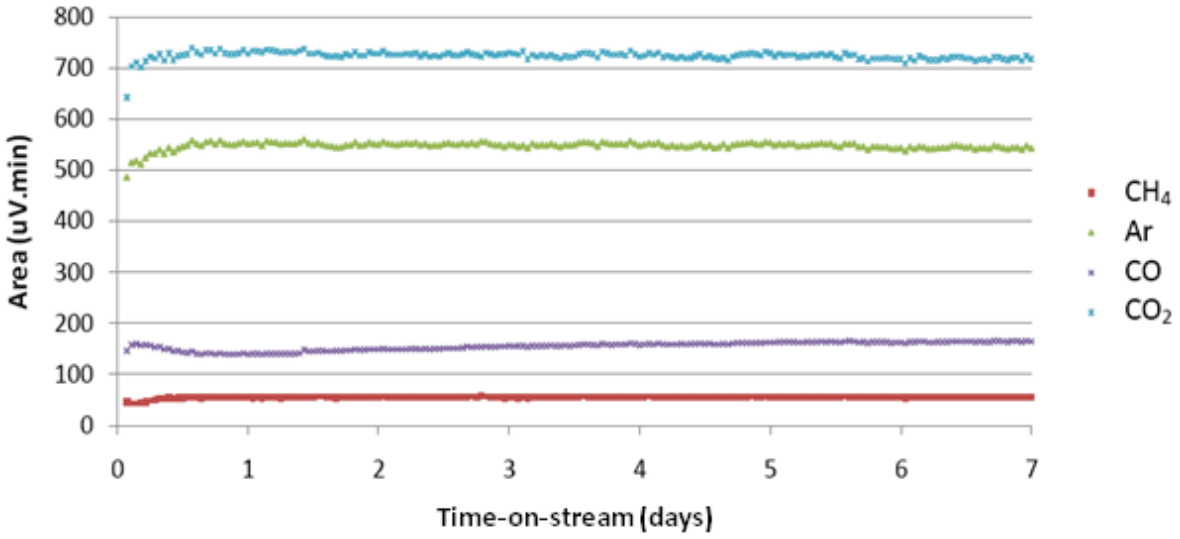

Figure 6.1: Chromatographic peak areas of the permanent gases analyzed on the GC-TCD channel 2 for the Fe-FT Expt. 1

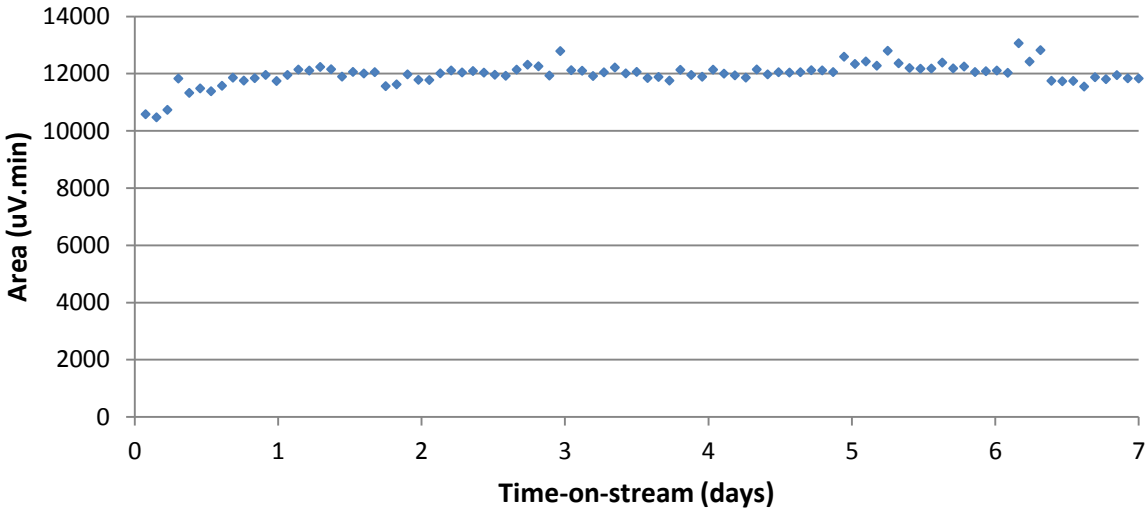

Figure 6.2: Total chromatographic peak area of components analysed on the GC-FID for the Fe-FT Expt. 1

.

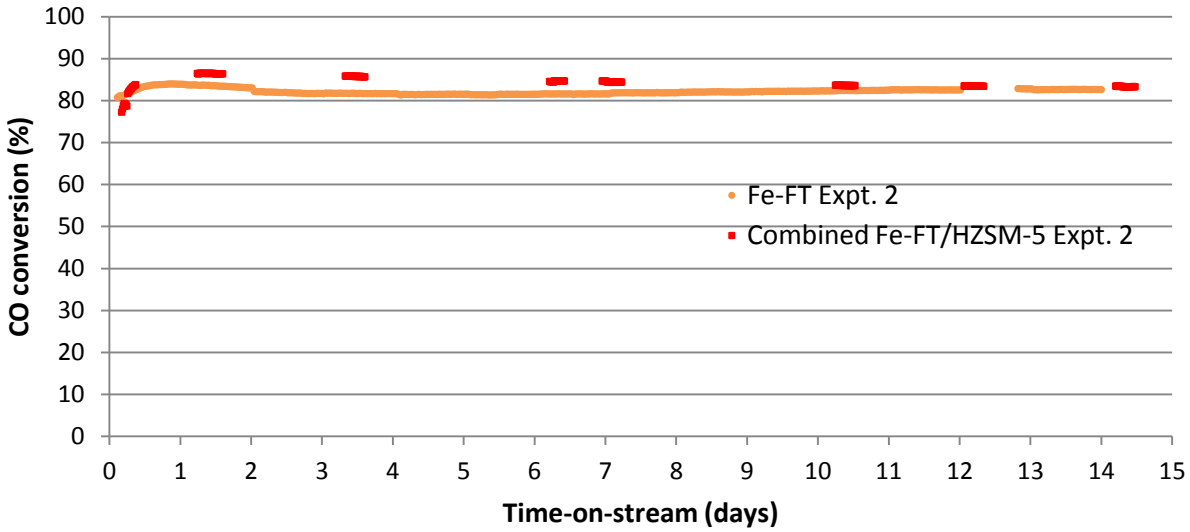

Figure 6.3: CO conversions for both the Fe-FT experiments and combined Fe-FT/HZSM-5 experiments

6.1.3 WGS equilibrium

To verify whether the WGS reaction reached equilibrium, the equilibrium constant (K_p) calculated from the Gibbs free energy and the partial pressures were determined (Appendix III) to be 15.8 and 16.9, respectively. The similar magnitudes of the K_p values obtained suggests that the WGS reaction was very close to equilibrium under the conditions of this study and, therefore, justifying the concept of the Ribblett ratio used in this study to determine the feed composition.

6.2 Fe-FT performance

6.2.1 Fe-FT activity and selectivity

The CO, $CO+CO_2$ and H_2+CO_2 conversions for the Fe-FT experiments are presented in Figure 6.4, Figure 6.5 and Figure 6.6, respectively. The $CO+CO_2$ conversion is the appropriate way of presenting Fe-FT activity as this negates the extent of the water-gas shift, which is not considered to be part of the FT reaction. From Figures 6.5 and 6.6, the $CO+CO_2$ and H_2+CO_2 conversions obtained for both the Fe-FT experiments were very similar and appeared to be stable with time-on-stream, with a very slight decline in the $CO+CO_2$ conversion in the first 7 days on-stream. The low H_2+CO_2 conversions obtained was as a result of the excess H_2 in the feed, which was intentional for purposes of obtaining a Ribblett ratio of 1, and the validity of this choice has been discussed earlier in Section 6.1.3.

The CH_4 selectivities for the Fe-FT experiments are presented in Figure 6.7, from which it can be seen that there was a very slight and gradual increase in the CH_4 selectivity with time-on-stream for both experiments, an occurrence that may be due to various reasons including the deposition of elemental carbon via the Boudouard reaction (Section 2.1.7).

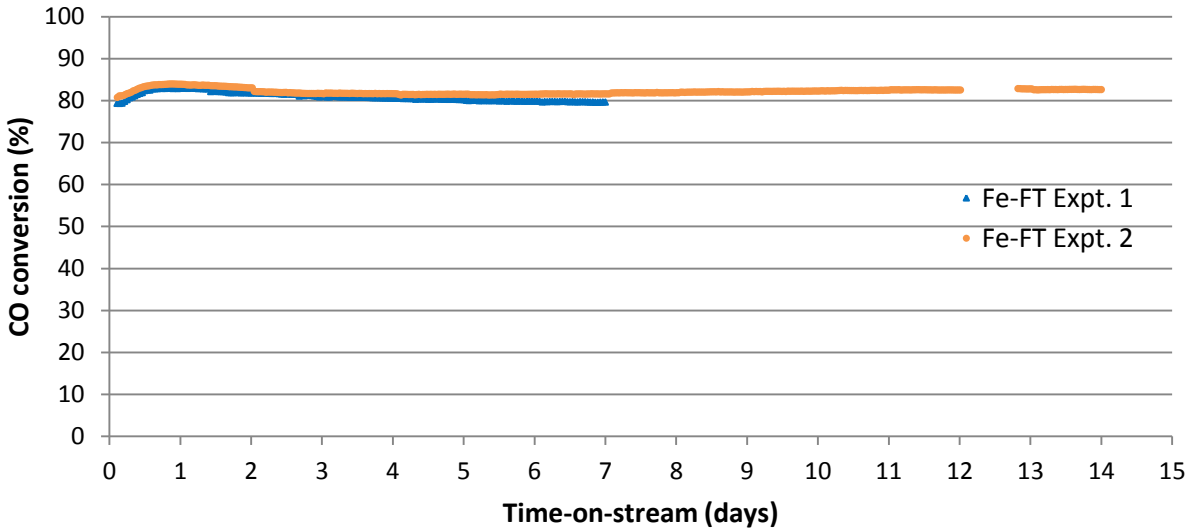

Figure 6.4: CO conversions for the Fe-FT experiments

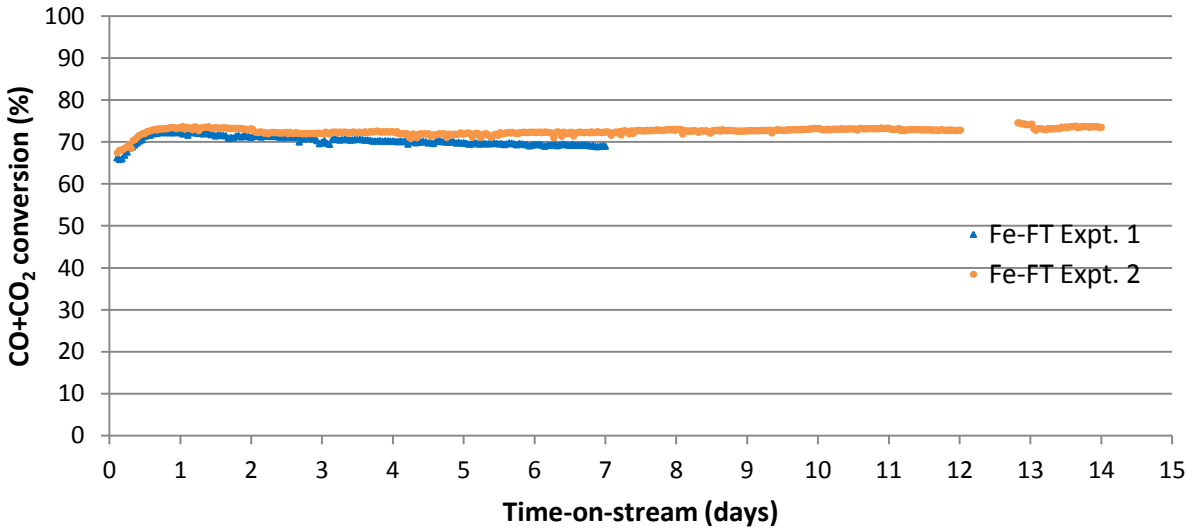

Figure 6.5: $CO+CO_2$ conversions for the Fe-FT experiments

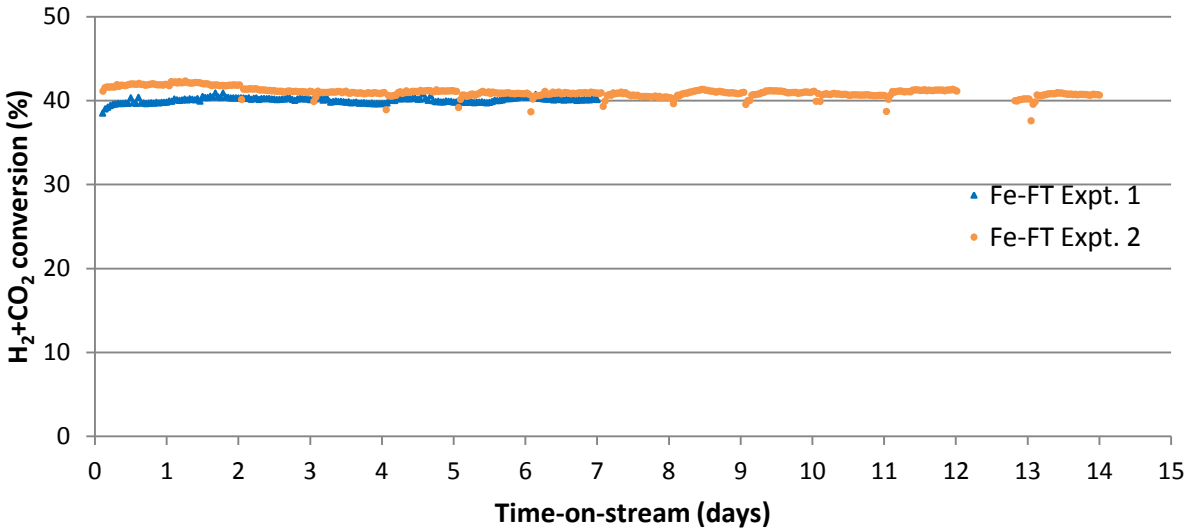

Figure 6.6: Conversion of H_2+CO_2 for the Fe-FT experiments

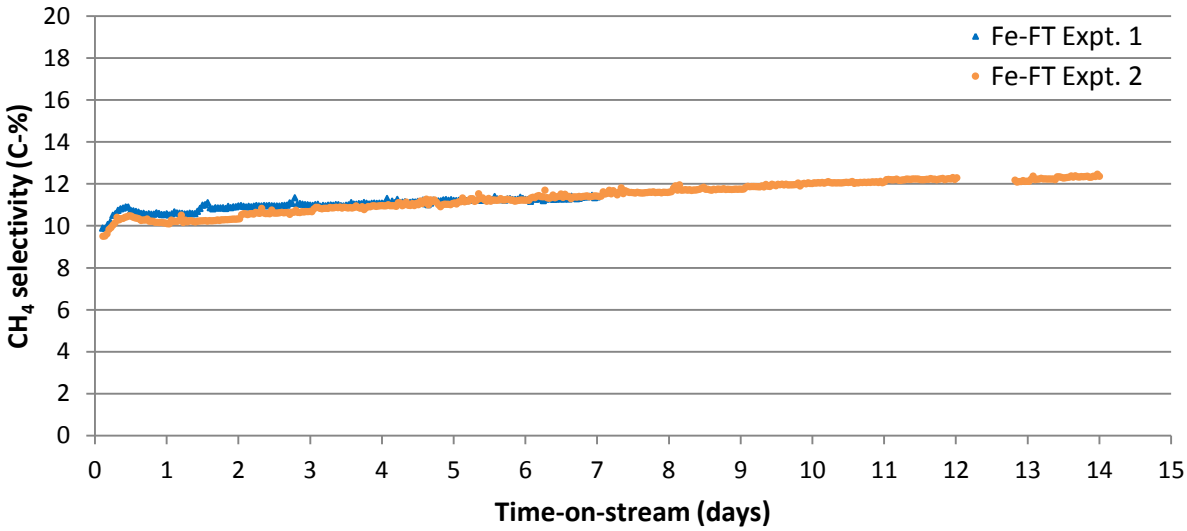

Figure 6.7: CH_4 Selectivities for the Fe-FT experiments

6.2.2 Product distribution

6.2.2.1 Carbon number distribution

The chain growth probabilities (α) for both the Fe-FT experiments were obtained from the Anderson Schulz Flory (ASF) polymerization equation (see Section 5.5.2) and the resultant plots are presented in Figure 6.8 and Figure 6.9. As expected (Dry, 1981), the C_1 fraction is slightly higher while the C_2 fraction is slightly lower than that predicted by the ASF model. The $C_3 - C_{15}$ fraction was in accordance to the ASF model and thus a linear trend is observed in the ASF molar plot. There was not any noticeable olefin readsorption occurring, as the C_{15+} fraction was also in accordance with the ASF model.

The probabilities of chain growth (α) with time-on-stream for both Fe-FT experiments are presented in Figure 6.10, from which it can be seen that the α values for both experiments were very similar and stable with time-on-stream.

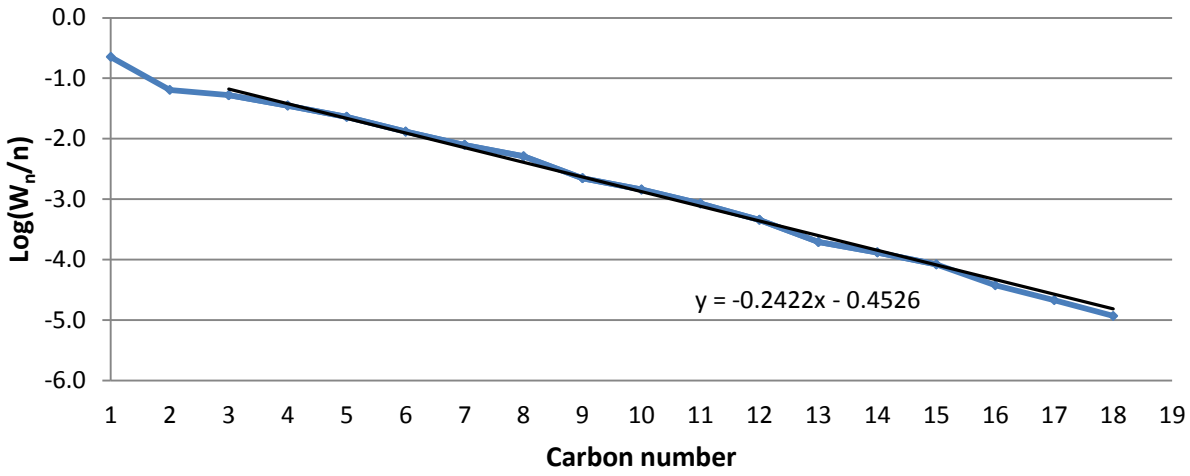

Figure 6.8: ASF Molar Plot for the Fe-FT Expt. 1 (2.5 days on-stream)

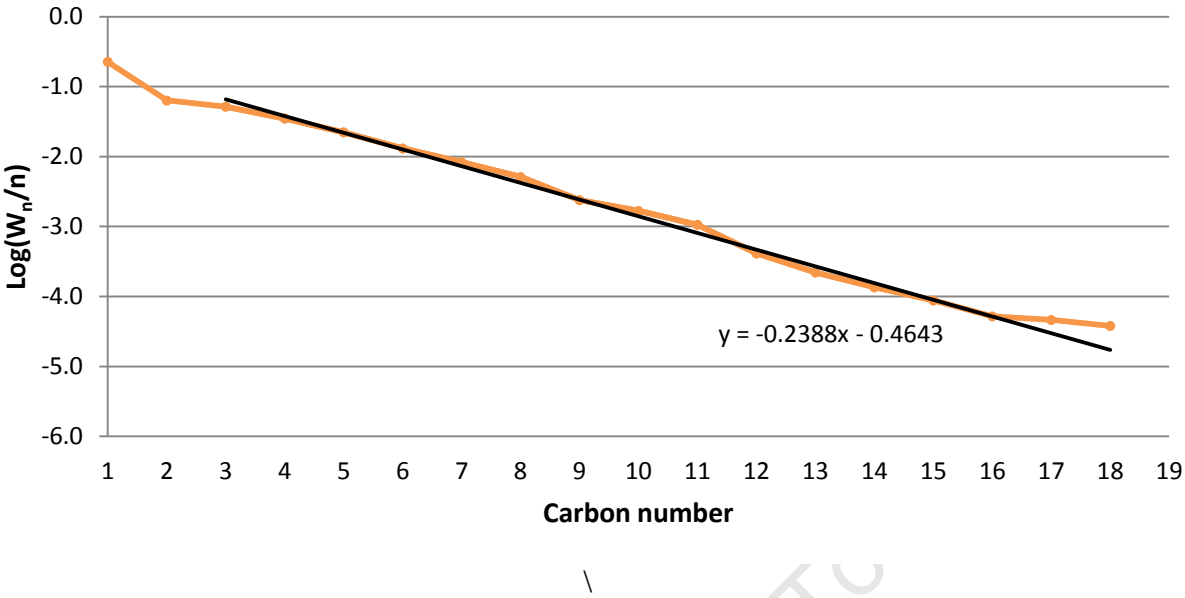

Figure 6.9: ASF molar plot for the Fe-FT Expt. 2 (2.5 days on-stream)

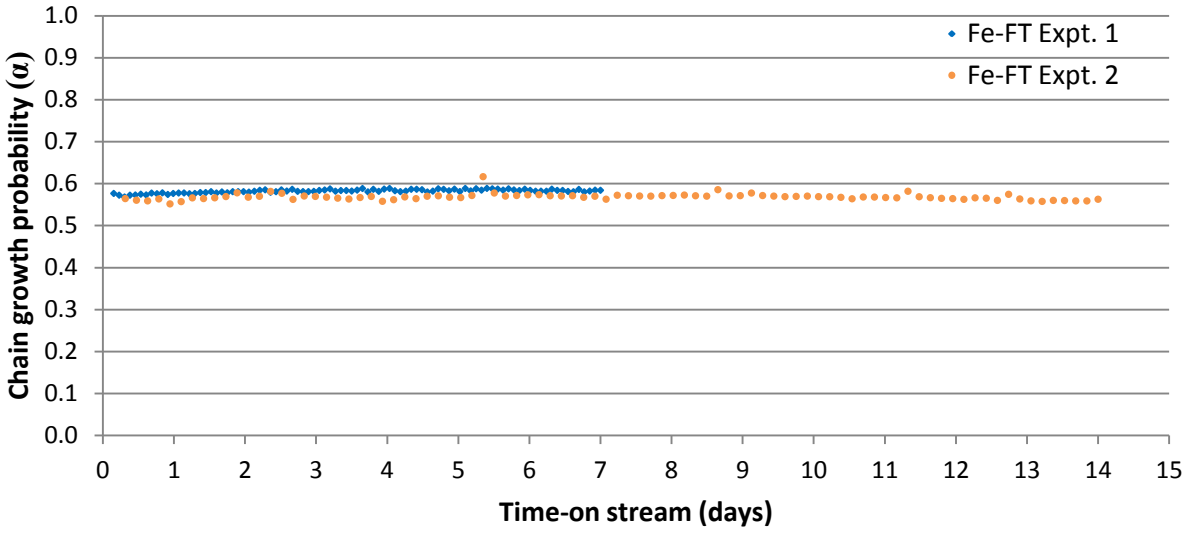

Figure 6.10: Chain growth probabilities (α) with time-on-stream for both Fe-FT experiments

In all the results presented henceforth, the Fe-FT experiment will be represented by the Fe-FT Expt. 2. Figure 6.11 compares the carbon number distributions of the total product for the Fe-FT Expt. 2 at 2.5 days and 14 days on-stream, from which it can be seen that there was a very slight shift towards a lighter product spectrum after 14 days on-stream. The product distribution versus the carbon number range at 2.5 days on-stream for the Fe-FT Expt. 2 is presented in Figure 6.12, from which it can be seen that the C_1 fraction comprised of approximately 6 C-% methanol, and the C_{2+} fraction was dominated by olefins.

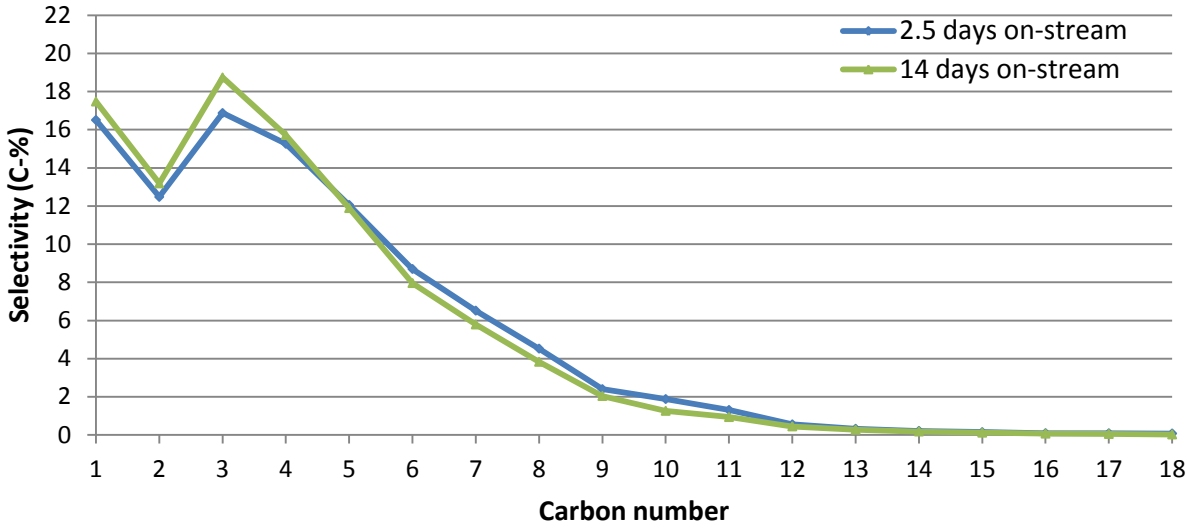

Figure 6.11: Carbon number distributions of the total product for the Fe-FT Expt. 2 (2.5 days and 14 days on-stream)

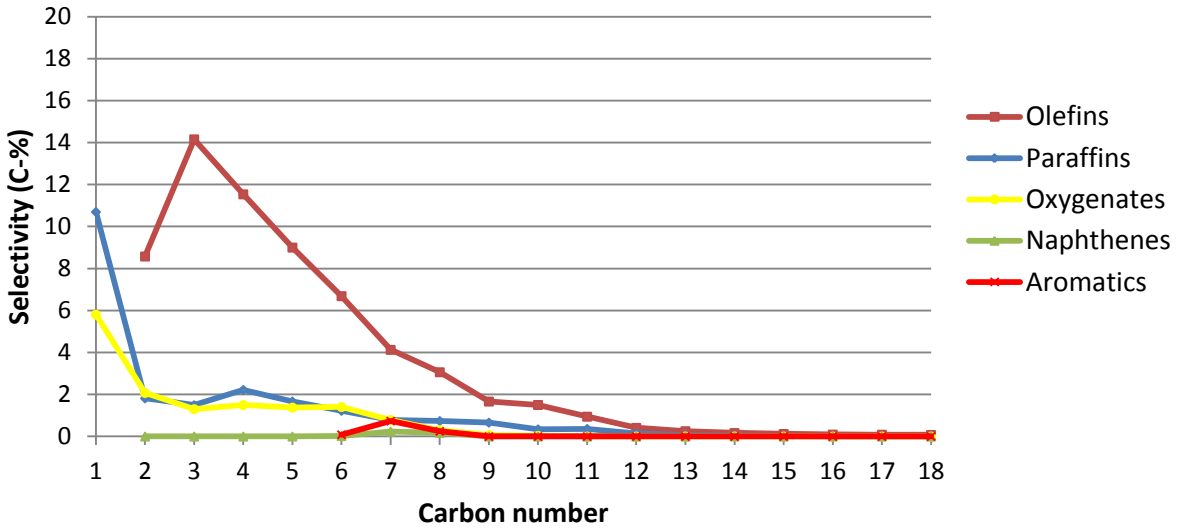

Figure 6.12: Product distribution versus carbon number range for the Fe-FT Expt. 2 (2.5 days on-stream)

6.2.2.2 Product-type distribution

The product distribution (C_{2+}) for the Fe-FT Expt. 2 is presented in Figure 6.13, and the olefin and paraffin distributions versus the carbon number range at 2.5 days on-stream for the Fe-FT Expt. 2 are presented in Figure 6.14 and Figure 6.15, respectively. From Figure 6.13, the selectivity to olefins over the Fe-FT catalyst appeared to increase as the selectivity to oxygenates decreased with time-on-stream, while there was not much of a change in the selectivity to paraffins, aromatics and naphthenes with time-on-stream. From Figures 6.14 and 6.15, as expected from literature (see Section 2.1.4), the Fe-FT product spectrum comprised mainly of linear α-olefins and approximately half of the C_{4+} paraffins formed were branched.

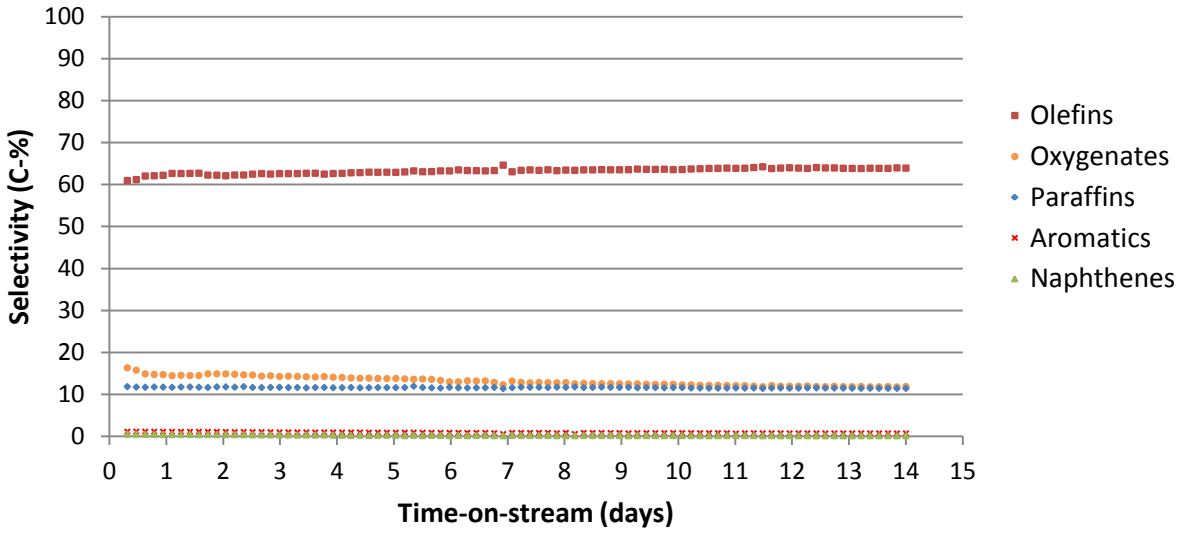

Figure 6.13: Product distribution (C_{2+}) with time-on-stream for the Fe-FT Expt. 2

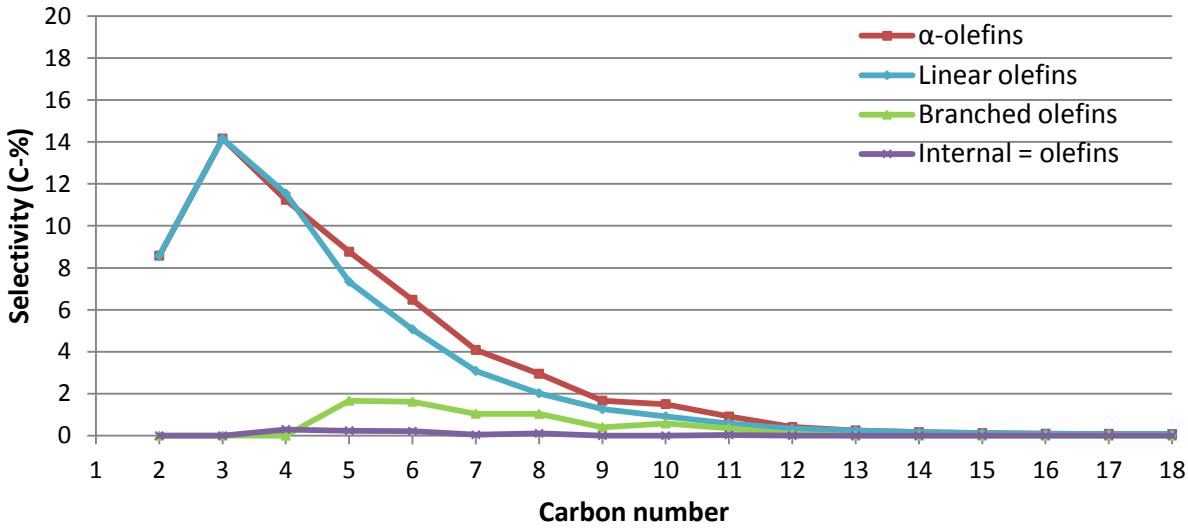

Figure 6.14: Olefin distribution versus carbon number range for the Fe-FT Expt. 2 (2.5 days on-stream)

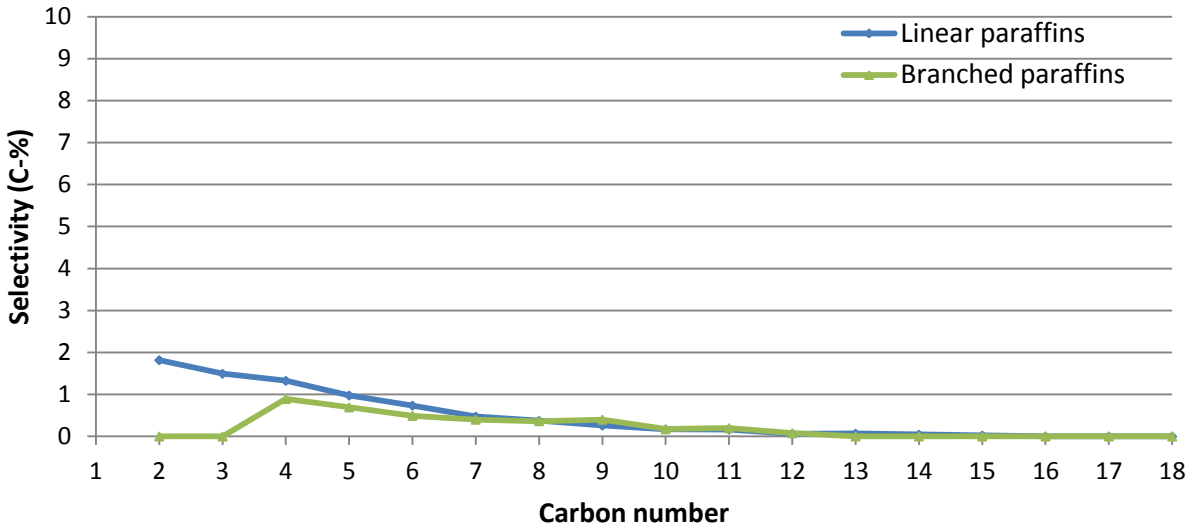

Figure 6.15: Paraffin distribution versus carbon number range for the Fe-FT Expt. 2 (2.5 days on-stream)

6.2.3 Gasoline selectivity and distribution

The gasoline selectivity for the Fe-FT Expt. 2 is presented in Figure 6.16, from which it can be seen that the gasoline selectivity remained relatively stable with a gradual decrease with time-on-stream, which was attributed to the slight shift of the overall hydrocarbon product towards a lighter product spectrum.

The gasoline distribution for the Fe-FT Expt. 2 is presented in Figure 6.17, from which it can be seen that the gasoline product spectrum of the Fe-FT experiment consisted mainly of olefins and a very small amount of aromatics.

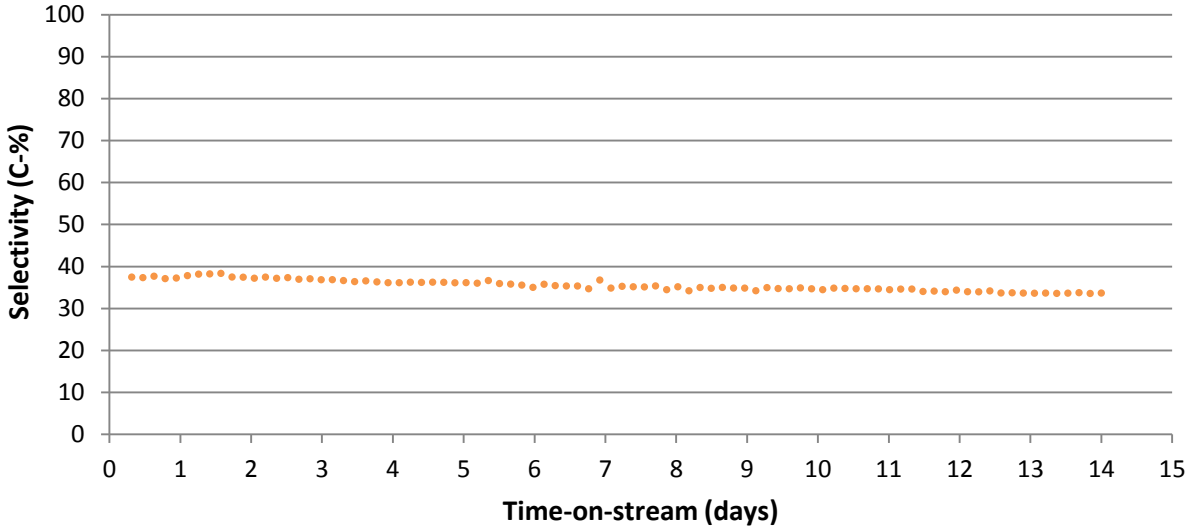

Figure 6.16: Gasoline ($C_5 - C_{11}$) selectivity for the Fe-FT Expt. 2

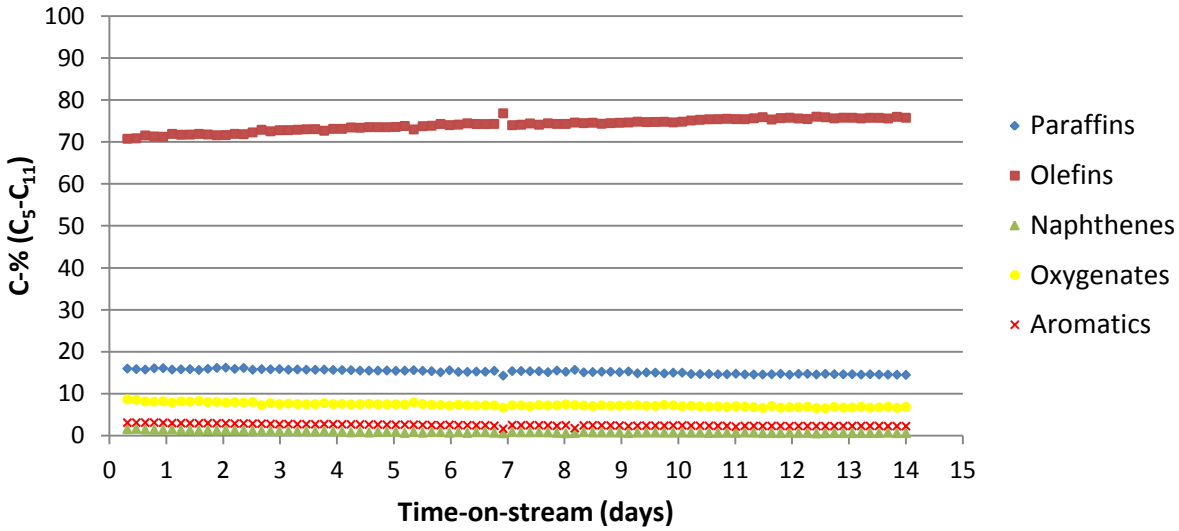

Figure 6.17: Gasoline ($C_5 - C_{11}$) distribution with time-on-stream for the Fe-FT Expt. 2

6.3 Combined Fe-FT/HZSM-5 performance

6.3.1 Fe-FT activity and selectivity

The CO, $CO+CO_2$ and H_2+CO_2 conversions for the combined Fe-FT/HZSM-5 experiments are presented in Figure 6.18, Figure 6.19 and Figure 6.20, respectively. Note that the results of the combined Fe-FT/HZSM-5 Expt. 1 are only presented from the first day of synthesis, as there was an air leak in channel 2 of the GC-TCD. There were slight discrepancies observed for the two combined experiments, as the $CO+CO_2$ conversion for the combined Fe-FT/HZSM-5 Expt. 2 was slightly higher than that of the combined Fe-FT/HZSM-5 Expt. 1, while the H_2+CO_2 conversion was lower. Nonetheless, the FT conversions could be compared with time-on-stream and, as was observed with the Fe-FT experiments, the FT conversions for the combined Fe-FT/HZSM-5 Expt. 2 stabilized after approximately 1 day on-stream, after which the FT conversions gradually declined with time-on-stream and then appeared to steady towards the end of both the combined Fe-FT/HZSM-5 experiments.

The CH_4 selectivities for the combined Fe-FT/HZSM-5 experiments are presented in Figure 6.21, from which it can be seen that the CH_4 selectivities gradually increased with time-on-stream for both combined Fe-FT/HZSM-5 experiments.

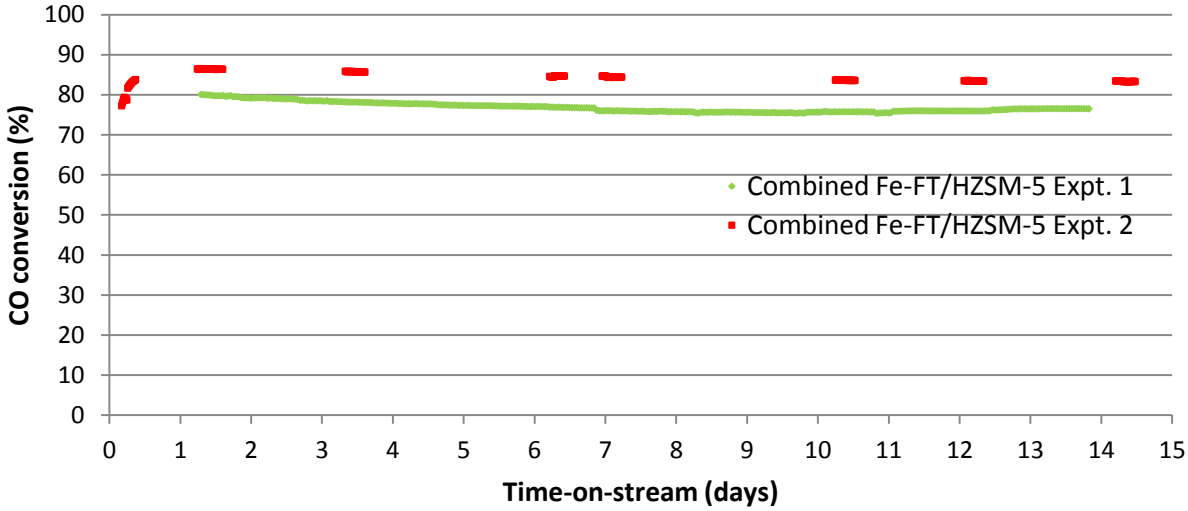

Figure 6.18: CO conversions for the combined Fe-FT/HZSM-5 experiments

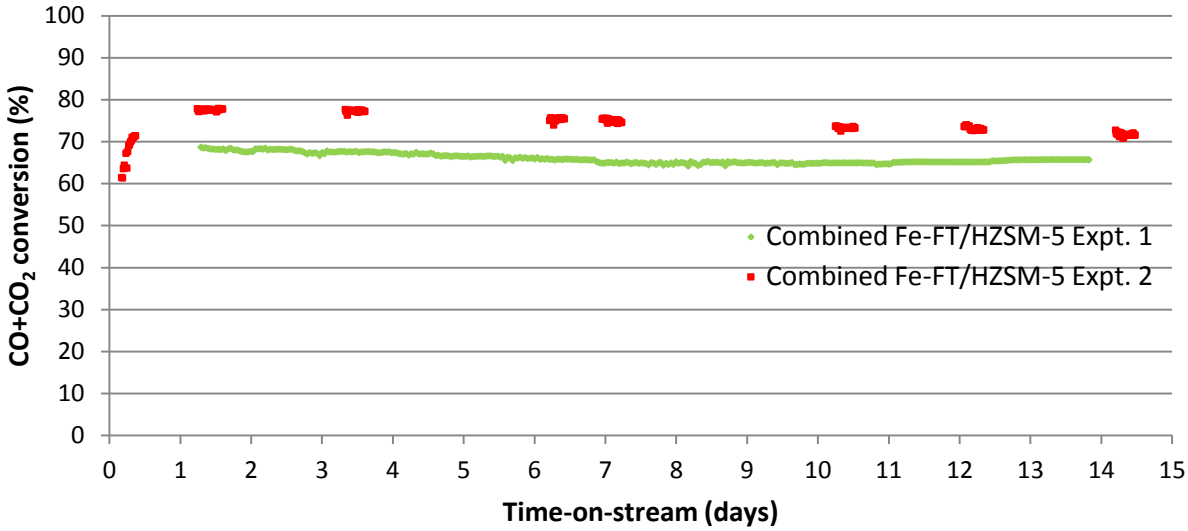

Figure 6.19: $CO+CO_2$ conversions for the combined Fe-FT/HZSM-5 experiments

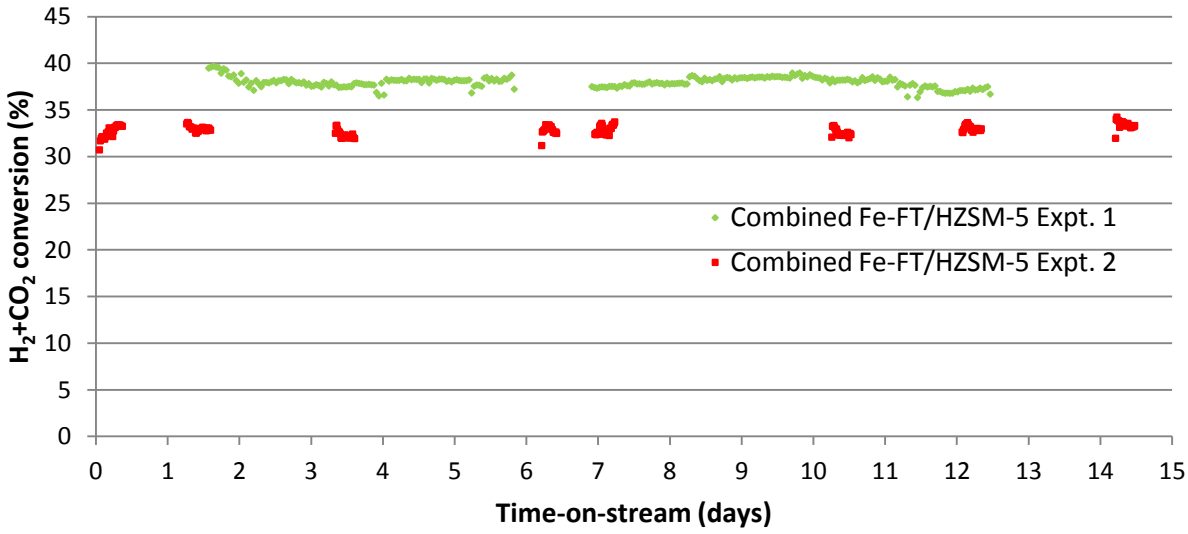

Figure 6.20: H_2+CO_2 conversions for the combined Fe-FT/HZSM-5 experiments

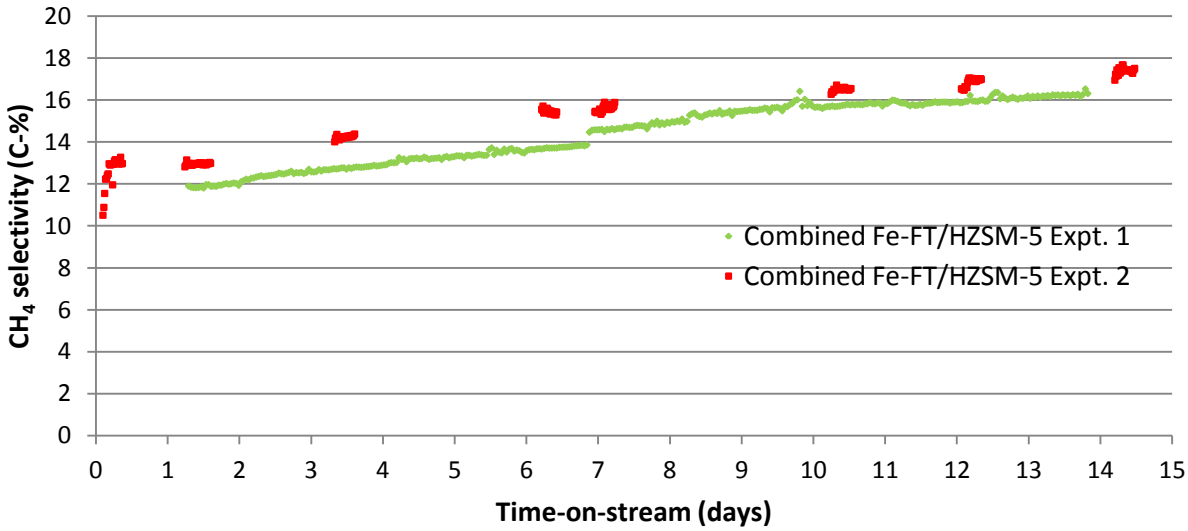

Figure 6.21: CH_4 selectivities for the combined Fe-FT/HZSM-5 experiments

6.3.2 HZSM-5 activity and selectivity

In all the results presented henceforth, the combined Fe-FT/HZSM-5 experiment will be represented by the combined Fe-FT/HZSM-5 Expt. 2. The zeolite activity is generally represented by its ability to carry out acid-catalyzed reactions and, therefore, the isomerization and aromatization activities of the acid co-catalyst are presented as the percentage of branched olefins (in the total olefins formed) and the selectivity to aromatics with time-on-stream, as shown in Figure 6.22 and Figure 6.23, respectively. However, since aromatization is the most demanding of the acid-catalyzed reactions, the amount of aromatics formed would be the best representative of the zeolite's activity with time-on-stream.

From Figure 6.22, there was a limited gradual decline in the percentage of branched olefins (in total olefins formed) with time-on-stream and, therefore, the zeolite's activity towards isomerization was not significantly affected over the duration of the combined Fe-FT/HZSM-5 experiment.

From Figure 6.23, however, the zeolite's activity towards aromatization was significantly affected over the duration of the combined experiment, as there was a rapid initial (ca. 2 days) decline in the aromatics selectivity after which the decline was relatively gradual with time-on-stream. This phenomenon was attributed to the rapid deactivation of the HZSM-5 zeolite within the first 2 days of synthesis time and consequently, the performance of HZSM-5 catalyst is best considered only after 2 days on-stream.

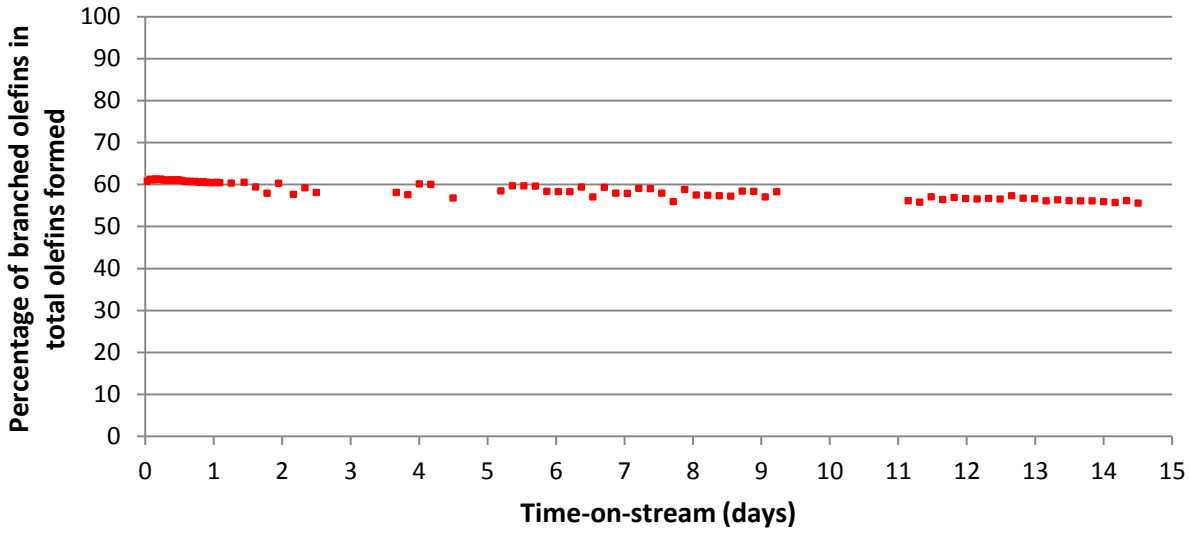

Figure 6.22: Percentage of branched olefins (in total olefins formed) for the combined Fe-FT/HZSM-5 Expt. 2

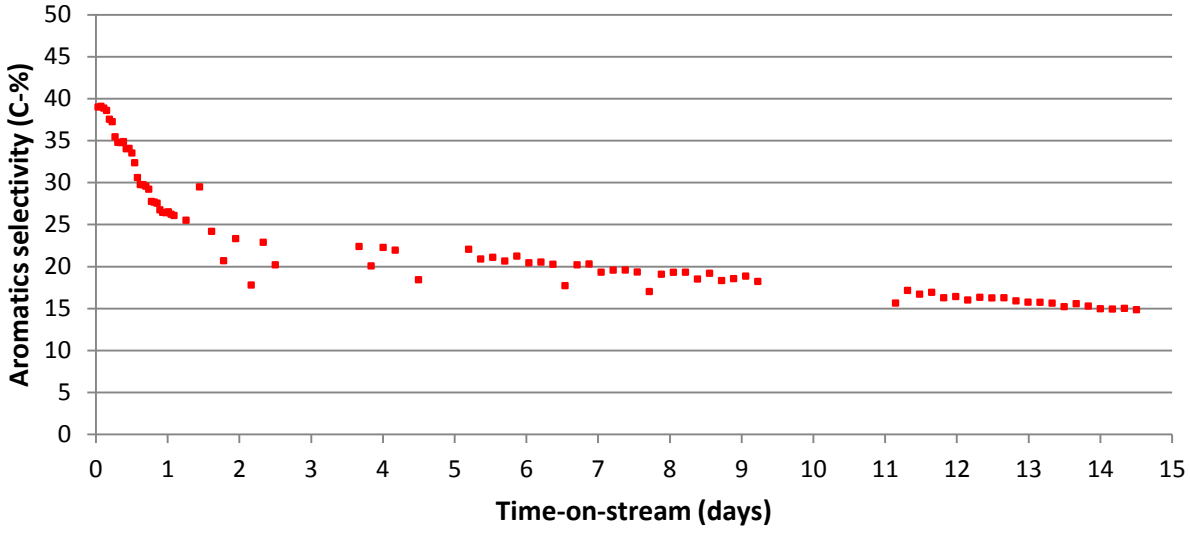

Figure 6.23: Aromatics selectivity for the combined Fe-FT/HZSM-5 Expt. 2

6.3.3 Product distribution

6.3.3.1 Product-type distribution

The product distribution (C_{2+}) with time-on-stream for the combined Fe-FT/HZSM-5 Expt. 2 is presented in Figure 6.24, from which it can be seen that the product selectivity stabilized after approximately 2 days on-stream with the addition of HZSM-5 to the Fe-FT process. This phenomenon, as mentioned previously, was attributed to the deactivation of the HZSM-5 zeolite, resulting in the initial rapid decrease in the aromatics selectivity and increase in the olefins selectivity. After 2 days on-stream, the zeolite gradually deactivated with time-on-stream, with a gradual decrease in the aromatics and paraffins selectivity and increase in the olefins selectivity with time-on-stream.

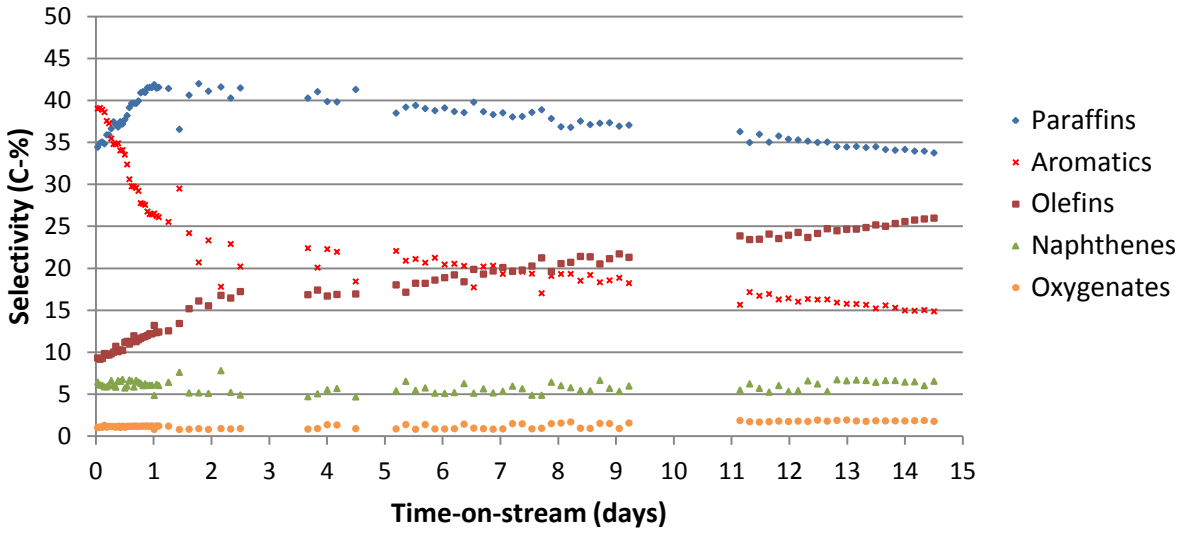

Figure 6.24: Product distribution (C_{2+}) with time-on-stream for the combined Fe-FT/HZSM-5 Expt. 2

The product distribution versus the carbon number range at 2.5 days on-stream for the combined Fe/HZSM-5 Expt. 2 is presented in Figure 6.25. The paraffin and olefin distribution at the beginning of the combined Fe-FT/HZSM-5 Expt. 2 are presented in Figure 6.26 and Figure 6.27, respectively. From Figure 6.25, the $C_3 - C_6$ fraction consisted mainly of paraffins, the $C_7 - C_{10}$ fraction consisted mainly of aromatics and there was a sharp cut-off of aliphatics around C_8. From Figures 6.26 and 6.27, the C_4 olefin distribution comprised only of n-butene and the C_{5+} olefin distribution consisted of a mixture of linear and branched olefins with the double bond in an internal position, while the C_{4+} paraffin distribution comprised mainly of branched paraffins.

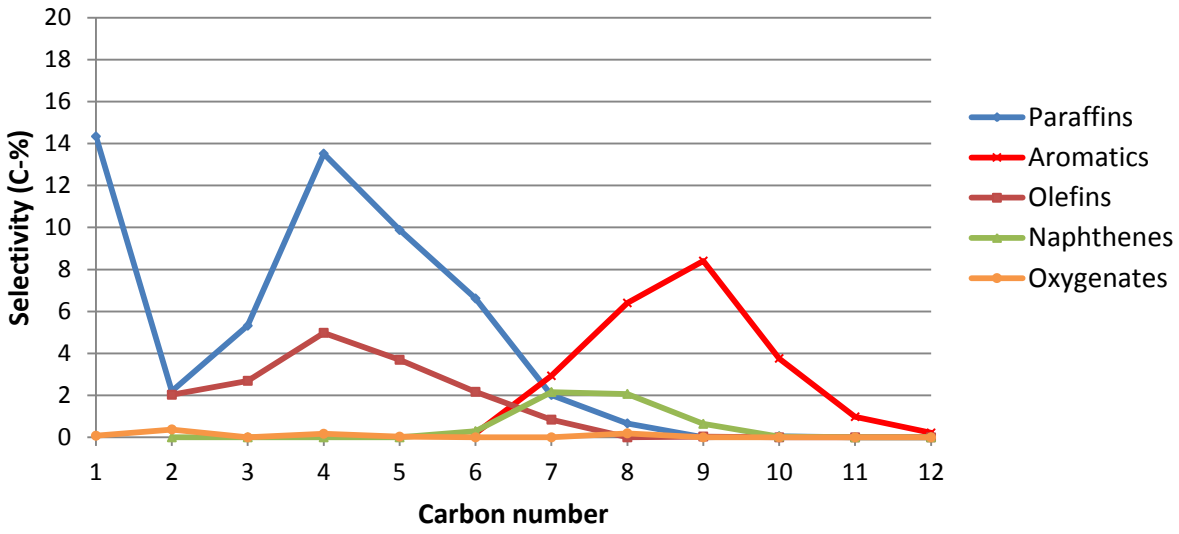

Figure 6.25: Product distribution versus carbon number range for the combined Fe-FT/HZSM-5 Expt. 2 (2.5 days on-stream)

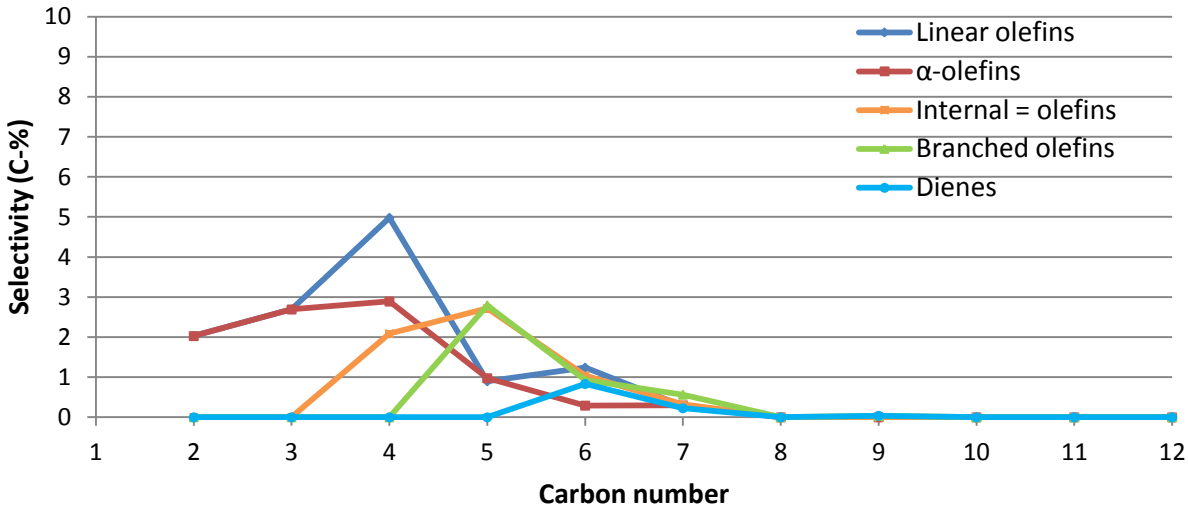

Figure 6.26: Olefin distribution versus carbon number range for the combined Fe-FT/HZSM-5 Expt. 2 (2.5 days on-stream)

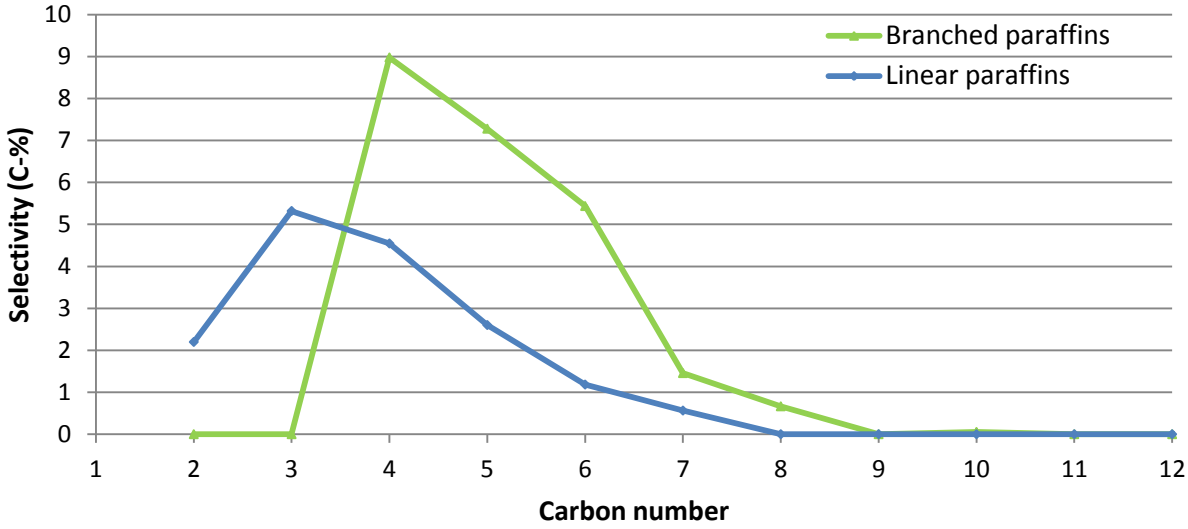

Figure 6.27: Paraffin distribution versus carbon number range for the combined Fe-FT/HZSM-5 Expt. 2 (2.5 days on-stream)

6.3.3.2 Carbon number distribution

The carbon number distributions of the total product at 2.5 days and 14 days on-stream for the combined Fe-FT/HZSM-5 Expt. 2 are presented in Figure 6.28, and the product distribution versus the carbon number range at 14 days on-stream for the combined Fe-FT/HZSM-5 Expt. 2 is presented in Figure 6.29. From Figure 6.28, there was a shift towards a lighter product spectrum after 14 days on-stream and from Figure 6.29 (in comparison to Figure 6.25), there was a significant decrease in the $C_7 - C_8$ aromatics and $C_4 - C_5$ paraffins selectivity, while the olefins selectivity increased. Moreover, at 14 days on-stream, there was still a sharp aliphatics cut-off around C_8, suggesting that cracking over the HZSM-5 zeolite was still readily occurring.

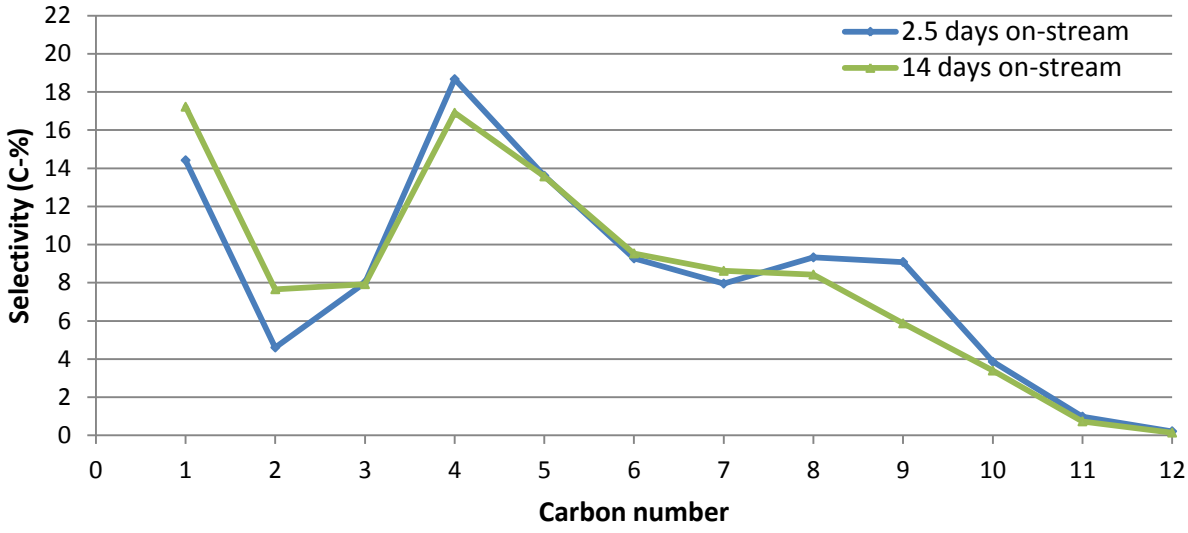

Figure 6.28: Carbon number distributions of the total product for the combined Fe-FT/HZSM-5 Expt. 2 (2.5 days and 14 days on-stream)

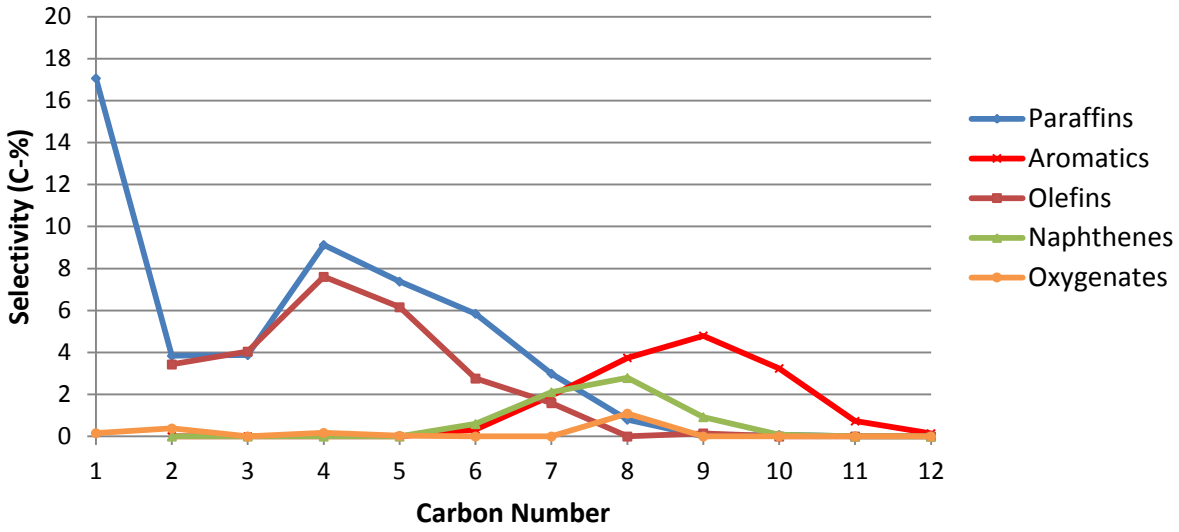

Figure 6.29: Product distribution versus carbon number range for the combined Fe-FT/HZSM-5 Expt. 2 (14 days on-stream)

6.3.3.3 Aromatics distribution

The aromatics distribution with time-on-stream for the combined Fe-FT/HZSM-5 Expt. 2 is presented in Figure 6.30, from which it can be seen that the C_8 and C_9 aromatics (mainly the xylenes, ethyl-toluenes and the 1,3,5-trimethyl-benzene as shown in Figure AIV.6 in Appendix IV) were the preferred aromatics for the combined Fe-FT/HZSM-5 experiment. After 2 days on-stream, the C_8 and C_9 aromatics percentage (in the total aromatics formed) gradually decreased with time-on-stream, whereas the other aromatics gradually increased (most significantly, the C_{10} aromatics).

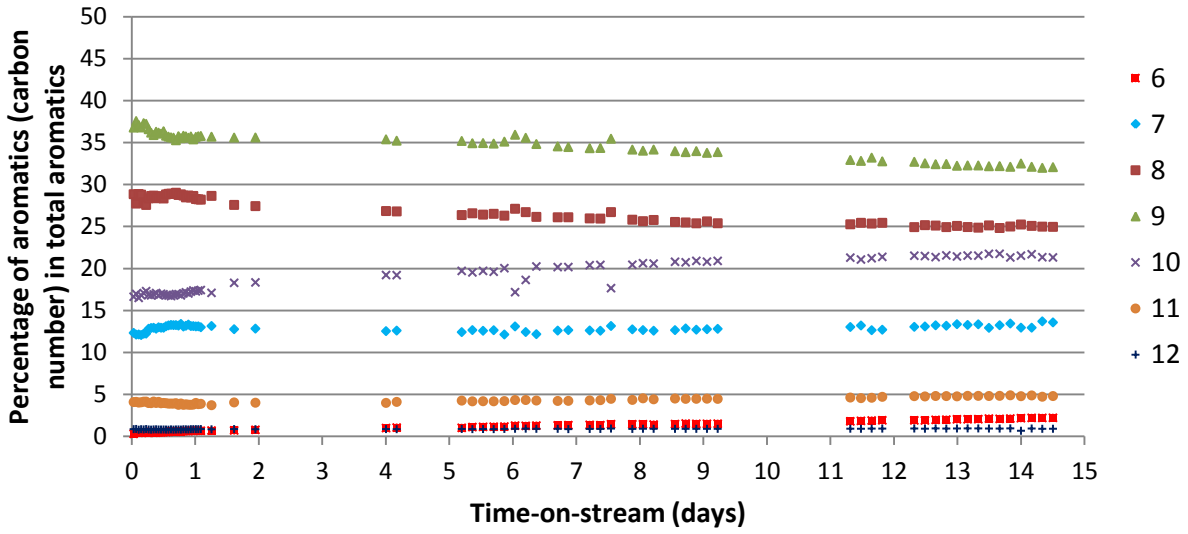

Figure 6.30: Aromatics distribution with time-on-stream for the combined Fe-FT/HZSM-5 Expt. 2

6.3.4 Gasoline selectivity and distribution

The gasoline selectivity and gasoline distribution for the combined Fe-FT/HZSM-5 Expt. 2 are presented in Figure 6.31 and Figure 6.32, respectively. From Figures 6.31 and 6.32, after 2 days on-stream, the gasoline selectivity slightly decreased with time-on-stream and appears to be almost stabilizing towards the end of the experiment. Similarly, the selectivity of aromatics gradually decreased, while the selectivity of paraffins and olefins gradually increased with time-on-stream.

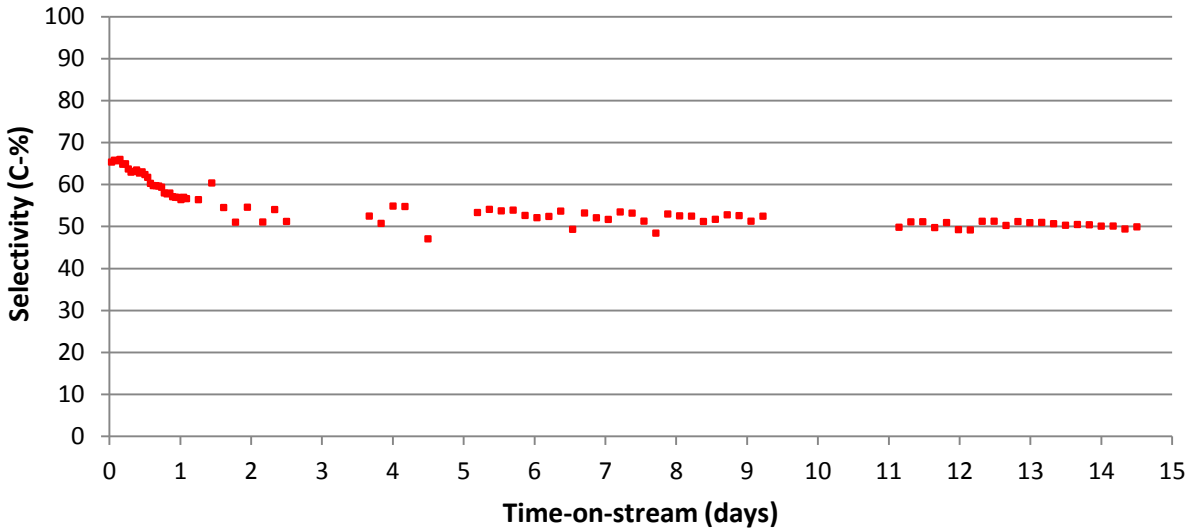

Figure 6.31: Gasoline ($C_5 - C_{11}$) selectivity for the combined Fe-FT/HZSM-5 Expt. 2

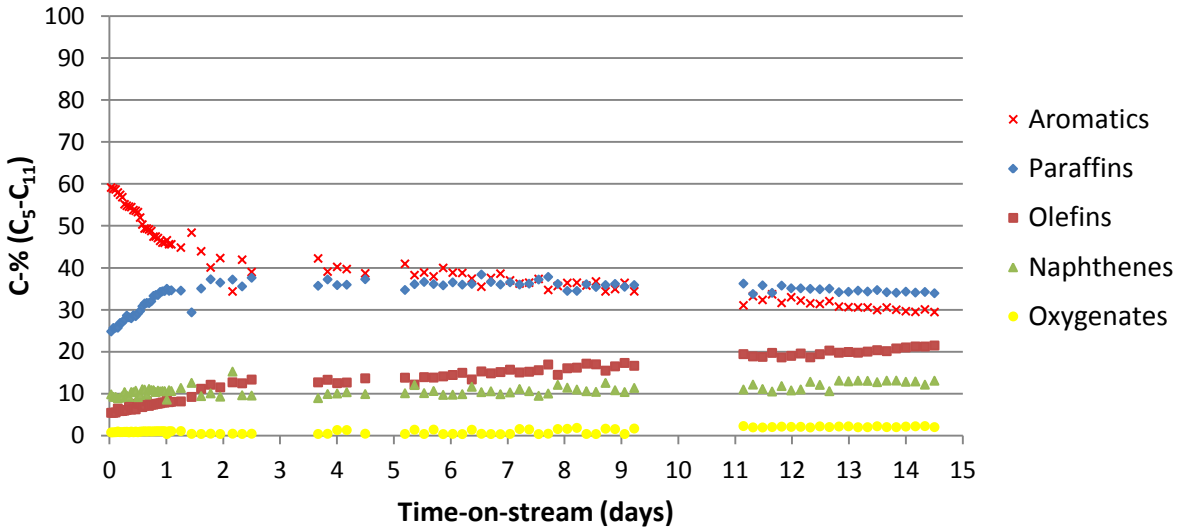

Figure 6.32: Gasoline ($C_5 - C_{11}$) distribution with time-on-stream for the combined Fe-FT/HZSM-5 Expt. 2

6.4 Catalyst characterization

6.4.1 Atomic absorption (AA) and atomic emission (AE) spectroscopy

The AA data obtained in this study was highly irreproducible and, consequently, the AAS results were not considered reliable in determining the potassium content in the fresh and spent catalysts. Nonetheless, the AAS results are recorded in Appendix IV.

The ICP-AE data was reproducible but the results were not used in the interpretation of the potassium migration, as significant potassium concentrations were measured in the fresh HZSM-5 catalyst, which is improbable as no potassium was intentionally added to the zeolite and only small amounts of potassium, if any, should be present in the fresh zeolite in the form of impurities. Likewise, the ICP-AES results are also recorded in Appendix IV.

6.4.2 X-Ray Fluorescence (XRF)

The XRF analysis of the fresh and spent Fe-FT and HZSM-5 catalysts are presented in Table 6.1, where all cations measured in the XRF spectrometer are presented as normal oxides in the table. For the combined Fe-FT/HZSM-5 experiments, there was a significant decrease in the potassium concentration in the spent Fe-FT catalysts as compared to the potassium concentration in the fresh Fe-FT catalyst, while there was a significant increase in the potassium concentration in the spent HZSM-5 as compared to the fresh HZSM-5 catalyst. Similarly, there was a significant decrease in the potassium concentrations of the spent Fe-FT catalysts as compared to the fresh Fe-FT catalyst for the Fe-FT experiments. A similar potassium concentration in the spent Fe-FT catalyst was obtained for the Fe-FT Expt. 2 and combined Fe-FT/HZSM-5 Expt. 1, both of which were run for ca. 14 days.

The Fe-FT and HZSM-5 catalysts were analyzed after reduction to see if any potassium migrates during the reduction process. The XRF analysis of the Fe-FT and HZSM-5 catalysts after the reduction procedure for the Fe-FT and combined Fe-FT/HZSM-5 catalyst configurations are shown in Table 6.2, from which it can be seen that the potassium concentrations of the reduced Fe-FT catalysts decreased by a similar amount for both catalyst configurations relative to the potassium concentration of the fresh Fe-FT catalyst, while there was no significant change in the potassium concentration of the HZSM-5 catalyst for the combined catalyst configuration.

Table 6.1: XRF analysis of the fresh and spent Fe-FT and HZSM-5 catalysts

Major Oxides (wt-%)*	**Fe-FT catalyst**					**HZSM-5 catalyst**		
	Fresh	*Fe-FT Expt. 1 (7 days)*	*Fe-FT Expt. 2 (14 days)*	*Combined Fe-FT/HZSM-5 Expt. 1 (14 days)*	*Combined Fe-FT/HZSM-5 Expt. 2 (15 days)*	*Fresh*	*Combined Fe-FT/HZSM-5 Expt. 1 (14 days)*	*Combined Fe-FT/HZSM-5 Expt. 2 (15 days)*
SiO_2	0.05	0.05	0.06	0.39	0.34	75.10	77.11	76.53
Al_2O_3	0.16	0.19	0.20	0.21	0.26	24.76	22.54	23.07
Fe_2O_3	99.54	99.58	99.60	99.26	99.24	0.14	0.18	0.27
K_2O	0.26	0.18	0.15	0.14	0.16	< 0.01	0.16	0.14
Fe	69.62	69.65	69.66	69.42	69.42	0.10	0.13	0.19
K	0.21	0.15	0.12	0.12	0.13	< 0.01	0.13	0.11
K/Fe	0.0030	0.0022	0.0018	0.0017	0.0019			

* Normalized to Si, Al, Fe, K and Cu oxides content

Table 6.2: XRF analysis of the Fe-FT and HZSM-5 catalysts after reduction

Major Oxide (wt-%)*	**Fresh catalyst**		**Fe-FT reduction experiment**	**Combined Fe-FT/HZSM-5 reduction experiment**	
	Fe-FT	*HZSM-5*	*Reduced Fe-FT*	*Reduced Fe-FT*	*HZSM-5*
SiO_2	0.09	75.43	0.12	0.15	75.11
Al_2O_3	0.16	24.49	0.22	0.26	24.47
Fe_2O_3	99.50	0.07	99.45	99.36	0.41
K_2O	0.25	< 0.01	0.21	0.22	0.01
Fe	69.60	0.05	69.56	69.50	0.29
K	0.21		0.18	0.18	
K/Fe	0.003		0.0025	0.0026	

* Normalized to Si, Al, Fe, K and Cu oxides content

7 DISCUSSION

7.1 Reproducibility

The reproducibility of the experiments carried out in the STIRR was tested by repeating both the Fe-FT and the combined Fe-FT/HZSM-5 experiments. From Figures 6.4 – 6.10, the conversions and selectivities obtained for the Fe-FT experiments were almost identical and followed similar trends and, therefore, the Fe-FT experiments were deemed sufficiently reproducible.

From Figures 6.18 – 6.21, there were slight discrepancies observed in the conversion and selectivity values obtained for the combined Fe-FT/HZSM-5 experiments, although the trends were similar with time-on-stream and, therefore, the combined Fe-FT/HZSM-5 experiments were deemed sufficiently reproducible for comparison of the catalytic performance with time-on-stream.

7.2 Comparison of Fe-FT catalyst performance to literature

The product selectivities obtained from the STIRR used in this study for the Fe-FT experiment were compared, in Table 7.1, to the product selectivities obtained in Sasol's synthol reactor (Dry, 1981) and a Berty reactor (Botes and Böhringer, 2004).

A similar Fe-FT product spectrum was obtained from the two internal recycle reactors with the most noticeable difference being the increase in oxygenates produced in the STIRR, which was probably due to the high amounts of copper-promotion of the Fe-FT catalyst used in this study (see Table 5.2). Therefore, the FT catalyst performance for the Fe-FT experiment carried out in

the STIRR under the experimental conditions was deemed credible when compared to the product spectrum obtained by Botes and Böhringer (2004).

There was a shift towards a lighter product spectrum when the product selectivities obtained from the two internal recycle reactors were compared to that obtained from Sasol's synthol reactor, but this may be due to various reasons including the different type and form of Fe-FT catalysts used, as well as the different reactor conditions and hydrodynamics experienced in an industrial reactor as compared to a lab reactor.

Table 7.1: Comparison of product selectivities obtained for the Fe-FT experiment in the STIRR to that obtained in a Berty reactor (Botes and Böhringer, 2004)

	This study[a]	Berty reactor[a,b]	Sasol[c]
CO Conversion	83	79	-
Syngas space velocity (ml/min/g unreduced Fe cat.)	159	200	-
Selectivities (C-%)			
CH_4	11	12	10
C_2-C_4 paraffins	6	5	8
C_2-C_4 olefins	35	37	25
C_5-C_{11}	37	38	40
C_{12+}	1	2	11
Water soluble chemicals	10	6	5
ASF α-value	0.6	0.65	0.7

[a] TOS - 1 day; [b] Old Berty reactor at 330°C and 20 bar (Botes and Böhringer, 2004);

[c] Iron fluidized bed at 325°C and 22 bar (Dry, 1981)

7.3 Fe-FT performance vs. combined Fe-FT/HZSM-5 performance

7.3.1 Fe-FT catalytic activity

The $CO+CO_2$ conversions for both the Fe-FT experiments and the combined Fe-FT/HZSM-5 experiments are compared in Figure 7.1, from which it can be seen that the addition of HZSM-5 to the Fe-FT process did not seem to significantly affect the Fe-FT activity with time-on-stream, as the $CO+CO_2$ conversion for the combined experiments gradually declined with time-on-stream in much the same manner as the $CO+CO_2$ conversion observed for the Fe-FT experiments.

The CH_4 selectivities for both the Fe-FT and combined Fe-FT/HZSM-5 experiments are compared in Figure 7.2, from which it can be seen that there was an initial increase in the CH_4 selectivity and a slightly more rapid increase with time-on-stream for both the combined Fe-FT/HZSM-5 experiments.

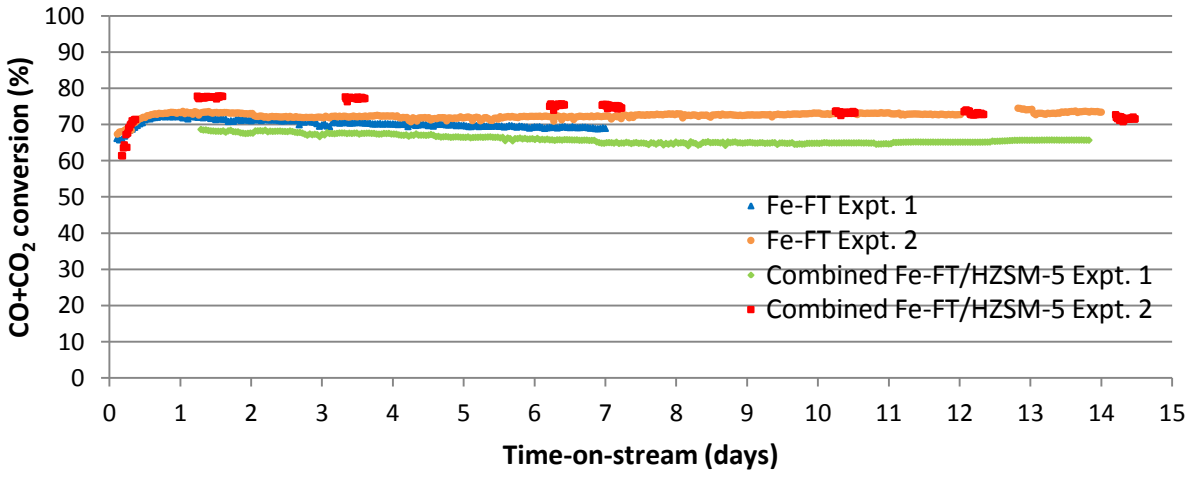

Figure 7.1: $CO+CO_2$ conversions for both the Fe-FT experiments and combined Fe-FT/HZSM-5 experiments

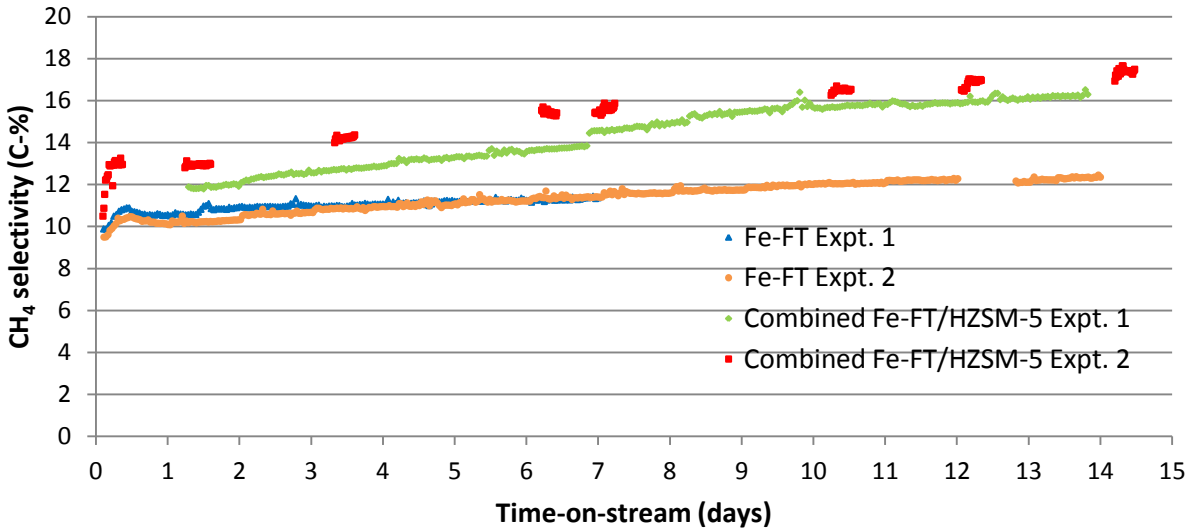

Figure 7.2: CH_4 selectivities for both the Fe-FT experiments and combined Fe-FT/HZSM-5 experiments

The H/C molar ratios of the overall product spectrum and of the C_{2+} fraction for the Fe-FT Expt. 2 and the combined Fe-FT/HZSM-5 Expt. 2 are compared in Figure 7.3 and Figure 7.4, respectively. From Figures 7.3 and 7.4, the hydrogen content of the combined Fe-FT/HZSM-5 product spectrum was lower than that of the Fe-FT product spectrum, and this was more noticeable in the C_{2+} fraction. HZSM-5 is not known to have a significant ability to activate molecular hydrogen and, therefore, it appears that the addition of HZSM-5 to the Fe-FT process changed the product selectivity over the Fe-FT catalyst to that of a less hydrogenated product spectrum. From Figure 7.3, there was a rapid initial increase in the H/C ratio of the overall product spectrum for the combined Fe-FT/HZSM-5 experiment followed by a gradual increase with time-on-stream, a trend that is reflected by the change in the CH_4 selectivity with time-on-stream. From Figure 7.4, the increase in the H/C ratio of the C_{2+} fraction was less rapid initially and slightly increased with time-on-stream. Therefore, excluding the effect of CH_4 on the overall hydrocarbon product spectrum and considering that HZSM-5 is not known to have a significant ability to activate molecular hydrogen, it appears that

the selectivity of the Fe-FT catalyst (towards saturated products) is not significantly affected with time-on-stream for the combined Fe-FT/HZSM-5 experiment.

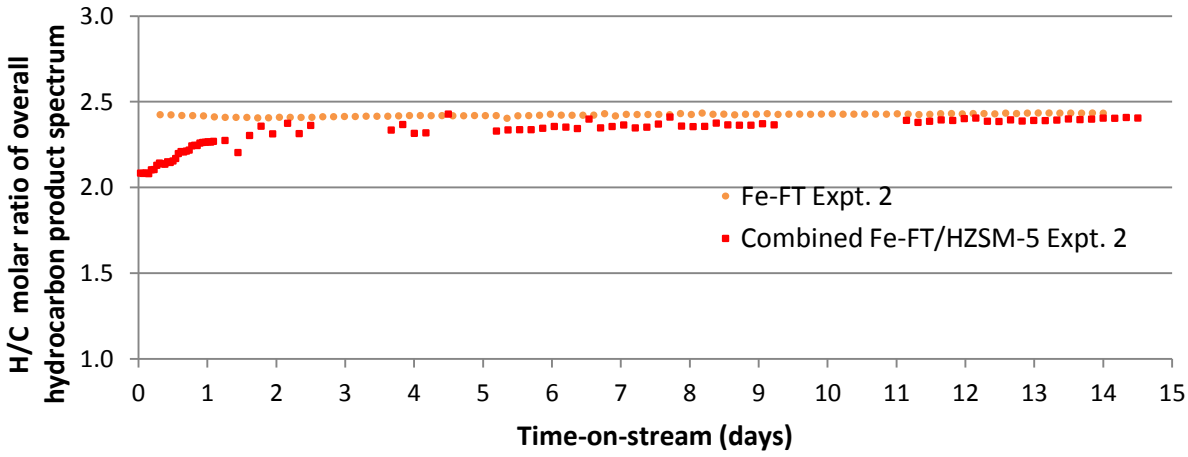

Figure 7.3: H/C molar ratio of overall hydrocarbon product spectrum for the Fe-FT Expt. 2 and the combined Fe-FT/HZSM-5 Expt. 2

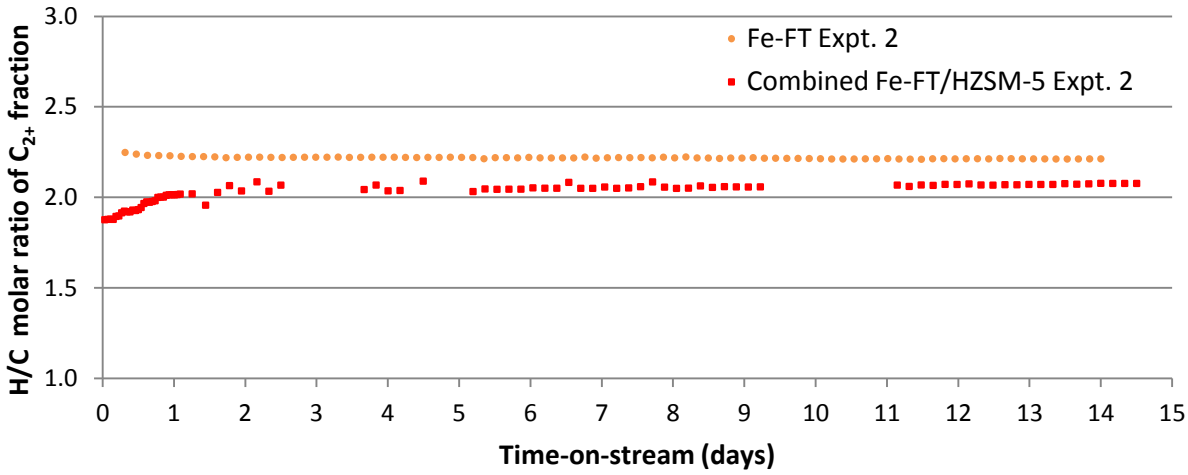

Figure 7.4: H/C molar ratio of C_{2+} fraction of overall hydrocarbon product spectrum for the Fe-FT Expt. 2 and the combined Fe-FT/HZSM-5 Expt. 2

7.3.2 Carbon number and product type distribution

Comparing Figure 6.13 to Figure 6.24, the addition of HZSM-5 to the Fe-FT process led to the formation of a significant amount of aromatics and paraffins. The olefins that had initially formed over the Fe-FT catalyst were mostly consumed due to the oligomerization of the lighter olefins and also due to the formation of aromatics and co-product paraffins over the HZSM-5 zeolite. The formation of paraffins over the HZSM-5 zeolite occurs primarily through the transfer of protons and hydride ions to olefins during the formation of aromatic rings and secondarily through the cracking of heavier paraffins (whereby long chain paraffin cracks into an olefin and a paraffin). Initially, the zeolite deactivated rapidly, as indicated in Figure 6.24 by the rapid decline in aromatics selectivity, after which (ca. 2 days on-stream), there was a gradual decrease in the aromatics and paraffins selectivity and an increase in the olefins selectivity, as less olefins were being converted into aromatics with the progressing deactivation of the HZSM-5 zeolite. The initial increase in the paraffins selectivity is not contradicting the decrease in co-product aromatics, but instead it reflects the initial deep cracking of the aliphatics product fraction.

The carbon number distributions at 2.5 days on-stream for the Fe-FT Expt. 2 and the combined Fe-FT/HZSM-5 Expt. 2 are compared in Figure 7.5, from which it can be seen that the addition of HZSM-5 to the Fe-FT process led to a substantial increase in the C_4 and $C_7 - C_{10}$ selectivity, and decrease in the $C_1 - C_3$ selectivity. The originally highly olefinic and alcohol containing FT product (with its maximum in carbon number distribution at C_3 (14 C-% propene, see Figure 6.12), followed by steady exponential decline) is converted over the acid zeolite into a predominantly aromatic/paraffinic product with a bimodal carbon number distribution. The C_1 selectivity decreased since the rather large amounts of methanol that had formed on the Fe-FT catalyst (6 C-%, see Figure 6.12) were readily converted into olefins and subsequently aromatics and paraffins over HZSM-5 (see methanol-free product distribution from the combined Fe-FT/HZSM-5 catalyst system, Figure 6.25). The increase in the $C_7 - C_{10}$ selectivity was due to

the formation of aromatics (particularly of the C_8 – C_9 aromatics) with the addition of HZSM-5 to the Fe-FT process. The high selectivity to C_3 – C_6 paraffins was likely due to the limited reactivity of light paraffins over HZSM-5, rapid cracking of the longer aliphatics into lighter olefins and paraffins, and the transfer of proton and hydride ions to form paraffins during aromatization. The C_4 – C_6 fraction mainly comprised of branched paraffins, reflecting the isomerization activity of HZSM-5. The percentage of olefins remaining was low and hardly any oxygenates were left.

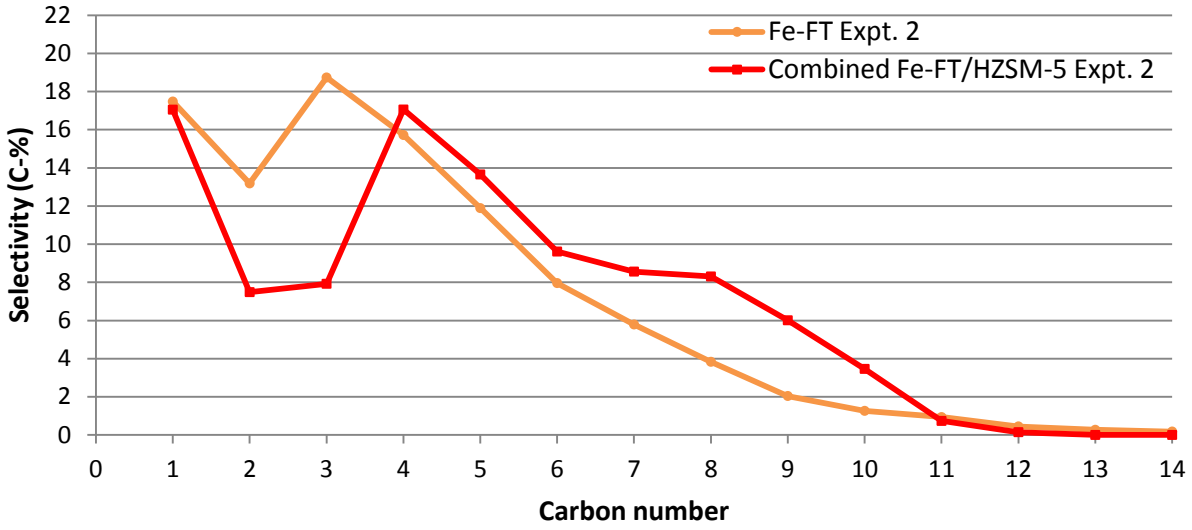

Figure 7.5: Carbon number distributions for the Fe-FT Expt. 2 and the combined Fe-FT/HZSM-5 Expt. 2 (2.5 days on-stream)

7.3.3 Gasoline selectivity and quality

The gasoline selectivities for the Fe-FT Expt. 2 and the combined Fe-FT/HZSM-5 Expt. 2 are compared in Figure 7.6, from which it can be seen that there was a significant increase in the gasoline selectivity (approximately 1.5 times as much) when HZSM-5 was added to the Fe-FT process. The rapid initial decline, followed by a gradual decline of the gasoline selectivity with

time-on-stream for the combined Fe-FT/HZSM-5 experiment was attributed to the deactivation of the HZSM-5 zeolite.

The gasoline compositions at 2.5 days and 14 days on-stream for the Fe-FT Expt. 2 and the combined Fe-FT/HZSM-5 Expt. 2 are compared in Table 7.2. The gasoline quality was assessed by its content of aromatics and branched aliphatic compounds, due to their high octane numbers (see Section 2.1.1). As expected (Dry, 1981), the Fe-FT product spectrum comprised mainly of linear aliphatics (mostly linear olefins) and small amounts of aromatics, which indicates a low gasoline quality in terms of its octane rating. From Table 7.2, it is evident that the addition of HZSM-5 to the Fe-FT process considerably improved the gasoline quality, due to the ability of the zeolite to produce aromatics and branched aliphatic compounds, although the latter may be partially offset by the increased amount of paraffins (particularly linear paraffins) formed.

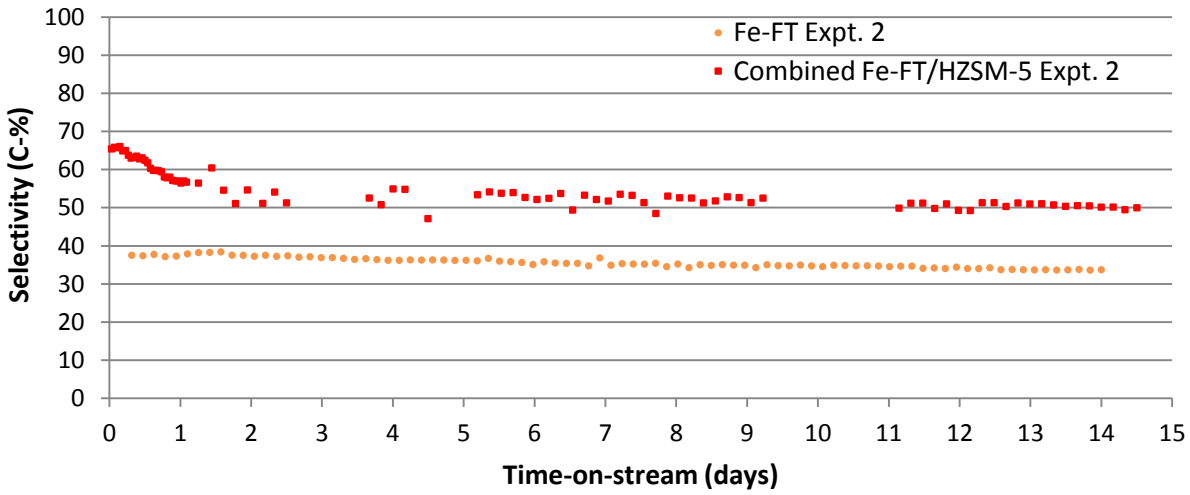

Figure 7.6: Gasoline (C_5-C_{11}) selectivities for the Fe-FT Expt. 2 and the combined Fe-FT/HZSM-5 Expt. 2

Table 7.2: Gasoline (C_5-C_{11}) compositions (C-%) for the Fe-FT Expt. 2 and combined Fe-FT/HZSM-5 Expt. 2

		TOS – 2.5 days		TOS – 14 days	
		Fe-FT Expt. 2	*Combined Fe-FT/HZSM-5 Expt. 2*	*Fe-FT Expt. 2*	*Combined Fe-FT/HZSM-5 Expt. 2*
Olefins		72	13	76	21
	Linear	75	35	79	28
	Branched	25	65	21	72
Paraffins		16	38	14	34
	Linear	54	24	58	23
	Branched	46	76	42	77
Naphthenes		1	10	1	13
Aromatics		3	39	2	30
Oxygenates		8	< 1	7	2

7.4 Comparison of the combined Fe-FT/HZSM-5 catalyst performance to literature

7.4.1 Fe-FT and HZSM-5 catalytic activity

Botes and Böhringer (2004), Botes (2005) and Pour et al. (2008a) observed a significant loss in the Fe-FT activity and increase in the CH_4 selectivity with time-on-stream, while Schulz et al. (1991a) observed a stable Fe-FT activity but a rapid initial increase in the CH_4 selectivity, followed by a very slight and gradual increase with time-on-stream, when the two catalysts in the combined Fe-FT/HZSM-5 experiment were in intimate contact. In this study, there was no significant change in the Fe-FT activity with time-on-stream in the combined catalyst system but there was an increase in the CH_4 selectivity with the addition of HZSM-5 to the Fe-FT process.

Botes and Böhringer (2004), Botes (2005), Martinez and Lopez (2005) and Pour et al. (2008a) observed that the HZSM-5 zeolite deactivates most rapidly in the initial period of synthesis followed by a gradual decrease with time-on-stream for the combined catalyst system. Likewise, a rapid initial deactivation of the HZSM-5 zeolite followed by a gradual decline with time-on-stream was observed in this study.

The decline in the performance of the combined Fe-FT/HZSM-5 catalyst system has been claimed, by some authors, to be a result of alkali migrating away from the Fe-FT catalyst and onto the acidic sites of the HZSM-5 zeolite (Butter et al., 1981; Udaya et al., 1990; Botes and Böhringer, 2004; Botes, 2005; Pour et al., 2008a).

7.4.2 Carbon number and hydrocarbon distribution

The carbon number distribution of the combined Fe-FT/HZSM-5 experiment showed a significant decrease in the $C_2 - C_3$ selectivity, a considerable increase in the $C_7 - C_{10}$ selectivity and a sharp cut-off in the product spectrum around C_{11} with the addition of HZSM-5 to the Fe-FT process, as was observed by Schulz et al. (1991a) and Botes and Böhringer (2004). In addition, the $C_3 - C_6$ selectivity consisted mainly of paraffins (largely branched), whereas the $C_7 - C_{10}$ selectivity consisted mainly of aromatics (predominantly the C_8-C_9 aromatics).

Furthermore, a significant increase in the gasoline selectivity and a highly aromatic and branched hydrocarbon product distribution was obtained, as was observed by numerous authors (Chang and Lang, 1978; Caesar et al., 1979; Rao and Gormley, 1980; Brennan et al., 1981; Butter et al., 1981; Dwyer and Garwood, 1982; Varma et al., 1986; Varma et al., 1987; Schulz et al., 1991a; Botes and Böhringer, 2004; Botes, 2005; Martinez and Lopez, 2005; Pour et al., 2008a; Pour et al., 2009).

7.5 Potassium balance

From the results presented in Section 6.4, the XRF analyses of the fresh and spent Fe-FT and HZSM-5 catalysts show that a noticeable and similar amount of potassium was lost from the Fe-FT catalyst in both the Fe-FT and combined Fe-FT/HZSM-5 experiments, and the amount of potassium lost was dependent on the duration of the individual experiments. Likewise, similar amounts of potassium were lost from the Fe-FT catalysts during the reduction procedure for both the Fe-FT and combined Fe-FT/HZSM-5 catalyst configurations.

It is not clear as to where the potassium diffuses to during the Fe-FT experiment but in the presence of the HZSM-5 zeolite, it is clear from the analyses that HZSM-5 traps this potassium in the combined Fe-FT/HZSM-5 experiment. However, potassium does not appear to be accessible to HZSM-5 under reduction conditions as there was no significant change in the potassium concentration of the HZSM-5 catalyst for the combined Fe-FT/HZSM-5 catalyst configuration and, therefore, it appears that the potassium required synthesis conditions (most likely with the increase of water vapour) to migrate to the zeolite.

7.6 Interpretation of catalyst characterization results with the performance of the combined Fe-FT/HZSM-5 catalyst system

The XRF analyses show that potassium did migrate to the HZSM-5 zeolite in the combined Fe-FT/HZSM-5 experiments, but the extent to which deactivation of the HZSM-5 proceeded due to coking or poisoning of the zeolite's acid sites by potassium was not apparent. However, the amount of potassium that migrated from the Fe-FT catalyst to the zeolite (approximately half of the originally present amount, see Table 6.2) could only have neutralized about 12% of the acid sites in the fresh HZSM-5 zeolite. Therefore, in this study, coking appears to be the more

significant contributor towards the deactivation of the HZSM-5 zeolite as compared to poisoning of the zeolite acid sites by potassium.

The XRF analyses of the fresh and spent Fe-FT catalysts shows that there were similar amounts of potassium lost from the Fe-FT catalysts for both the Fe-FT and combined Fe-FT/HZSM-5 experiments despite the observed increase in the CH_4 selectivity with the addition of HZSM-5 to the Fe-FT process (see Figure 7.2). Therefore, the catalyst characterization results refute the hypothesis of potassium migration away from the Fe-FT catalyst being the cause of the increase in CH_4 selectivity with the addition of HZSM-5 to the Fe-FT process. Indeed, the decline in activity of the Fe-FT catalysts that would have accompanied an effective loss of potassium was not observed (see Figure 7.1). Furthermore, it appears, see Table 6.2, that the loss of potassium from the Fe-FT catalyst is limited and the potassium content stabilizes after several days on-stream.

It is known that coke formation over a zeolite is generally associated with CH_4 formation (Langner, 1982; Schulz et al., 1991a; Schulz et al., 1993; Bauer et al., 1994; Bauer et al., 1996; Schulz and Wei, 1999), such that the increased CH_4 values of the combined Fe-FT/HZSM-5 experiments may reasonably be ascribed to declining zeolite performance (by coking) and not to a decline in the chain growth probability of the Fe-FT catalysts by a loss of potassium promoter. Activated hydrogen from the reaction of light alkanes over zeolites is known to react with coke or coke precursors to form small volatile compounds such as CH_4 (Bauer et al., 1994; Bauer et al., 1996). In the presence of molecular hydrogen and an FT catalyst as in this study, a source of activated hydrogen is likely to be the Fe-FT catalyst, where the activated hydrogen migrates to the zeolite crystallites and surface by spillover. In addition, methanol (that is produced at ca. 6 C-% selectivity over the Fe-FT catalyst) is well known to convert, to some extent, to CH_4 over zeolites at temperatures similar to those used in this study (Langner, 1982; Schulz et al., 1991b; Schulz et al., 1993; Schulz and Wei, 1999).

8 CONCLUSIONS AND RECOMMENDATIONS

This work confirms the Fe-FT catalyst performance in a STIRR under typical high temperature FT conditions when compared to the performance obtained by other authors. The performance of the combined Fe-FT/HZSM-5 catalyst system was similar to what is observed in literature in relation to the carbon number and product distribution, and the more rapid increase in the CH_4 selectivity observed with time-on-stream when HZSM-5 is added to the Fe-FT process.

It has been reconfirmed that a highly aromatic and branched hydrocarbon product, and a significant increase in the gasoline selectivity is obtained with the addition of HZSM-5 to the Fe-FT process, but also that the gasoline and aromatic selectivities decline with time-on-stream. This work also confirms the somewhat higher level and more rapid increase in the CH_4 selectivity observed with time-on-stream when HZSM-5 is added to the Fe-FT process.

Furthermore, this study also shows that no relationship exists between potassium migration and the more rapid increase in the CH_4 selectivity with the addition of HZSM-5 to the Fe-FT process, as similar amounts of potassium were lost from the Fe-FT catalyst for both the Fe-FT and combined Fe-FT/HZSM-5 experiments. Moreover, the Fe-FT activity, as determined by the $CO+CO_2$ conversion, is unchanged by both, the partial loss of potassium promoter and the presence of the HZSM-5 zeolite. The deactivation of HZSM-5 was primarily a result of zeolite coking in this study, which was also ascribed to be the cause of the observed increase in the CH_4 selectivity in the combined system. Nonetheless, to further confirm that no relationship exists between potassium migration and the increase in CH_4 selectivity, it is recommended that the performance of an Fe-FT and combined Fe-FT/HZSM-5 catalyst system (containing an Fe-FT catalyst with no alkali promotion) be tested and compared.

REFERENCES

Anderson, R., 1956. Kinetics and reaction mechanism of the Fischer-Tropsch synthesis: In P.H. Emmetty, ed. *Catalysis.* Reinhold Publishing Corporation. Vol. IV, p. 257-372.

Anderson, R., 1984. *The Fischer-Tropsch Synthesis.* Orlando: Academic Press.

Arakwa, H. and Bell, A., 1983. Effects of potassium promotion on the activity and selectivity of iron Fischer-Tropsch Catalysis. *Industrial and Engineering Chemistry Process Design and Development*, 22, p. 97-103.

Barthomeuf, D., 1987. Zeolite acidity dependence on structure and chemical environment. Correlations with catalysis, *Materials Chemistry and Physics*, 17, p. 49-71.

Bauer, F., Geidel, E. and Petzold, E., 1994. Reactivation of coked HZSM-5 by hydrogen and by alkane treatment. *Studies in Surface Science and Catalysis*, 84, p. 1749-1755.

Bauer, F., Ernst, H., Geidel, E. and Schödel, R., 1996. Reactivation of coked HZSM-5 by treatment with hydrogen and alkane. *Journal of Catalysis*, 164, p. 146-151.

Berty, J., 1974. Reactor for vapour-phase catalytic studies. *Chemical Engineering Progress*, 70 (5), p. 76-84.

Botes, F., 2002. The addition of HZSM-5 to the Fischer-Tropsch process for improved gasoline production. MSc dissertation. University of Cape Town.

Botes, F. and Böhringer, W., 2004. The addition of HZSM-5 to the Fischer-Tropsch process for improved gasoline production. *Applied Catalysis A: General*, 267, p. 217-225.

Botes, F., 2005. The effect of a higher operating temperature on the Fischer-Tropsch/HZSM-5 bifunctional process. *Applied Catalysis A: General*, 284, p. 21-29.

Brennan, J., Caesar, P., Pitman, J. and Garwood, W., 1981. U.S Patent 4304871.

Brosius, R. and Fletcher, J., 2010. Direct measurement of recycle ratios in internal recycle laboratory reactors. *Chemical Engineering Journal*, 161, p. 196-203.

Bussemeier, B., Frohning, C. and Cornels, B., 1976. *Hydrocarbon Processing*, 55 (11), p. 105-110.

Butter, S., Chester A. and Schwartz, A., 1981. U.S Patent 4298695 to Mobil Oil Corporation.

Caeser, P., Brennan, J., Garwood, W. and Ciric, J., 1979. Advances in Fischer-Tropsch chemistry. *Journal of Catalysis*, 56, p. 274-278.

Carberry, J., 1964. Designing laboratory catalytic reactors. *Industrial and Engineering Chemistry*, 56 (39), p. 39-46.

Chang, C., Lang, W. and Silvestri, A., 1978. U.S Patent 4086262 to Mobil Oil Corporation.

Claeys, M. and van Steen, E., 2004. Basic studies. In A. Steynberg and M. Dry, eds. Fischer-Tropsch Technology. *Studies in Surface Science and Catalysis*. Vol. 152. Elsevier. Ch. 8.

Csicsery, S., 1986. Catalysis by shape selective zeolite – science and technology. *Pure and Applied Chemistry*, 58 (6), p. 841-856.

Derouane, E. and Gabelica, Z., 1980. *Journal of Catalysis*, 65, p. 486.

Dry, M., 1981. In J. Anderson and M. Boudart, eds. *Catalysis Science and Technology*. Vol. I. Springer-Verlag, p. 159-255.

Dry, M., 1990. Fischer-Tropsch synthesis over iron catalysts. *Catalysis Letters*, 7, p. 241-252.

Dry, M., 1996. Practical and theoretical aspects of the catalytic Fischer-Tropsch process. *Applied Catalysis A: General*, 138, p. 319-344.

Dry, M., 2002. The Fischer-Tropsch Process: 1950-2000. *Catalysis Today*, 71 (3-4), p. 227-241.

Dry, M., 2004a. Chemical concepts used for engineering purposes. In A. Steynberg and M. Dry, eds. Fischer-Tropsch Technology. *Studies in Surface Science and Catalysis*. Vol. 152. Elsevier. Ch. 3.

Dry, M., 2004b. FT catalysts. In A. Steynberg and M. Dry, eds. Fischer-Tropsch Technology. *Studies in Surface Science and Catalysis*. Vol. 152. Elsevier. Ch. 7.

Dry, M., 2004c. Commercial FT process applications. In A. Steynberg and M. Dry, eds. Fischer-Tropsch Technology. *Studies in Surface Science and Catalysis*. Vol. 152. Elsevier. Ch. 5.

Dry, M., 2008. The Fischer-Tropsch (FT) synthesis processes. *Handbook of Heterogeneous Catalysis* 6. 3rd ed. p. 2965-2994.

Dwyer, F. and Garwood, W., 1982. U.S Patent 4361503 to Mobil Oil Corporation.

Ertl, G., Prigge, D., Schlogl, R. and Weiss, M., 1983. *Journal of Catalysis*, 79, p. 359.

Fraenkel, D., Cherniavsky, M. and Levy, M., 1984. *Proceedings: 8th International Congress on Catalysis*. Berlin, Vol. IV, p. 545-554.

Gates, B., Katzer, J. and Schuit, J., 1979. *Chemistry of Catalytic Processes*. USA: McGraw-Hill.

Guan, N., Liu, Y. and Zhang, M., 1996. Development of catalysts for the production of aromatics from syngas. *Catalysis Today*, 30, p. 207-213.

Guisnet, M. and Magnoux, P., 1989. Coking and deactivation of zeolites: influence of the pore structure. *Applied Catalysis*, 54 (1), p. 1-27.

Guisnet, M. and Magnoux, P., 1997. Deactivation by coking of zeolite catalysts. Prevention of deactivation. Optimal conditions for regeneration. *Catalysis Today*, 36, p. 477-483.

Guisnet, M., Costa, L. and Ribeiro, F., 2009. Prevention of zeolite deactivation by coking. *Journal of Molecular Catalysis A: Chemical*, 305, p. 69-83.

Gwagwa, Y. and van Steen, E., 2009. Migration of potassium in an Fe_2O_3/H-ZSM-5 composite catalyst. *Chemical Engineering and Technology*, 32 (5), p. 826-829.

Haag, W. and Huang, T., 1981. U.S Patent 4279830 to Mobil Oil Corporation.

Horsley, J., Corma, A., Derouane, E. and Guisnet, M., 1993. New zeolite applications in the petroleum and petrochemical industries. *Catalytica Studies Division*, p. 223.

Haag, W. and Chen, N., 1981. *Catalysis Design Progress and Perspectives*. John Wiley and Sons.

IZA (International Zeolite Association – Structure Commission), 2002. Database of Zeolite Structures, [Online]. Available at: http://www.iza-structure.org/databases/ [accessed 31 June 2010].

Jacobs, A. and Martens, A., 1991. Introduction to acid catalysis with zeolites in hydrocarbon reactions. In H. van Bekkum, E. Flanigen and J. Jansen, eds. Introduction to Zeolite Science and Practise. *Studies in Surface Science and Catalysis*. Vol. 58. Elsevier. Ch. 12.

Jager, B., and Espinoza, R., 1995. Advances in low temperature Fischer-Tropsch synthesis. *Catalysis Today*, 23 (1), p. 17-28.

Jothimurugesan, K. and Gangwal, S., 1998. Titania-supported bimetallic catalysts combined with HZSM-5 for Fischer-Tropsch synthesis. *Industrial Engineering Chemical Reserves*, 37, pp. 1181-1188.

Kaiser, R. 1969. *Chromatographie in der gasphase*. Bibliographisches Insitut, Mannheim.

Langner, B., 1982. Reactions of methanol on zeolites with different pore structures. *Applied Catalysis*, 2, p. 289-302.

Loggenberg, P., Dry, M. and Copperthwaite, R., in press, *ECASIA 89,* Antibes, France.

Martens, J. and Jacobs, P., 1997. Reaction mechanisms of acid-catalyzed hydrocarbon conversions in zeolites. In G. Ertl, H., Knozinger and J. Weitkamp, eds. *Handbook of Heterogeneous Catalysis*. Wiley, Vol. 3.

Martinez, A. and Lopez. C., 2005. The influence of ZSM-5 zeolite composition and crystal size on the situ conversion of Fischer-Tropsch products over hybrid catalysts. *Applied Catalysis A: General*, 294, p. 251-259.

Maxwell, I. and Stork, W., 1991. *Studies in Surface Science and Catalysis*, 58, p. 571.

Muller, K., Deckwer, H. and Ralek, M., 1982. Fischer-Tropsch synthesis on polyfunctional manganese/iron-pentasil zeolite catalysts. *Studies in Surface Science and Catalysis*, 12, p. 267-274.

Nenitzescu, C., 1968. *Carbenium Ions*. In G. Olah and P. Von R. Sclayer eds. New York: John Wiley. Ch. 13, Vol. 2.

Niederberger, H., 1988. *Time Change of Activity and Selectivity during the Conversion of Syngas, that is rich in CO, over an Iron/H-ZSM-5 Composite Catalyst*. Dr.-Ing. Dissertation, University of Karlsruhe.

Olson, D., Haag, W. and Lago, R., 1980. *Journal of Catalysis*, 61, p. 390.

Park, K. and Ihm, S., 2000. Comparison of Pt/Zeolite Catalysts for n-hexadecane hydroisomerization. *Applied Catalysis A: General*, 203, p. 201-209.

Perry, R. and Green, W., 1997. *Perry's Chemical Engineers' Handbook*. 7th ed. USA: Mc-Grew-Hill.

Polinski, L., Rao, V. and Stencel, J., 1984. *The Science and Technology of Coal and Coal Utilization*. In B. Cooper and W. Ellingson eds. Plenum, p. 381.

Pour, A., Shahri, S., Zamani, Y., Irani, M. and Tehrani, S., 2008a. Deactivation studies of bifunctional Fe-HZSM-5 catalyst in Fischer-Tropsch process. *Journal of Natural Gas Chemistry*, 17, p. 242-248.

Pour, A., Zamani, Y., Tavasoli, A., Shahri, S., and Taheri, S., 2008b. Study on products distribution of iron and iron-zeolite catalysts in Fischer-Tropsch synthesis. *Fuel*, 87, p. 2004-2012.

Pour, A., Zare, M., Shahri, S., Zamani, Y. and Alei, M., 2009. Catalytic behaviors of bifunctional Fe-HZSM-5 catalyst in Fischer-Tropsch synthesis. *Journal of Natural Gas Science and Engineering*, 1, p. 183-189.

Pradhan, R., Lin. T., Chen, W., Jong, S., Wu. J., Chao, K. and Liu, S., 1991. EPR and NMR studies of coke induced selectivation over H-ZSM-5 zeolite during ethylbenzene disproportionation reaction. *Journal of Catalysis*, 184, p. 29-38.

Rao, V. and Gormley, R., 1980. Make olefins from syngas. *Hydrocarbon Processing*, 59 (11), p. 139-142.

Rao, V., Gormley, R., Shamsi, A., Petrick, T., Stencel, J., Schehl, R., Chi, R. and Obermyer, R., 1985. Promotion and characterisation of zeolitic catalysts used in the synthesis of hydrocarbons from syngas. *Journal of Molecular Catalysis*, 29, p. 271-283.

Rastelli, H., Lok, B., Duisman, J., Earls, D. and J., M., 1982. Characterization of zeolite acidity: the cracking of 2 mole% n-butane over a fixed zeolite bed. *Canadian Journal of Chemical Engineering*, 60, p. 44.

Riedel, T., Claeys, M., Schultz, H., Schaub, G., Nam, S., Jun, K., Choi, M., Kishan, G. and Lic, K., 1999. Comparative study of Fischer-Tropsch synthesis with H_2/CO and H_2/CO_2 syngas using Fe- and Co-based catalysts. *Applied Catalysis A: General*, 186, p. 201-213.

Rollmann, L. and Walsh D., 1979. Shape selectivity and carbon formation in zeolites. *Journal of Catalysis*, 56 (1), p. 139.

Sandler, S., 1999. *Chemical and Engineering Thermodynamics*. 3rd ed. USA: John Wiley and Sons, Inc.

Schulz, H., Beck, K. and Erich, E., 1988a. Kinetics of Fischer-Tropsch selectivity. *Fuel Processing Technology*, 18 (3), p. 293-304.

Schulz, H., Beck, K. and Erich, E., 1988b. Mechanism of the Fischer-Tropsch process. *Studies in Surface Science and Catalysis*, 36, p. 457-471.

Schulz, H., Niederberger, H., Kneip, M. and Weil, F., 1991a. Synthesis gas conversion on Fischer-Tropsch iron/HZSM-5 composite catalysts. *Studies in Surface Science and Catalysis*, 61, p. 313-323.

Schulz, H., Barth, D. and Siwei, Z., 1991b. Deactivation of HZSM-5 zeolite during methanol conversion: kinetic probing of pore-architecture and acidic properties. *Studies in Surface Science and Catalysis*, 68, p. 783-790.

Schulz, H., Böhringer, W. and Siwei, Z., 1993. Comparison of shape selectivity of coke formation in different zeolites. *Proceedings of the 9th International Zeolite Conference*, Montreal, Butterworth-Heinemann, p. 567-574.

Schulz, H., van Steen, E. and Claeys, M., 1994. *Studies in Surface Science and Catalysis*, 81, p. 45-50.

Schulz, H. and Wei, M., 1999. Deactivation and thermal regeneration of zeolite HZSM-5 for methanol conversion at low temperatures (260-290^{o}C). *Microporous and Mesoporous Materials*, 29, p. 205-218.

Shamsi, A., Udaya, V., Rao, S., Gormley, R., Obermyer, R., Schehl, R. and Stencel, J., 1984. Zeolite-supported cobalt catalysts for the conversion of synthesis gas to hydrocarbon products. *Industrial and Engineering Chemistry Product Research and Development*, 23, p. 513-519.

Shamsi, A., Rao, V., Gormley, R., Obermyer, R., Schehl, R. and Stencel, J., 1986. Influence of preparative procedure on the activity and selectivity of Fe/ZSM-5 catalysts in syngas conversion. *Applied Catalysis*, 27, p. 55-68.

Schermuly, O. and Luft, G., 1977. Studies on low-pressure methanol synthesis in a jet reactor. *Chemie Ingenieur Technik*, 49 (11), p. 907.

Skoog. D. and West, D., 1980. *Principles of Instrumental Analysis.* 2nd ed. Philadelphia: Saunders College.

Stencel, J., Rao, V, Diehl, J., Rhee, K., Dhere, A. and De Angelis, R., 1983. *Journal of Catalysis*, 84, p. 109.

Steynberg, A., Espinoza, R., Jager, B. and Vosloo, A., 1999. High temperature Fischer-Tropsch synthesis in commercial practise. *Applied Catalysis A: General*, 186, p. 41-54.

Udaya, V., Rao, S. and Gormley, R., 1990. Bifunctional catalysis in syngas conversions, *Catalysis Today*, 6 (3), p. 207-234.

Vallabh, H., 2008. Characterization of a novel laboratory internal recycle reactor for HTFT studies. MSc dissertation. University of Cape Town.

Valyon, J. Mihalyfi, J., Beyer, H. and Jacobs, P., 1979. *Processing Workshop on Absorption*. Berlin, DDR.

van Bekkum, H., Flanigen, E., Jacobs, P. and Jansen, J. (eds.), 2001. *Introduction to Zeolite Science and Practise*. 2nd ed. Elsevier.

van Steen, E. and Claeys, M., 2008. Fischer-Tropsch catalysis for the biomass-to-liquid process. *Chemical Engineering Technology*, 31 (5), p. 655-666.

van Santen, R., 1994. *Studies in Surface Science and Catalysis*, 85, p.271.

Varma, R., Jothimurugesan, K., Bakhshi, N., Mathews, J. and Ng, S., 1986. Direct conversion of synthesis gas to aromatic hydrocarbons: variation of product distribution with time-on-stream. *The Canadian Journal of Chemical Engineering*, 64, p. 141-148.

Varma, R., Bakhshi, N., Mathews, J. and Ng, S., 1987. Performance of dual-reactor system for conversion of syngas to aromatic-containing hydrocarbons. *Industrial Engineering Chemical Reserves*, 26, p. 183-188.

Vedrine, J., Dejaive, P., Garlowski, E. and Derouane, G., 1980. *Catalysis by Zeolites*. In B. Imelik ed. New York: Elsevier, p. 29.

Willard, H., Merrit, L., Dean, J. and Settle, F., 1981. *Instrumental Methods of Analysis.* 7th ed. California: Wadsworth publishing Company.

Willis, J., 1999. Instrumental parameters and data quality for routine major and trace element determinations by WDXRFS. Abstract from Department of Geological Sciences, University of Cape Town database. Available at: web.uct.ac.za/depts./geolsci/facilities/xrf/X40CALIB.doc [accessed 7 June 2010].

Yang, Y., Xiang, H., Xu, Y., Bai, L. and Li, Y., 2004. Effect of potassium promoter on precipitated iron-manganese catalyst for Fischer-Tropsch synthesis. *Applied Catalysis A: General*, 266, p. 181-194.

APPENDICES

Appendix I: Pictures of the reactor

Figure AI.1: Photograph of reactor base, internal draft tube, felts and metal sieve plates

Figure AI.2: Photograph of closed reactor with magnedrive

Figure AI.3: Photograph of the top view of the catalyst bed with Fe-FT catalyst uniformly spread out within the holes of the metal sieve plate

Figure AI.4: Photograph of reactor base and lid with impellers

Figure AI.5: Photograph of reactor test unit

Appendix II: GC-FID peak identification and product chromatograms

Table AII.1: Identification table of the Fe-FT experiment product spectrum (GC-FID)

Peak Name	Residence Time (min)	Correction Factor
Methane	3.71	1.00
Ethylene	4.11	1.00
Ethane	4.36	1.00
Propylene	6.07	1.00
Propane	6.27	1.00
Isobutene	8.59	1.00
Acetaldehyde	8.99	1.82
1-butene	9.64	1.00
Butane	10.00	1.00
t-2-butene	10.40	1.00
c-2-butene	10.95	1.00
Methanol	11.61	1.82
3-me-1-butene	12.15	1.00
Ethanol	12.67	1.29
2-me-butane	12.78	1.00
Acetone	13.12	1.43
1-pentene	13.29	1.00
2-me-1-butene	13.52	1.00
Pentane	13.68	1.00
t-2-pentene	13.91	1.00
c-2-pentene	14.18	1.00
2-me-2-butene	14.33	1.00
X1	14.43	-
propanal, 2-methyl-	14.87	1.29
2,2-dime-butane +	15.04	1.00
1-propanol	15.08	1.18
3-me-1-pentene	15.52	1.00
4-me-1-pentene	15.58	1.00
acetic acid	15.71	1.90
2,3-dime-butane	15.84	1.00
2-me-pentane	15.90	1.00
Butanal	15.99	1.29
2-butanone	16.09	1.29
2-propanol + 3-me-	16.36	1.18 / 1.00
1-hexene	16.48	1.00
ethyl acetate	16.67	1.87
Hexane	16.81	1.00
3-hexene, (E)-	16.91	1.00
2-pentene, 2-methyl-	17.00	1.00
1-propanol, 2-methyl-	17.12	1.09
2-hexene, (Z)-	17.21	1.00
2-pentene, 3-methyl-,	17.32	1.00
cyclopentane, methyl-	17.40	1.00
1-butanol	18.05	1.13
1-hexene, 3-methyl	18.17	1.00
1-hexene, 5-methyl-	18.32	1.00
propanoic acid /	18.35	1.46
1-hexene, 4-methyl-	18.40	1.00
2-pentanone	18.67	1.22
hexane, 2-methyl-	18.71	1.00
pentane, 2,3-dimethyl-	18.84	1.00
pentanal + 3-me-	18.93	1.22 / 1.00
2-butanol	19.04	1.13
1-hexene, 2-methyl-	19.18	1.00
1-heptene	19.22	1.00
X6	19.43	-
Heptane	19.51	1.00
2-heptene	19.60	1.00
3-heptene, (Z)-	19.67	1.00
1-butanol, 3-methyl-	19.90	1.10
1-butanol, 2-methyl-	20.05	1.10
Vinylcyclopentane	20.30	1.00
methylcyclohexane	20.43	1.00
2-pentanone, 3-	20.53	1.17
1-pentanol	20.67	1.10
1-heptene, 3-methyl-	20.83	1.00
1-heptene, 5-methyl-	20.94	1.00
1-heptene, 4-methyl-	21.05	1.00
heptane,2-methyl-	21.17	1.00
2-hexanone / toluene	21.24	1.18
heptane,4-methyl-	21.28	1.00
heptane, 3-methyl-	21.41	1.00
Hexanal	21.56	1.18
1-heptene, 2-methyl-	21.67	1.00
1-octene	21.76	1.00
Octane	22.03	1.00
2-octene	22.25	1.00
1-pentanol, 3-methyl-	22.37	1.08
2-heptene, 3-methyl-	22.45	1.00
1-pentanol, 2-methyl-	22.51	1.08
cyclohexane, dimethyl, a	22.86	1.00
cyclohexane, dimethyl, b	22.93	1.00
1-hexanol	23.27	1.08
1-octene, 3-methyl	23.52	1.00
octane, 2-methyl	23.72	1.00
2-heptanone / ethylbenzene	23.76	1.15
octane, 4-methyl-	23.93	1.00
octane, 3-methyl-	23.98	1.00
Heptanal	24.17	1.15
1-nonene	24.37	1.00
Nonane	24.71	1.00
1-heptanol	26.03	1.07
1-nonene, a-methyl-	26.23	1.00
nonane, a-methyl-	26.46	1.00
2-octanone	26.75	1.00
1-nonene, 2-methyl	26.88	1.00
1-decene	27.17	1.00
Decane	27.42	1.00
1-decene, c-methyl-	28.79	1.00
1-octanol	28.90	1.06
1-decene, b-methyl-	29.01	1.00
1-decene, a-methyl-	29.12	1.00
decane, d-methyl-	29.24	1.00
decane, c-methyl-	29.30	1.00
decane, b-methyl-	29.53	1.00
2-nonanone	29.60	1.11
decane, a-methyl-	29.71	1.00
1-decene, 2-methyl	29.82	1.00
1-undecene	30.05	1.00
Undecane	30.27	1.00
2-undecene	30.45	1.00
1-undecene, b-methyl-	31.71	1.00
1-nonanol	31.77	1.05
1-undecene, a-methyl-	31.83	1.00
undecane, b-methyl-	32.25	1.00
2-decanone	32.35	1.10
undecane, a-methyl-	32.52	1.00
1-dodecene	32.88	1.00
Dodecane	33.16	1.00
1-tridecene	35.68	1.00
Tridecane	35.93	1.00
1-tetradecene	38.42	1.00
Tetradecane	38.63	1.00
1-pentadecene	41.07	1.00
Pentadecane	41.30	1.00
1-hexadecene	43.59	1.00
Hexadecane	43.90	1.00
1-heptadecene	46.01	1.00
Heptadecane	46.19	1.00
1-octadecene	48.34	1.00
Octadecane	48.55	1.00

Table AII.2: Identification table of the combined Fe-FT/HZSM-5 experiment product spectrum (GC-FID)

Peak name	Residence time (min)	Correction factor
Methane	3.67	1.00
Ethylene	4.07	1.00
Ethane	4.33	1.00
Propylene	6.05	1.00
Propane	6.24	1.00
Isobutane	8.60	1.00
1-butene	9.58	1.00
Butane	9.98	1.00
t-2-butene	10.38	1.00
c-2-butene	10.93	1.00
Methanol	11.60	1.82
3-me-1-butene	12.13	1.00
ethanol	12.64	1.29
2-me-butane	12.78	1.00
1-pentene	13.27	1.00
2-me-1-butene	13.50	1.00
pentane	13.66	1.00
t-2-pentene	13.90	1.00
c-2-pentene	14.17	1.00
2-me-2-butene	14.32	1.00
3-me-1-pentene	15.56	1.00
4-me-1-pentene	15.61	1.00
2,3-dime-butane	15.89	1.00
2-me-pentane	15.93	1.18
2-butanone	16.06	1.29
3-me-pentane	16.34	1.00
1-hexene	16.45	1.00
hexane	16.79	1.00
3-hexene, (E)-	16.96	1.00
2-pentene, 2-methyl-	17.01	1.00
2-pentene, 3-methyl-, (Z)-	17.11	1.00
2-hexene, (Z)-	17.20	1.00
X1	17.36	1.00
2-pentene, 3-methyl-, (E)-	17.41	1.00
X2	17.58	1.00
hexadiene	17.73	1.00
cyclopentane, methyl-	17.78	1.00
2-butanone, 3-methyl-	17.96	1.22
1-hexene, 3-methyl-	18.13	1.00
1,3-pentadiene, 3-methyl-	18.30	1.00
benzene	18.35	1.00
cyclohexane	18.50	1.00
X3	18.54	1.00
2-me-hexane	18.66	1.00
2,3-dimethyl-pentane	18.81	1.00
3-me-hexane	18.92	1.00
X4	19.02	1.00
1-hexene, 2-methyl-	19.21	1.00
cyclopentane, 1,3-dimethyl-, cis	19.26	1.00
cyclopentane, 1,3-dimethyl-, trans	19.30	1.00
cyclopentane, 1,2-dimethyl-, trans	19.41	1.00
3-heptene, (E)-	19.45	1.00
heptane	19.53	1.00
1-pentene, 2,3-dimethyl-	19.60	1.00
3-hexene, 2-methyl-, (Z)-	19.66	1.00
1,3-pentadiene, 2,3-dimethyl-	19.70	1.00
1,4-hexadiene, 4-methyl-	19.84	1.00
3-hexene, 2-methyl-, (E)-	19.90	1.00
2-hexene, 3-methyl-, (E)-	19.97	1.00
cyclopentene, 3,5-dimethyl-	20.01	1.00
cyclopentane, 1,2-dimethyl-, cis-	20.38	1.00
methylcyclohexane	20.42	1.00
ethylcyclopentane	20.59	1.00
cyclopentane, 1,2,4-trimethyl-	20.81	1.00
cyclopentene, 1,2,3-trimethyl-	20.88	1.00

Peak name	Residence time (min)	Correction factor
cyclopentene, 4,4-dimethyl	21.00	1.00
X5	21.04	1.00
heptane, 2-methyl-	21.21	1.00
toluene	21.26	1.00
heptane, 3-methyl-	21.48	1.00
hexane, 3-ethyl-	21.52	1.00
cyclohexane, 1,2-dimethyl-	21.71	1.00
cyclohexane, 1,4-dimethyl-	21.88	1.00
X6	21.93	1.00
cyclohexanol, 2,4-dimethyl-	22.02	1.06
cyclopentene, 1-ethyl-5-methyl-	22.14	1.00
cyclohexene, 1-ethyl-	22.25	1.00
cyclopentene, 1-ethyl-2-methyl-	22.42	1.00
cyclohexane, 1,3-dimethyl-	22.57	1.00
cyclohexene, 3-ethyl-	22.72	1.00
cyclohexene, 1,3-dimethyl	22.97	1.00
cyclohexene, 3,5-dimethyl-	23.04	1.00
cyclohexene, 1,4-dimethyl	23.09	1.00
cyclopentane, 1,1,3,3-tetramethyl-	23.16	1.00
cyclohexene, 1,2-dimethyl-	23.35	1.00
cyclohexane, ethyl-	23.50	1.00
ethylbenzene	23.75	1.00
m-xylene+p-xylene	23.95	1.00
cyclohexene, 3,3,5-trimethyl-	24.19	1.00
1,3-hexadiene, 3-ethyl-2-methyl-	24.28	1.00
cyclohexane, 1,3-dimethyl-2-methylene-, cis-	24.33	1.00
cyclohexane, (1-methylethylidene)-	24.51	1.00
p-xylene	24.67	1.00
cyclohexane, 1-ethyl-3-methyl	24.88	1.00
ethylidenecycloheptane	24.92	1.00
C9-naphtene, a	25.00	1.00
1,3-heptadiene, 5,5-dimethyl-	25.18	1.00
cyclohexane, 1-ethyl-4-methyl	25.39	1.00
benzene, (1-methylethyl)-	25.55	1.00
C9-naphtene, b	25.75	1.00
C10-naphtene, a	25.92	1.00
pinane, trans-	26.08	1.00
cyclopentanone, 2-methyl-3-(1-methylethyl)-	26.14	1.11
benzene-propyl	26.36	1.00
m-ethyl-toluene	26.59	1.00
p-ethyl-toluene	26.67	1.00
5-me-nonane	26.72	1.00
o-ethyl-toluene	27.12	1.00
C10-naphtene, b	27.41	1.00
benzene, 1,3,5-trime-	27.61	1.00
C10-aromatic, a	27.66	1.00
C10-aromatic, b	28.18	1.00
C10-aromatic, c	28.39	1.00
benzene, 1,3-diethyl-	29.07	1.00
benzene, 1-methyl-3-propyl-	29.13	1.00
benzene, 1,4-diethyl-	29.23	1.00
benzene, 2-ethyl-1,4-dimethyl-	29.95	1.00
benzene, 1-ethyl-2,4-dimethyl-	30.01	1.00
benzene, 4-ethyl-1,2-dimethyl-	30.12	1.00
C11-aromatic, a	30.33	1.00
C11-aromatic, b	31.14	1.00
C11-aromatic, x	31.33	1.00
C11-aromatic, c	31.54	1.00
C11-aromatic, d	31.97	1.00
C11-aromatic, e	32.03	1.00
C11-aromatic, f	32.30	1.00
C11-aromatic, g	32.36	1.00
C11-aromatic, h	32.47	1.00
C12-aromatic, a	32.69	1.00
C12-aromatic, b	35.82	1.00

Figure AII.1: Typical GC-FID chromatogram of product analyzed for the Fe-FT experiment (2.5 days on-stream)

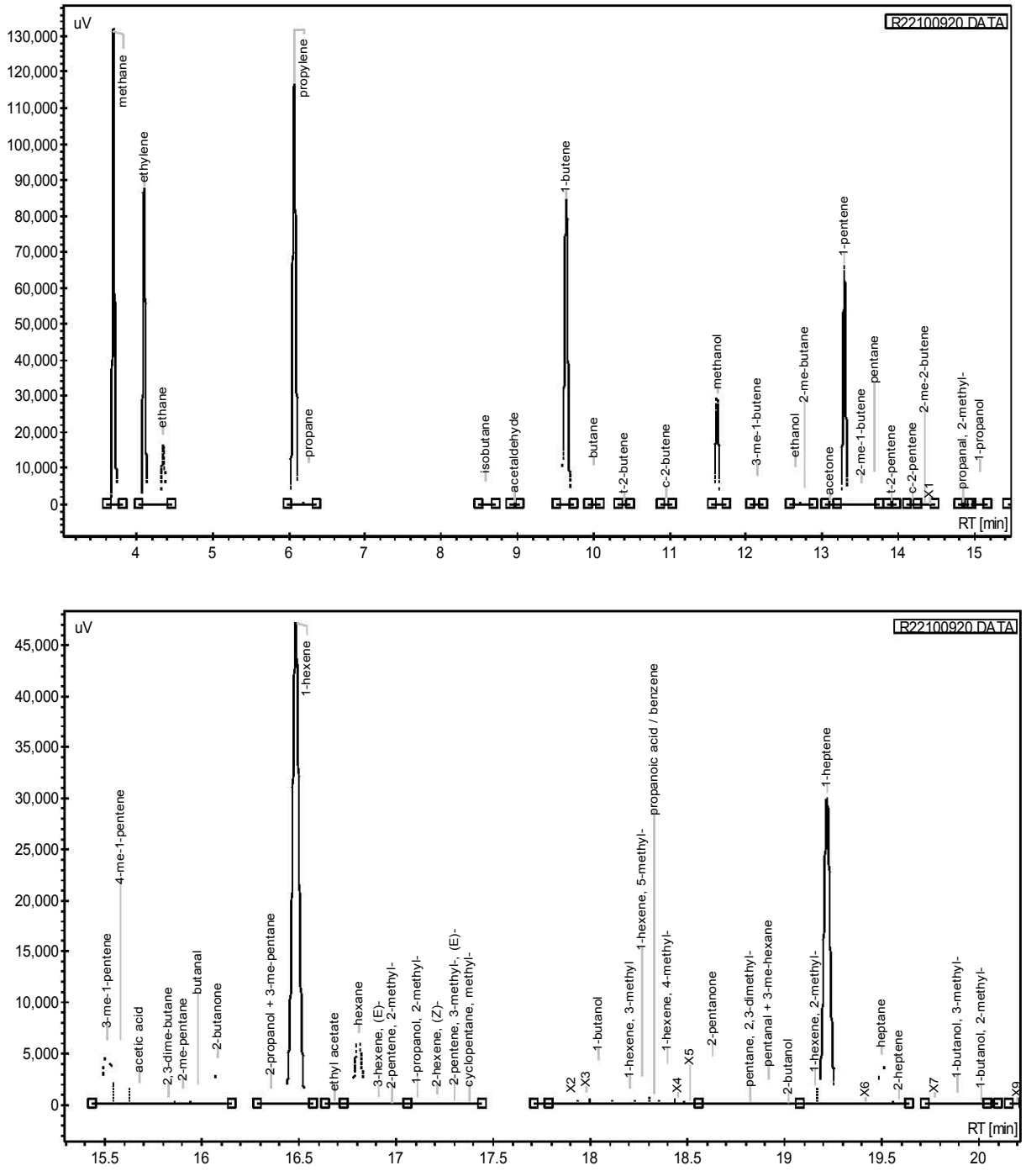

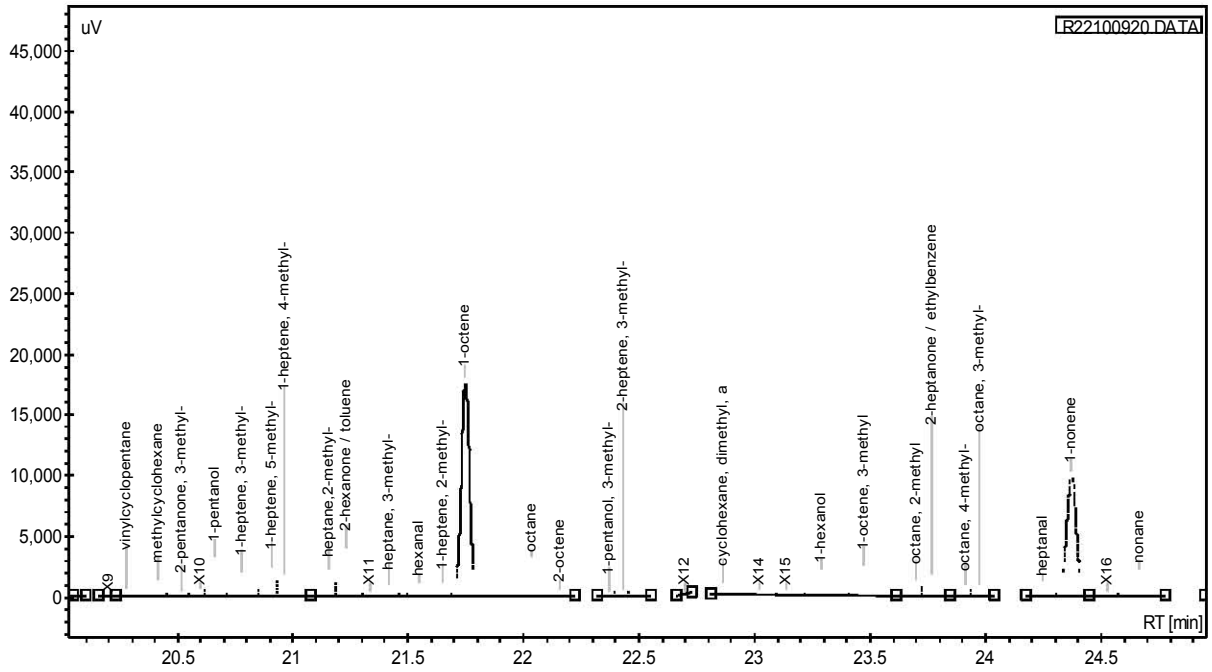
uV
R22100920.DATA
45,000
40,000
35,000
30,000
25,000
20,000
15,000
10,000
5,000
0
X9
vinylcyclopentane
methylcyclohexane
2-pentanone, 3-methyl-
X10
1-pentanol
1-heptene, 3-methyl-
1-heptene, 5-methyl-
1-heptene, 4-methyl-
heptane,2-methyl-
2-hexanone / toluene
X11
heptane, 3-methyl-
hexanal
1-heptene, 2-methyl-
1-octene
octane
2-octene
1-pentanol, 3-methyl-
2-heptene, 3-methyl-
X12
cyclohexane, dimethyl, a
X14
X15
1-hexanol
1-octene, 3-methyl
octane, 2-methyl
2-heptanone / ethylbenzene
octane, 4-methyl-
octane, 3-methyl-
heptanal
1-nonene
X16
nonane
RT [min]
20.5
21
21.5
22
22.5
23
23.5
24
24.5

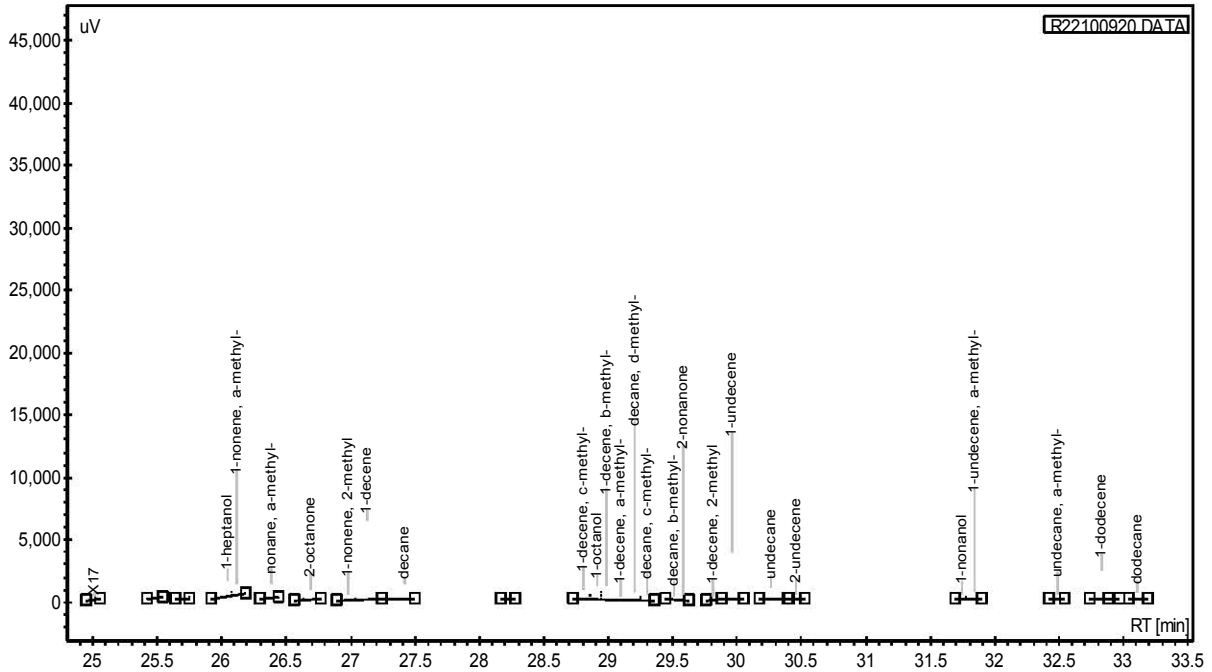
uV
R22100920.DATA
45,000
40,000
35,000
30,000
25,000
20,000
15,000
10,000
5,000
0
X17
1-heptanol
1-nonene, a-methyl-
nonane, a-methyl-
2-octanone
1-nonene, 2-methyl
1-decene
decane
1-decene, c-methyl-
1-octanol
1-decene, b-methyl-
1-decene, a-methyl-
decane, c-methyl-
decane, d-methyl-
decane, b-methyl-
2-nonanone
1-decene, 2-methyl
1-undecene
undecane
2-undecene
1-nonanol
1-undecene, a-methyl-
undecane, a-methyl-
1-dodecene
dodecane
RT [min]
25
25.5
26
26.5
27
27.5
28
28.5
29
29.5
30
30.5
31
31.5
32
32.5
33
33.5

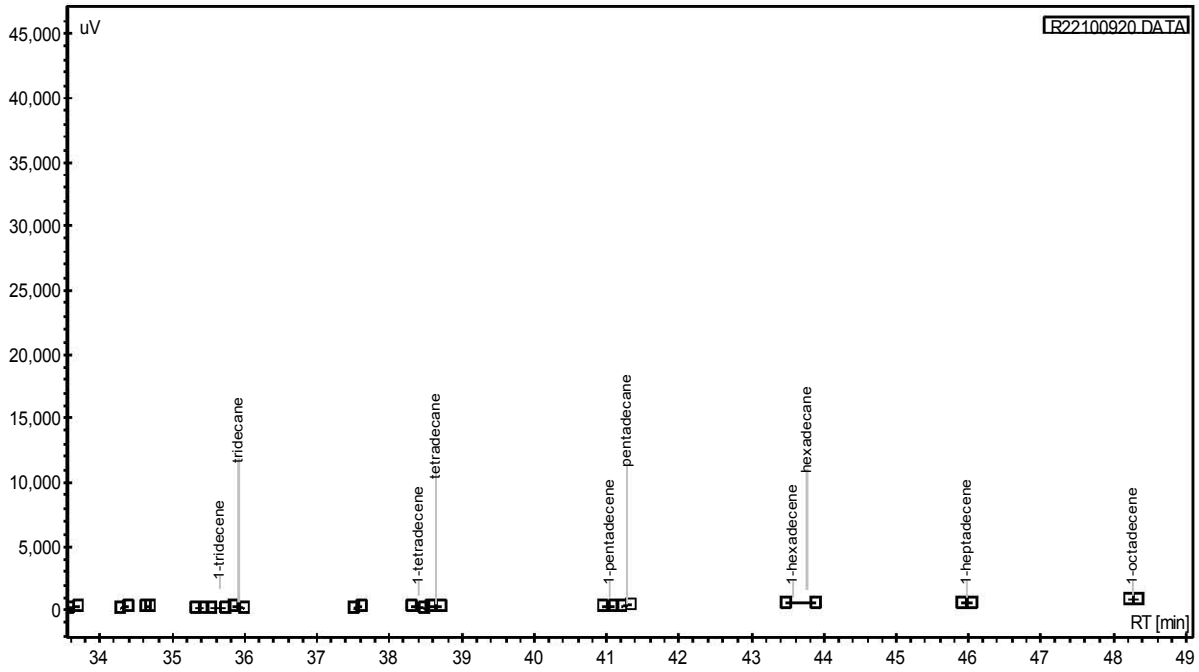
uV
R22100920.DATA
45,000
40,000
35,000
30,000
25,000
20,000
15,000
10,000
5,000
0
1-tridecene
tridecane
1-tetradecene
tetradecane
1-pentadecene
pentadecane
1-hexadecene
hexadecane
1-heptadecene
1-octadecene
RT [min]
34
35
36
37
38
39
40
41
42
43
44
45
46
47
48
49

Figure AII.2: Typical GC-FID chromatogram of product analyzed for the combined Fe-FT/HZSM-5 experiment (2.5 days on-stream)

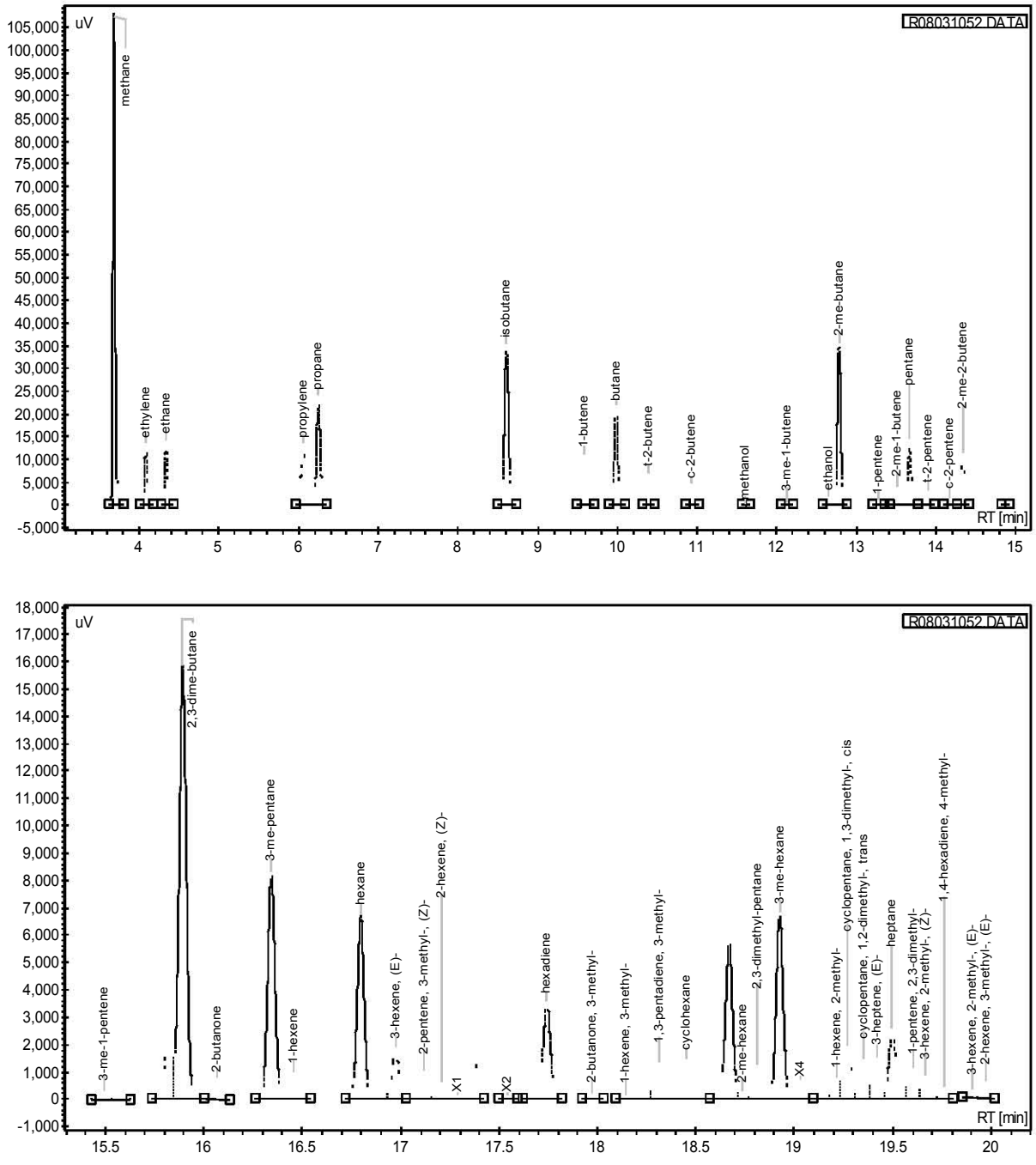

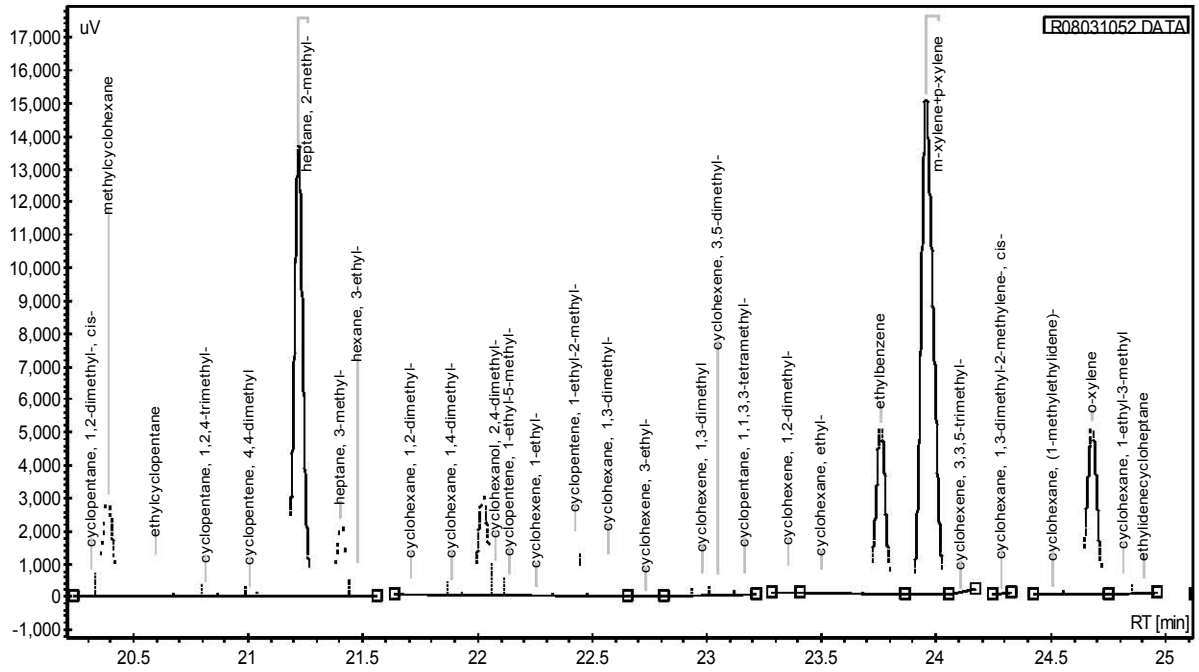
uV
R08031052.DATA
cyclopentane, 1,2-dimethyl-, cis-
methylcyclohexane
ethylcyclopentane
cyclopentane, 1,2,4-trimethyl-
cyclopentene, 4,4-dimethyl
heptane, 2-methyl-
heptane, 3-methyl-
hexane, 3-ethyl-
cyclohexane, 1,2-dimethyl-
cyclohexane, 1,4-dimethyl-
cyclohexanol, 2,4-dimethyl-
cyclopentene, 1-ethyl-5-methyl-
cyclohexene, 1-ethyl-
cyclopentene, 1-ethyl-2-methyl-
cyclohexane, 1,3-dimethyl-
cyclohexene, 3-ethyl-
cyclohexene, 1,3-dimethyl
cyclohexene, 3,5-dimethyl-
cyclopentane, 1,1,3,3-tetramethyl-
cyclohexene, 1,2-dimethyl-
cyclohexane, ethyl-
ethylbenzene
m-xylene+p-xylene
cyclohexene, 3,3,5-trimethyl-
cyclohexane, 1,3-dimethyl-2-methylene-, cis-
cyclohexane, (1-methylethylidene)-
o-xylene
cyclohexane, 1-ethyl-3-methyl
ethylidenecycloheptane
RT [min]

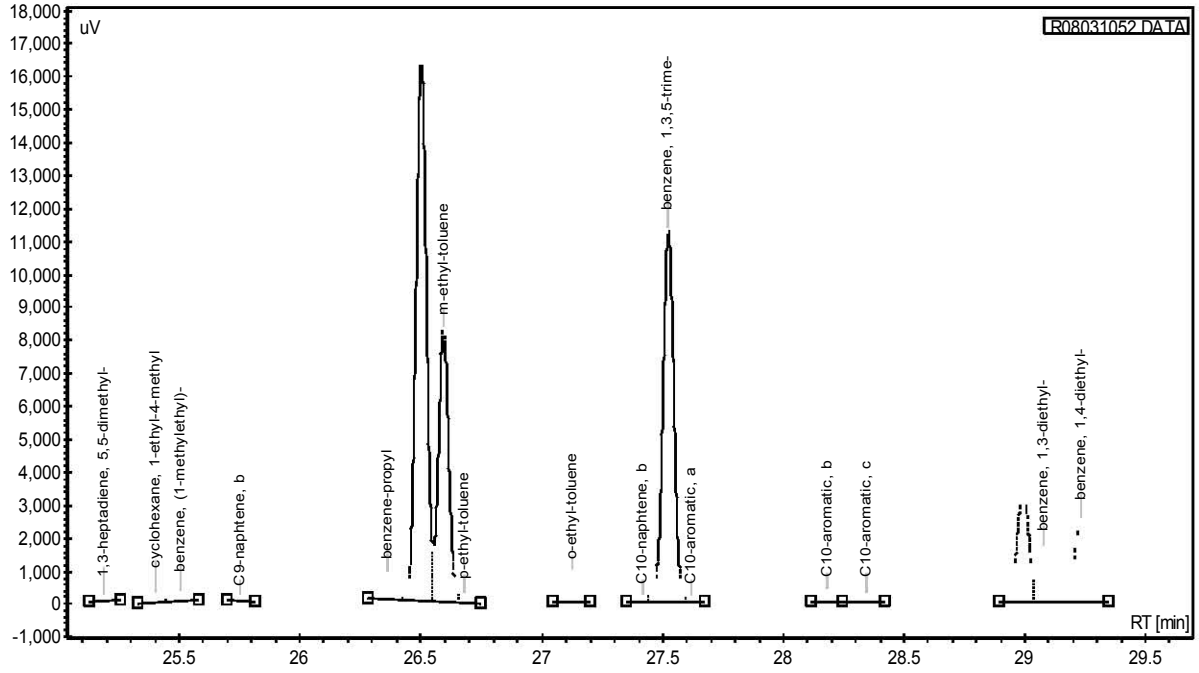
uV
R08031052.DATA
1,3-heptadiene, 5,5-dimethyl-
cyclohexane, 1-ethyl-4-methyl
benzene, (1-methylethyl)-
C9-naphtene, b
benzene-propyl
m-ethyl-toluene
p-ethyl-toluene
o-ethyl-toluene
C10-naphtene, b
benzene, 1,3,5-trime-
C10-aromatic, a
C10-aromatic, b
C10-aromatic, c
benzene, 1,3-diethyl-
benzene, 1,4-diethyl-
RT [min]

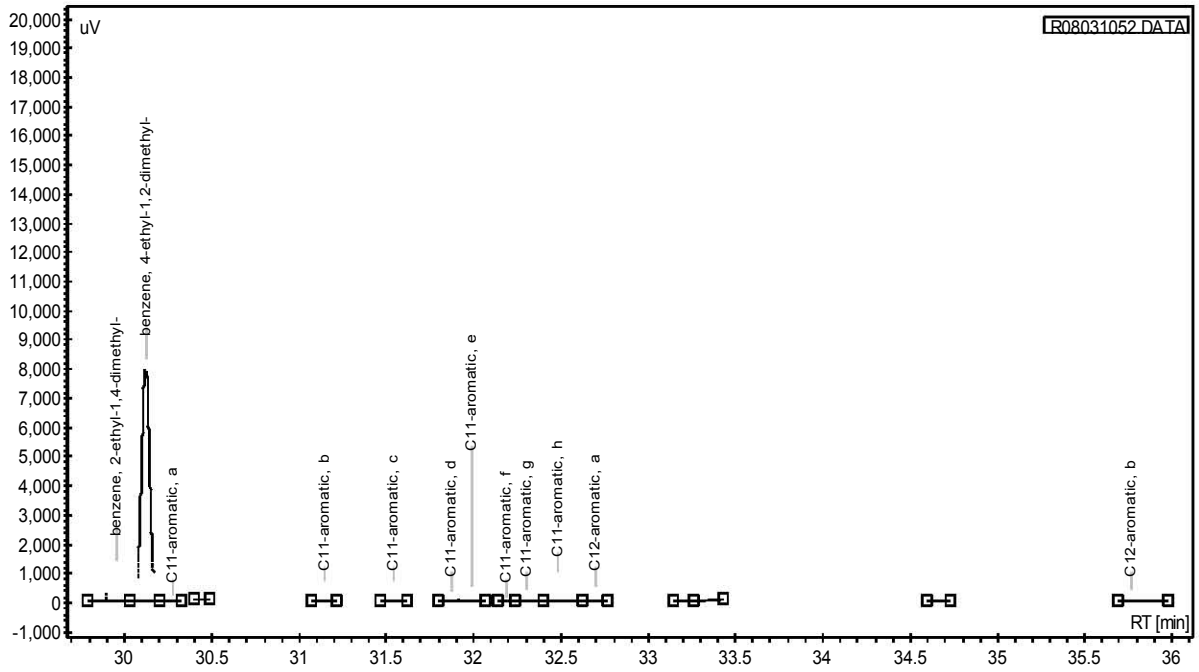
uV
R08031052.DATA
benzene, 2-ethyl-1,4-dimethyl-
benzene, 4-ethyl-1,2-dimethyl-
C11-aromatic, a
C11-aromatic, b
C11-aromatic, c
C11-aromatic, d
C11-aromatic, e
C11-aromatic, f
C11-aromatic, g
C11-aromatic, h
C12-aromatic, a
C12-aromatic, b
RT [min]

Appendix III: Additional feed and product gas analysis

WGS equilibrium

It is well known that iron catalyzes the WGS reaction and at high temperature FT conditions the WGS reaction approaches equilibrium and in this situation, CO_2 is best treated as a reactant (Dry, 2004a). To determine the stoichiometric ratio when CO_2 is a reactant, both Equations A.1 and A.2 need to be considered.

Heavier hydrocarbons: $$nCO + 2nH_2 \rightarrow (-CH_2-)_n + nH_2O \quad \text{(A.1)}$$

Reverse WGS reaction: $$CO_2 + H_2 \rightarrow CO + H_2O \quad \text{(A.2)}$$

Dividing Equation A.1 by n and adding it to Equation A.2 gives:

$$CO_2 + 3H_2 \rightarrow (-CH_2-)_n + 2H_2O \quad \text{(A.3)}$$

From Equation A.1 and Equation A.3., two H_2 molecules are consumed by each CO molecule and three H_2 molecules are consumed by each CO_2 molecule, respectively, to form the desired ($-CH_2-$) product. Therefore, when the reactants are in stoichiometric balance, the Ribblett ratio (H_2 / $2CO+3CO_2$) equals one (Dry, 2004 (a)).

Data work-up

- To determine whether the WGS reaction was at equilibrium, the following equations were applied:

WGS reaction: $$CO + H_2O \rightarrow CO_2 + H_2 \quad \text{(A.4)}$$

At equilibrium, the equilibrium constant (K_p) is related to the Gibbs free energy for reaction at the specific temperature as follows:

$$K_p = e^{\frac{-\Delta \underline{G}^{rxn}(T)}{R.T}} \quad \text{(A.5)}$$

Where,

$$\Delta \underline{G}^{rxn}(T) = T.\left[\frac{\Delta \underline{G}^{rxn}(298K)}{298K} + \Delta \underline{H}^{rxn}(T).\left(\frac{1}{T} - \frac{1}{298K}\right)\right] \quad \text{(A.6)}$$

$$\Delta \underline{G}^{rxn}(298K) = \sum \nu.\Delta \underline{G}^{f}(298K) \quad \text{(A.7)}$$

ΔH^{rxn} is also a function of temperature and is related to the specific heat capacity (C_p) as follows:

$$\left(\frac{\delta \Delta \underline{H}^{rxn}}{\delta T}\right)_P = \nabla C_p = \nabla a - \nabla b.T - \nabla c.T^2 - \nabla d.T^3 \quad \text{(A.8)}$$

Integrating ΔH^{rxn} gives

$$\Delta \underline{H}^{rxn}(T) = \Delta \underline{H}^{rxn}(298K) - \nabla a.T - \nabla b.\frac{T^2}{2} - \nabla c.\frac{T^3}{3} - \nabla d.\frac{T^4}{4} \quad \text{(A.9)}$$

Table AIII.1: Heat capacity coefficients (Sandler, 1999)

	C_p (J/mol)			
	a	*b*10²*	*c*10⁵*	*d*10⁹*
CO_2	22.243	5.977	-3.499	7.464
H_2	29.088	-0.192	0.400	-0.870
CO	28.142	0.167	0.537	-2.221
H_2O	32.218	0.192	1.055	-3.593
	-9.029	5.426	-4.691	12.408

and

$$\Delta \underline{H}^{rxn}(298K) = \sum \nu.\Delta \underline{H}^{f}(298K) \quad \text{(A.10)}$$

Table AIII.2: Gibbs free energy of formation and enthalpies of formation at 298K (Sandler, 1999)

	KJ/mol	
	ΔG^f (298K)	ΔH^f (298K)
CO_2	-394.36	-393.51
H_2	-	-
CO	-137.2	-110.5
H_2O	-228.6	-241.8

In addition, the equilibrium constant for the WGS reaction is also given as:

$$K_p = \frac{p_{CO_2}.p_{H_2}}{p_{CO}.p_{H_2O}} = \frac{y_{CO_2}.P_T.y_{H_2}.P_T}{y_{CO}.P_T.y_{H_2O}.P_T} = \frac{y_{CO_2}.y_{H_2}}{y_{CO}.y_{H_2O}} = \frac{n_{CO_2,out}.n_{H_2,out}}{n_{CO,out}.n_{H_2O,out}} \quad \text{(A.11)}$$

The composition in the reactor was assumed to be the same as the composition in the reactor outlet stream since the Berty reactor is an internal recycle reactor and thus assumed to be well mixed (see Section 2.4 for more details). The moles of CO, CO_2 and H_2 in the reactor outlet were determined from the GC-TCD results.

The moles of H_2O out were determined by doing an oxygen mass balance as shown below:

$$m_{O[CO],in} + m_{O[CO_2],in} = m_{O[CO],out} + m_{O[CO_2],out} + m_{O[oxygenates],out} + m_{O[H_2O],out} \quad \text{(A.12)}$$

Where the mass of oxygen in each oxygenate was calculated as follows:

$$m_{O[i]} = n_{O(i)}.M_O.N_{O(i)} \quad \text{(A.13)}$$

and the moles of oxygenates were obtained from the GC-FID results.

The moles of H_2O out were then calculated as follows:

$$n_{H_2O,out} = \frac{m_{O(H_2O),out}}{M_O} \quad \text{(A.14)}$$

The reaction is at equilibrium if the K_p from the Gibbs free energy is equal to the K_p calculated from the partial pressures.

Appendix IV: Additional results

Fe-FT performance

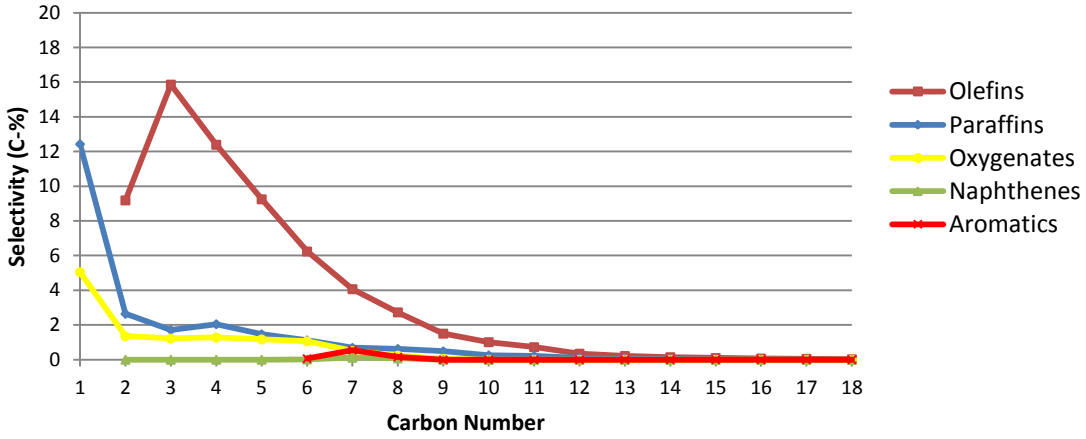

Figure AIV.1: Product distribution versus carbon number range for the Fe-FT Expt. 2 (14 days on-stream)

Combined Fe-FT/HZSM-5 performance

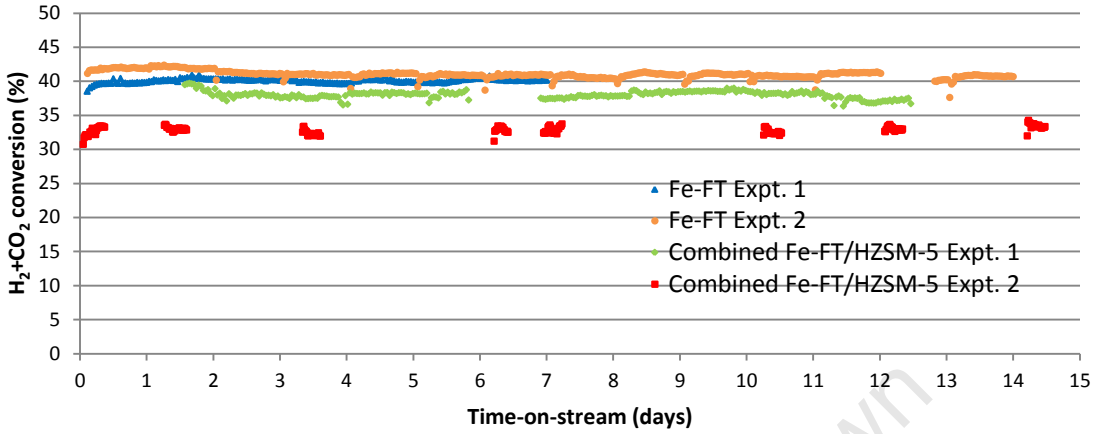

Figure AIV.2: H_2+CO_2 conversions for the Fe-FT and combined Fe-FT/HZSM-5 experiments

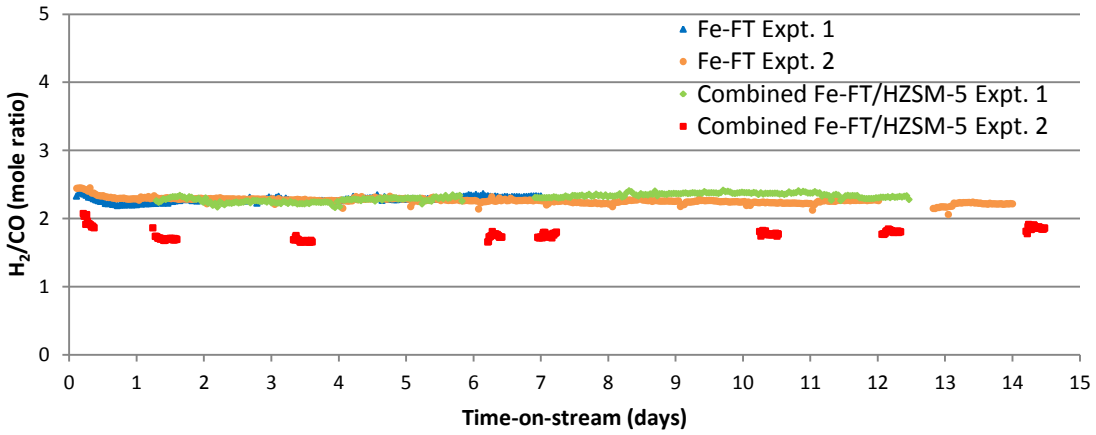

Figure AIV.3: H_2/CO usage ratios for the Fe-FT and combined Fe-FT/HZSM-5 experiments

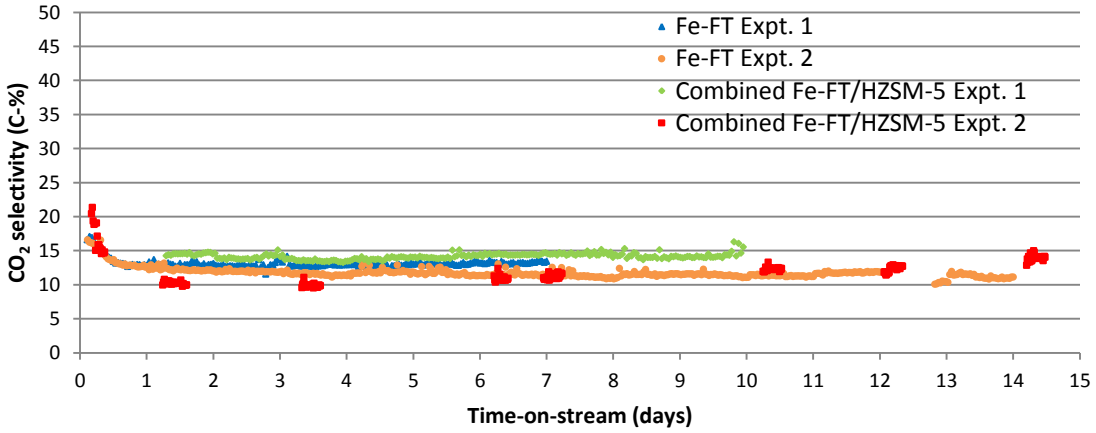

Figure AIV.4: CO_2 selectivities for the Fe-FT and combined Fe-FT/HZSM-5 experiments

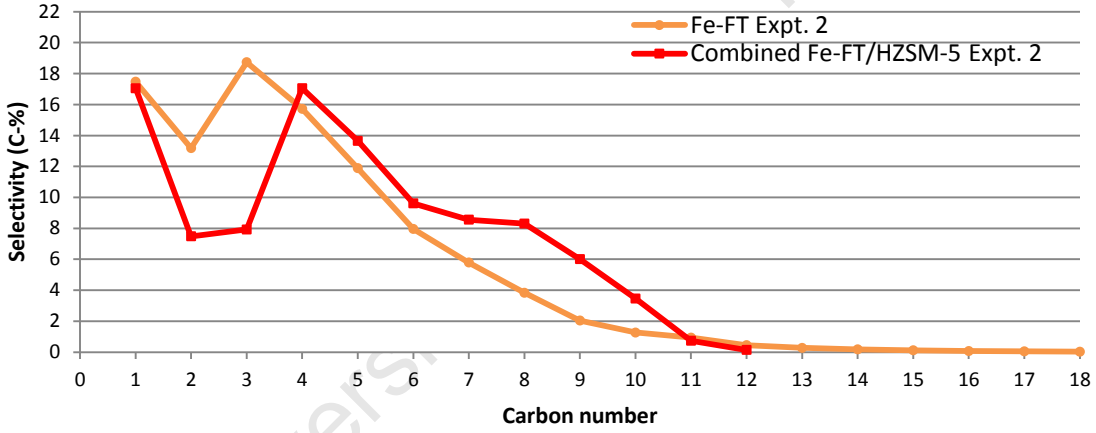

Figure AIV.5: Carbon number distribution for the Fe-FT Expt. 2 and the combined Fe-FT/HZSM-5 Expt. 2 (14 days on-stream)

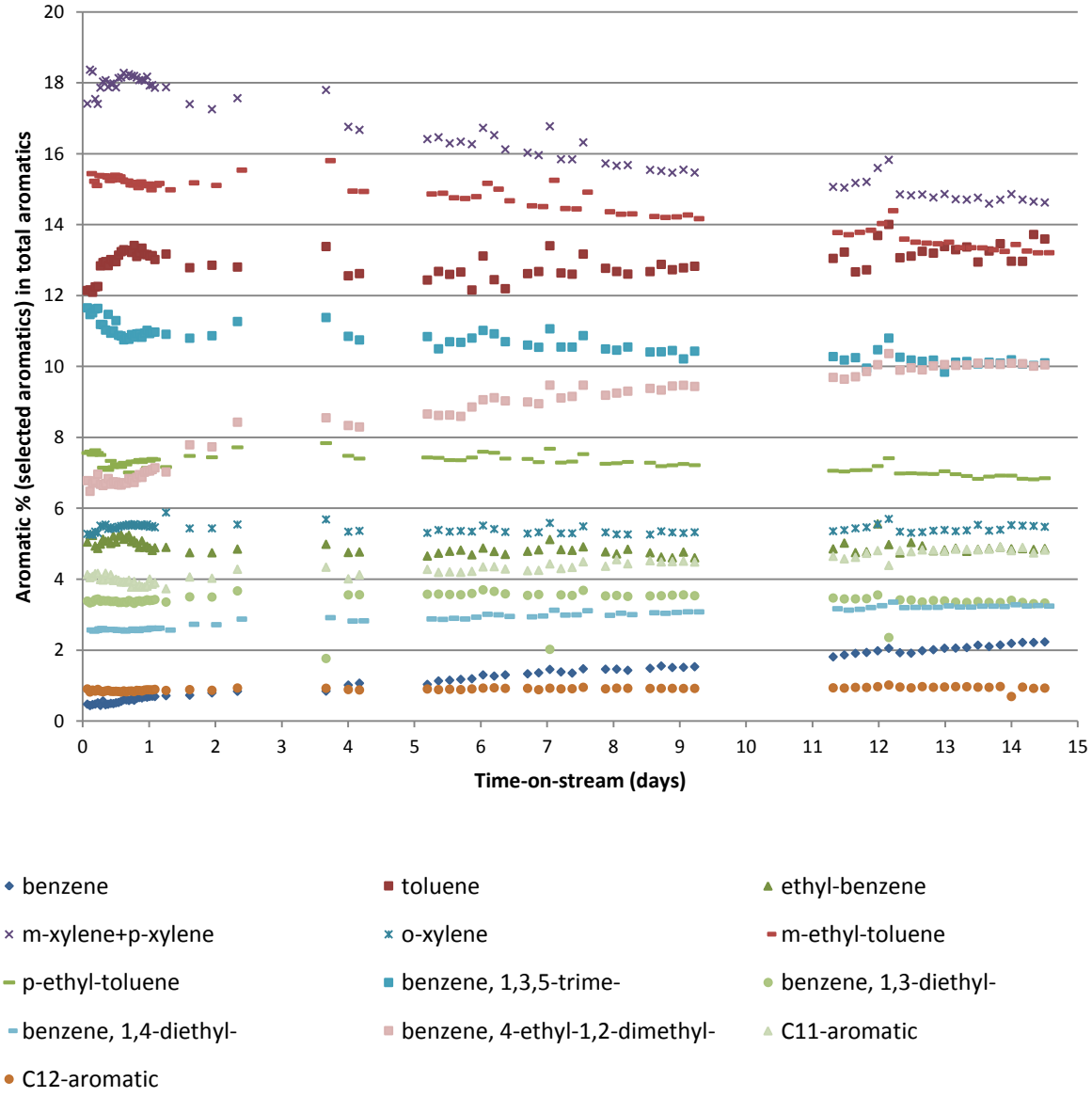

Figure AIV.6: Distribution of selected aromatics with time-on-stream for the combined Fe-FT/HZSM-5 Expt. 2

Catalyst characterization

Table AIV.1: AAS analysis of the fresh and spent Fe-FT and HZSM-5 catalysts

	K (wt-%)	Fe (wt-%)	K/Fe
Fresh Fe-FT Catalyst	2.39 ± 0.23	60.95 ± 5.46	0.039 ± 0.004
Spent Fe-FT catalyst of Fe-FT Expt. 2	1.88 ± 0.82	61.51 ± 3.69	0.030 ± 0.013
Spent Fe-FT catalyst for combined Fe-FT/HZSM-5 Expt. 2	1.62 ± 1.16	59.36 ± 3.73	0.028 ± 0.020
Fresh HZSM-5	1.91 ± 0.23	0.15 ± 0.02	
Spent HZSM-5 for combined Fe/HZSM-5 Expt. 2	1.44 ± 0.90	0.14 ± 0.04	

Table AIV.2: ICP-AES analysis of the fresh and spent Fe-FT and HZSM-5 catalysts

	Fe-FT catalyst			**HZSM-5 catalyst**	
	Fresh	*Fe-FT Expt. 2*	*Combined Fe-FT/HZSM-5 Expt. 1*	*Fresh*	*Combined Fe-FT/HZSM-5 Expt. 1*
Fe (wt-%)	60.9 ± 1.70	58.2 ± 0.53	56.7 ± 2.30	1.88 ± 0.71	1.43 ± 0.04
K (wt-%)	0.40 ± 0.04	0.29 ± 0.03	0.25 ± 0.02	0.16 ± 0.02	0.24 ± 0.01
K/Fe	0.0066 ± 0.0006	0.0050 ± 0.0005	0.0044 ± 0.0005		